Characterization of Subunit Interactions versus Catalysis in Yeast Enolase

Alessandra Padovani

A Thesis

in

The Department

of

Chemistry and Biochemistry

Presented in Partial Fulfilment of the Requirements
for the Degree of Master of Science at
Concordia University
Montreal, Quebec, Canada

March, 2003

Abstract

Characterization of Subunit Interactions versus Catalysis in Yeast Enolase

Alessandra Padovani

A protocol has been established for the over-expression and purification of large quantities of yeast enolase from *E. coli* cells. Yields have frequently exceeded 200 mg of >90% pure enzyme. Homogeneity of the preparations was assessed using both SDS-PAGE and analytical ultracentrifugation. Site-directed mutagenesis was successfully utilized to effect amino acid substitutions at two positions involved in subunit contacts. The residues in question are tryptophan 56, which was changed to phenylalanine (W56F), and glutamic acid 188, which was changed to aspartic acid (E188D). The mutants were characterized both structurally and catalytically, in order to study the effects of these substitutions on the enzyme.

Both mutants are partially dissociated in the 'apo' form, and are significantly more readily dissociable than is wild type in the presence of $NaClO_4$, a chaotropic salt. Each mutant shows a decreased conformational stability, or $\Delta G_{(H2O)}$, with respect to wild type. Secondary structural studies show proper folding, with a greater susceptibility to denaturation when subjected to heat, as reflected by lower T_m values. Circular dichroism and fluorescence spectroscopy reveal important changes in the aromatic environments within the variant proteins, indicative of a more loosely held hydrogen bond contact at the

subunit interface. Binding of cofactor and substrate allow the mutants to associate more fully and protect against dissociation when incubated with $NaClO_4$, although the holo-enzymes remain significantly more readily dissociable than wild type enolase.

A survey of the mutants' kinetic properties reveals a decrease in k_{cat} in the presence of the cofactors, Mg^{2+} and Mn^{2+}. Metal cofactor K_m values were not appreciably affected in these cases. W56F shows a greater reduction in catalytic efficiency in the presence of both metals, dropping by as much as two-fold when titrated with Mn^{2+}. The mutants are equally less prone to inhibition by Mg^{2+}, which inhibits the native enzyme's activity at high concentrations, whereas Mn^{2+} inhibits as expected. The modified Mg^{2+} inhibition reveals a change in metal ion specificity at enolase's third and inhibitory metal ion binding site. This finding in both mutants suggests that this site may lie in close proximity to the subunit interface, if not at the interface.

The effects of these mutations on both structure and catalysis reveal the integral importance of dimerization for the enzyme's function, and, more specifically, the role of the Pro35-Gly60 loop in maintaining this delicate balance.

Acknowledgments

To begin, I would like to extend a very appreciative thank you to my research supervisor Dr. Judith Kornblatt for her guidance, reliability and availability. I gratefully thank my examining committee members Dr. Justin Powlowski and Dr. Paul Joyce for their time and effort in following the progress of my work. A special thank you to Dr. Peter Ulycznyj of the Concordia Center for Structural and Functional Genomics for patiently running my endless samples in the analytical ultracentrifuge. To my good friend Isabelle Rajotte, I say thank you for the support and encouragement, as well as for being such a great example of diligence and dedication. Lastly, I thank my mother whose selflessness put me on the path I follow today.

Table of Contents

Chapter 2 Materials and Methods

List of Figures

List of Tables

Abbreviations

Ala	Alanine
AUC	Analytical ultracentrifuge/ultracentrifugation
Arg	Arginine
Asp	Asparagine
CD	Circular dichroism
EDTA	Ethylenediaminetetraacetic acid
Glu	Glutamic acid
Gly	Glycine
His	Histidine
LB	Luria-Bertani medium
Lys	Lysine
MES	2-Morpholinoethanesulfonic acid
$NaClO_4$	Sodium perchlorate
$(NH_4)_2SO_4$	Ammonium sulfate
PEP	Phosphoenolpyruvate
2-PGA	2-Phosphoglyceric acid
PhAH	Phosphonoacetohydroxamate
Phe	Phenylalanine

Pro	Proline
SDS-PAGE	Sodium dodecyl sulfate polyacrylamide gel electrophoresis
Ser	Serine
TAE	Tris/Acetic acid/EDTA
TE	Tris/EDTA
T_m	Melting temperature
Tris	Tris-(hydroxymethyl)aminomethane
Trp	Tryptophan
Val	Valine

Chapter 1: Introduction

1.1 A basic overview of enolase

Enolase (EC 4.2.1.11) (phosphoenolpyruvate hydratase) catalyzes the interconversion of 2-phosphoglyceric acid (2-PGA) and phosphoenolpyruvate (PEP) in a committed step of the glycolytic pathway. The reverse reaction is involved in gluconeogenesis. Mammalian organisms have three genes for enolase which code for three isozymes, or the α, β, and γ subunits. These isozymes are tissue-specific: α-subunits are found mainly in cardiac muscle and other smooth muscle tissue; β-subunits are found mainly in skeletal muscle tissue, and γ-subunits are found mainly in neuronal tissue. These isozymes are different electrophoretic forms of the enzyme, as they possess differing isoelectric points. The subunits assemble to form homo- and hetero-oligomers of the enzyme. Both the homo- and hetero-forms are naturally occurring.

Two genes have been found to encode enolase in *S. cerevisiae*. These are the ENO8 and ENO46 genes (1). The product for the ENO46 gene is enolase 1 (p*eno*46), which was first sequenced by Chin *et al.* in 1981 (2, 3). The ENO8 gene codes for enolase 2 (p*eno*8). The mammalian enolase (ββ isozyme), isolated from rabbit muscle, was sequenced by Chin in 1990 (4). The levels of the two yeast isozymes are under metabolic and developmental control (5). Enolase 1 is the predominant form of the enzyme, which was first isolated by Warburg and Christian in 1942 (6).

All of the eukaryotic enolases studied thus far are dimers of identical subunits (7). All known enolases are dimeric, except those isolated from thermophilic bacteria; these enolases are octameric (8, 9, 10). Subunit weights range from 40-50 kDa (11). The polypeptide chain in yeast is 436 amino acid residues in length (3).

Enolase is highly conserved at the level of sequence. Mammalian and yeast enolases share 60-65% sequence identity (4, 12). Among the mammalian enolases, there is at least 80% sequence identity (4, 12). Enolases 1 and 2 from yeast exhibit 95% sequence identity (3). Recent findings in a prokaryotic organism, *Escherichia coli*, show that its sequence bears 50% identity with those of the eukaryotes lobster and yeast (13).

Crystal structures have been obtained for the yeast (12) and lobster (14, 15) enzymes, and, more recently, that from *E. coli* (13). The *E. coli* enzyme was crystallized as a component of the RNA degradosome complex (13). Its function within this complex is as yet unknown. These three crystal structures were superimposed by Kühnel and Luisi (13). A reproduction of this comparison is shown in Figure 1.1. It demonstrates conservation at the level of tertiary structure, which may also indicate conservation at the level of quaternary structure (13). The main region of structural variability lies in a loop, extending from residues 248 to 268 in *E. coli*, denoted by an asterisk in the figure. *E. coli* has a corresponding five residue deletion between residues 259 and 260 (13). In comparison to animal enolases, this loop is, on average, four residues shorter in prokaryotic enolases and two residues longer in plant enolases (16). The active sites of *E. coli*, yeast and lobster enolase are very similar, and all the residues involved in catalysis are conserved (13).

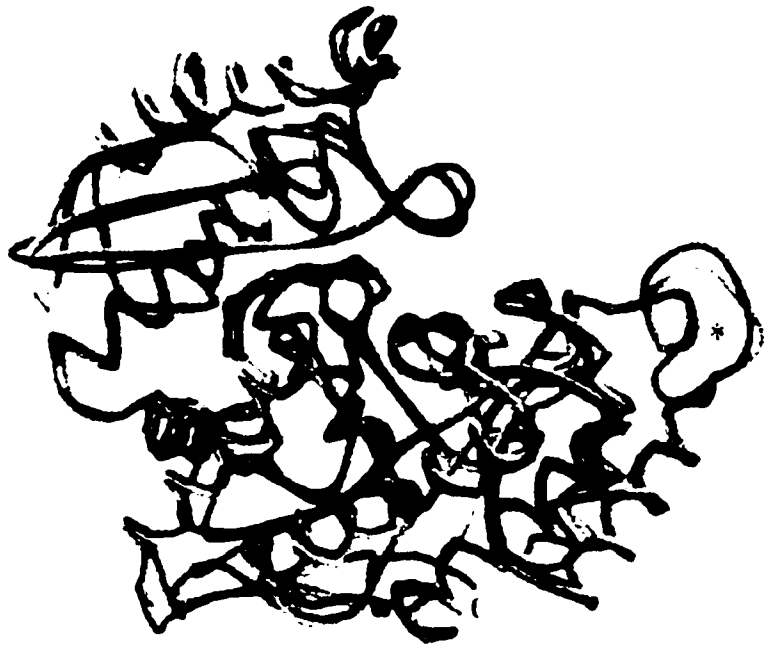

Figure 1.1 Superimposed enolase crystal structures. *E. coli* (red), yeast (yellow), and lobster (blue) crystal structures (13).

The best-characterized and most extensively-studied enolase is that from yeast. This is probably due to its simple purification in large quantities, and stability to laboratory manipulations (7). Detailed studies of this enzyme have been reviewed by Wold (11), and Brewer (7).

Enolase belongs to a group of functionally related enzymes, known as the enolase superfamily (17, 18, 19). The members of this superfamily can be assigned to three different subgroups, depending on their catalytic mechanism. The subgroups are represented by the

proteins mandelate racemase (EC 5.1.2.2), muconate cycloisomerase (EC 5.5.1.1), and enolase. Proteins belonging to these subgroups share both structural and functional similarity. For example, the active site in all of these enzymes is situated at the C-terminal end of the β-strands of an α/β–barrel. An important mechanistic similarity is the first step in the enzymes' reaction. In all cases, this involves the abstraction of the α-proton of a carboxylic acid to form an enolic intermediate (17). The interest sparked by the discovery of this functional relatedness is what prompted the search and discovery of their level of structural similarity. Structural details will be discussed in greater depth in the following section.

1.2 A structural overview of enolase

1.2.1 Overall 2° and 3° structure of enolase

Enolase, as it occurs in most organisms, is a dimer of two identical subunits, each of which consists of one continuous polypeptide chain. Figure 1.2 illustrates this clearly. Several high resolution crystal structures have been reported (12, 20, 21, 22, 23). These have provided us with a better understanding of the enzyme's overall tertiary fold, the architecture of the active site, including binding sites and protein ligands for cofactors and substrate, as well as the importance of polar side chains within the active site. This will be discussed more rigorously later.

Enolase consists of two domains (12, 22). The smaller N-terminal domain extends from residues 1-142, and is known as the α/β-domain. For the purposes of this discussion, this portion of the enzyme will be referred to as the small domain. It is composed of a three-stranded/amphiphilic/anti-parallel β-sheet with tight turns, followed by four α-helices with

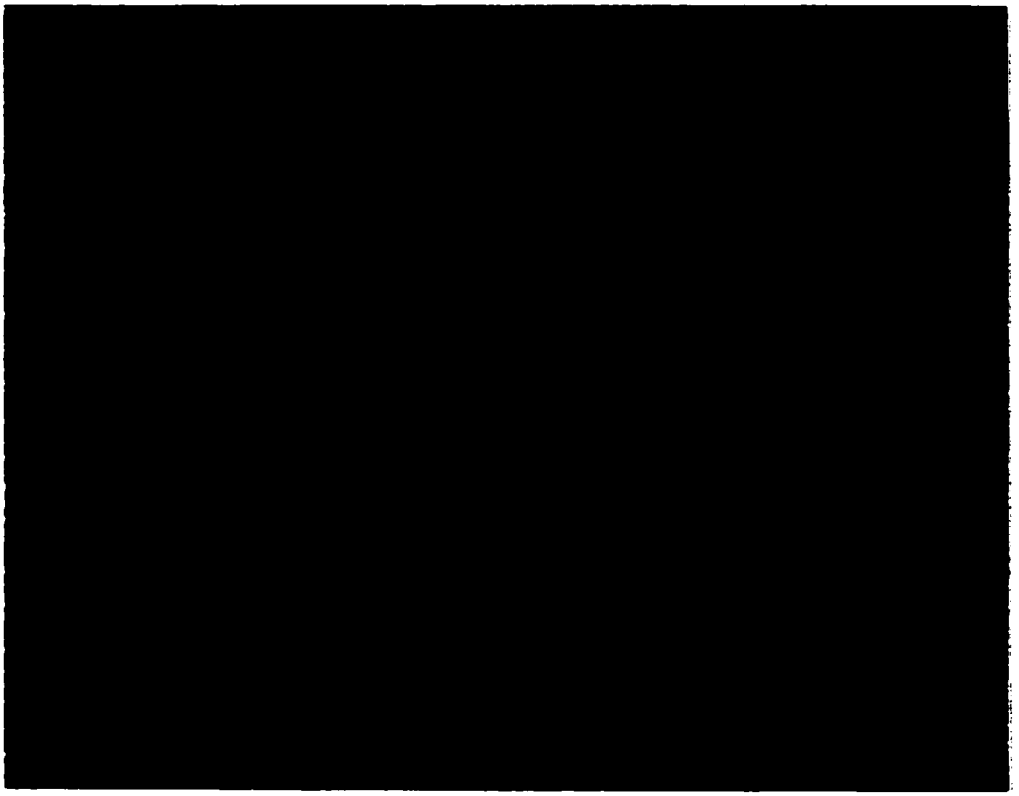

Figure 1.2 The butterfly enzyme. Yeast enolase (1one.pdb). Each enolase subunit is shown in a separate color (green and blue). The red spheres indicate substrate (2-PGA) bound, and the location of the active site. (Image generated using Rasmol, version 2.6.)

regular hydrogen bonding patterns. The principal domain, extending from residues 143-436 in yeast, consists of a cylindrical β-sheet, which is built of eight β-strands surrounded by eight α-helices (12, 22). This is known as an α/β-barrel. Here, it will be referred to as the large domain. The yeast enolase monomer (24) is depicted in Figure 1.3, where these structural features are illustrated with greater clarity. The eight-stranded α/β-barrel is a widely occurring form of protein architecture (25, 26). All enzymes belonging to the enolase superfamily have an unusual $\beta\beta\alpha\alpha(\beta\alpha)_6$ topology (12). This is in contrast to the more frequently occurring $(\beta\alpha)_8$ topology of the α/β-barrels represented by the enzyme triosephosphate isomerase (TIM) (EC 5.3.1.1) (27). This topological distinction is illustrated in Figure 1.4 (13). The hydrophobic side of the β-sheet in the small domain is in contact with the first helix (HI) and the third helix (HK) of the same domain. The other side is exposed to the solvent, where predominantly large hydrophilic side chains protect the polypeptide chain (22). This assembly forms a hydrophobic core, which is highly conserved among the prokaryotic and eukaryotic enolases (12, 13, 14, 15). Strands S9, S10, and the loop which connects S11 and helix HI, which closes onto the active site upon substrate binding, are part of the dimer interface (13). This region of the protein, of great interest in the study of dimer dissociation, will be discussed further. The topology reveals S2, the second barrel strand, to be anti-parallel to the other barrel strands. This is equally the case for HA, the first barrel helix. Helix HA, extending from residues 179-200, is also the longest helix in the protein (12, 13). It forms an extended entrance to the active site, and contributes residues to the dimer interface (13). The barrel helices are mainly amphiphilic, with the exception of the mainly hydrophobic helix HG, which extends from residues 382-389 of the

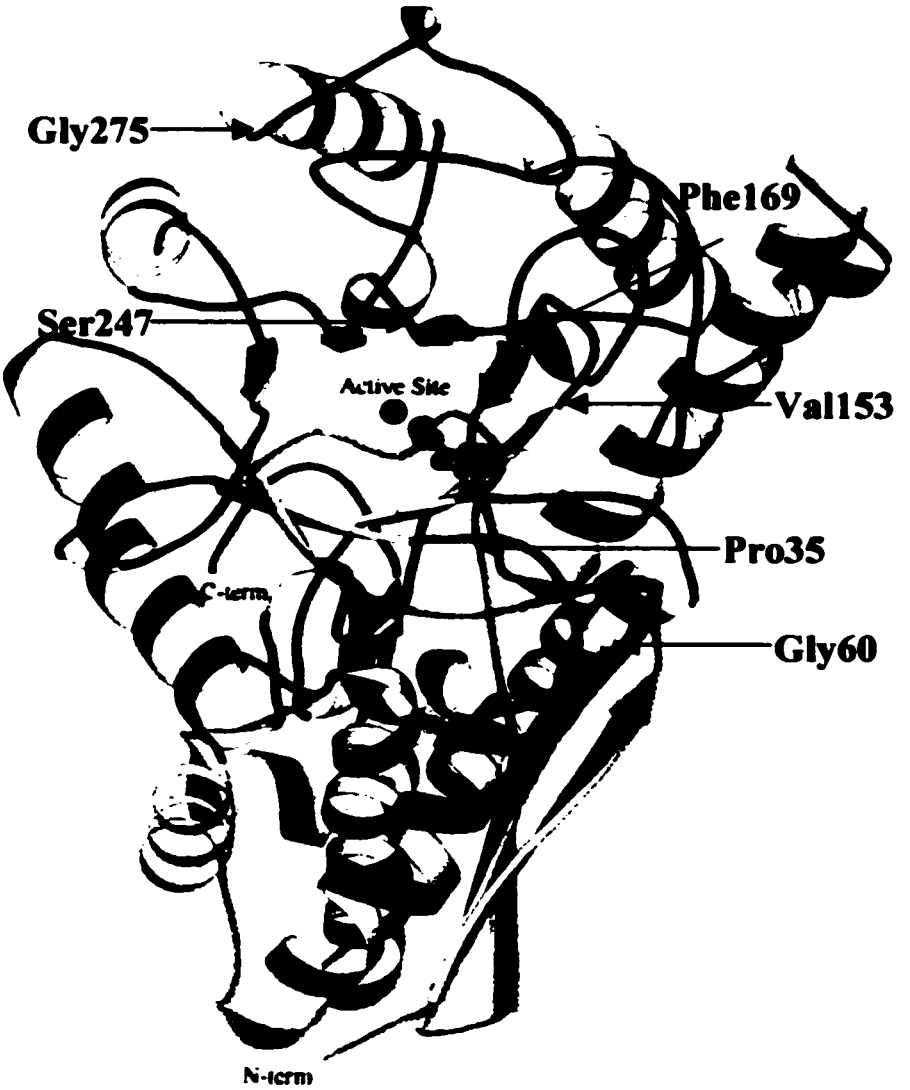

Figure 1.3 The yeast enolase monomer. The small domain is shown in green, and the large domain in blue. The active site is shown with substrate (red) and cofactor (dark blue) bound (24).

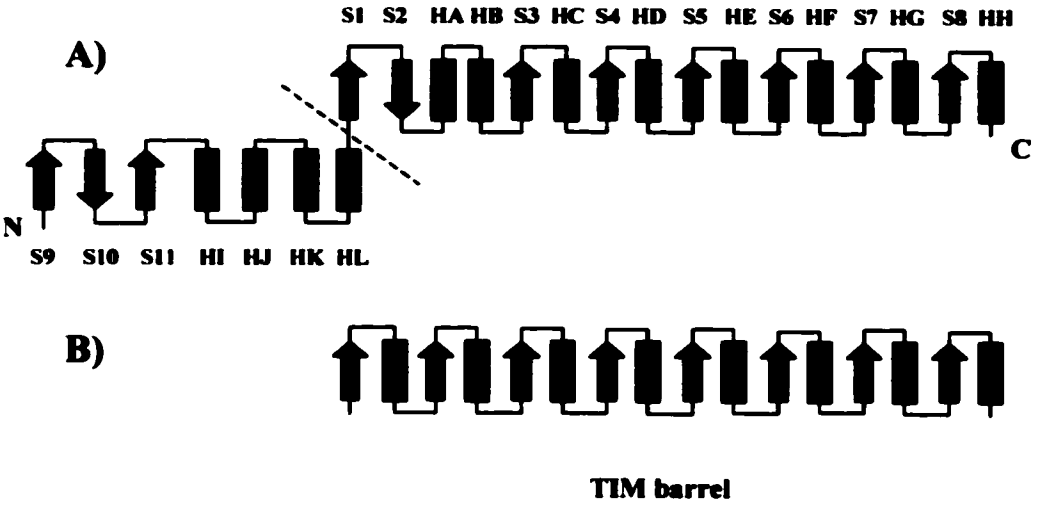

Figure 1.4 Topology of enolase. The enolase topology is shown in (A), and that of TIM in (B) (12). β-strands are denoted 'S', and are shown as dark arrows; α-helices are denoted 'H', and appear as red cylinders. The domain boundary is indicated by the line (13).

chain (12, 13, 22). This region is highly hydrophobic, and corresponds to the interface between the large and small domains (13). In addition, most of the helices in the barrel are on the outside of the molecule (22). This is depicted in Figure 1.5, taken from Lebioda *et al.* (23). The exception, again, is helix HG, which is almost completely buried (22). Its sequence is almost entirely conserved among all known enolases (22). The β–strands of the

large domain are 3-5 residues in length (13). In most cases, the first few amino acid residues of the strands are hydrophobic, whereas the last ones are hydrophilic and participate in the active site (13). A breakdown of the elements of secondary structure, and the residues they comprise, is presented in Table 1.1, reproduced from Lebioda *et al.* (12).

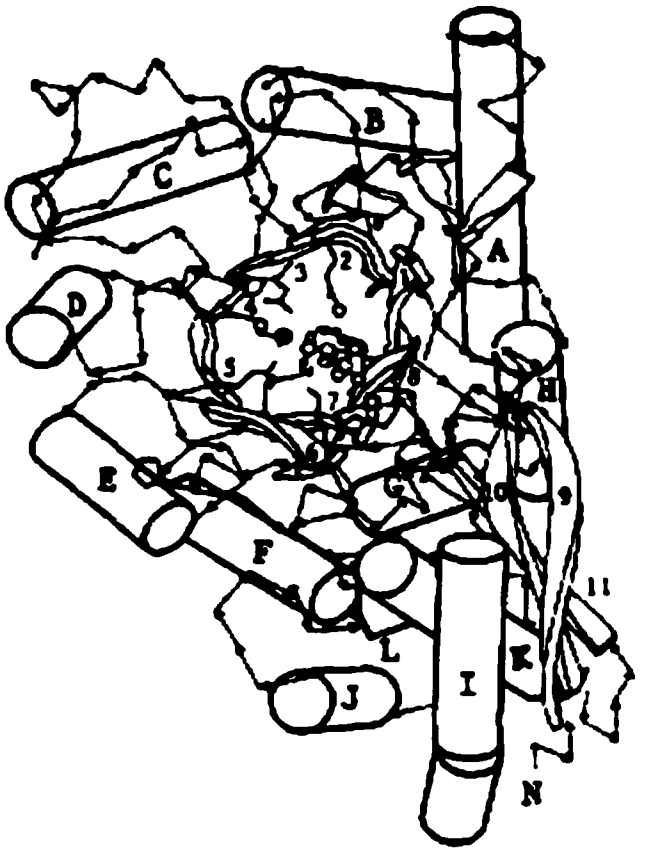

Figure 1.5 Stereoview of the enolase subunit. The subunit is seen along the barrel axis. The active site is located at the end of this deep cavity. The barrel helices (cylinders) surround the exterior of the molecule, whereas the β-strands (arrows) are mainly found in the barrel's interior, where they line the active site with a myriad of catalytically significant polar side chains (23).

Anti-parallel β meander	**Strand 9**	**5-13**
	Strand 10	**17-25**
	Strand 11	**29-35**
Helices of N-terminal domain	**Helix I**	**61-80**
	Helix J	**86-96**
	Helix K	**107-125**
	Helix L	**128-136**
8-fold	**Strand 1**	**150-153**
	Strand 2	**168-172**
	Helix A	**179-200**
	Helix B	**221-235**
	Strand 3	**241-247**
	Helix C	**275-288**
	Strand 4	**293-296**
	Helix D	**303-312**
	Strand 5	**316-320**
	Helix E	**327-336**
	Strand 6	**341-345**
	Helix F	**352-365**
	Strand 7	**368-373**
	Helix G	**382-389**
	Strand 8	**394-397**
	Helix H	**404-419**

Table 1.1 Enolase in pieces. Amino acid residues within the various secondary structural elements (12).

1.2.2 Active site architecture

The active site is situated in a deep conical shaped cavity, at the C-terminal end of the inner β-strands of the α/β-barrel (22). It sits among loops contributed by both subunit domains (23). Loops, as well as their structural importance, will be discussed further. The

active site residues are on all of the barrel strands, except the first (23). As stated, polar side chains line the active site. Figure 1.6 attests to this.

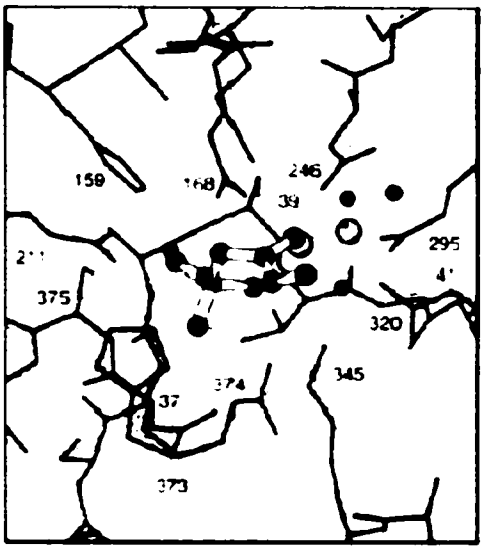

Figure 1.6 Enolase active site. Active site of enolase bound to Mg^{2+} (natural cofactor, seen as two light spheres), and a tight binding inhibitor (PhAH, seen in ball-&-stick form) (28). Some of the polar residues implicated in catalysis (Glu168, Glu211, Lys345, & His373), in active site stabilization (Glu168, Glu295, Asp320, & Lys345), and in substrate coordination (Asp246, His373, Arg374, & Ser375) are indicated (28, 29). Smaller dark spheres represent water molecules.

These residues are highly conserved among the various enolases sequenced, and their positions are the same in the substrate-bound crystal structures (12, 20, 23, 28). In effect, the active sites of *E. coli*, yeast and lobster enolase are very similar, and all of the residues involved in catalysis are conserved (12, 13, 14, 15).

1.2.3 Loop structures in enolase

Loops play a central role in enolase, both structurally and catalytically. One half of the polypeptide chain is in the form of loops and turns, which connect elements of secondary structure (22, 23). The loops which connect the strands and helices at the C-terminal end of the barrel, and thus lie in close proximity to the active site, are, on average, longer than those situated at the opposite end of the molecule (22, 23). Stec and Lebioda postulated in 1990 (22) that this extended entrance into the active site may play an important role in directing the substrate toward the site of catalysis.

The loop elements are of interest in the enolase structure for a number of reasons: a) they contain approximately one half of the aromatic amino acids in the yeast protein; b) specific movements are associated with cofactor and substrate binding, bringing some of the loop regions closer to the active site, and c) the loops contribute residues to both the active site and the subunit interface (23, 30). Kornblatt *et al.* in 1996 proposed that precise loop conformation is crucial in maintaining both structural integrity at the active site and the interactions at the dimer interface (30). Disrupting the loop conformations would, therefore, not only weaken the stability of the dimeric form of the enzyme, but also have an adverse effect on the active site architecture (30). This would explain the importance of dimerization for catalysis in enolase. The correlation between dimerization and function has been reported for other enzymes (31).

Three distinctly important loop regions have been revealed in the structure of enolase. The first extends from residues Pro35-Gly60. This loop extends from the small domain, and connects the third strand to the first helix of the same domain (16, 20, 23, 28).

The most mobile portion of this loop comprises Pro35-His43, and is known as the 'active site loop', since it closes over the active site upon cofactor and substrate binding (23). Its closure is necessary for catalysis to occur. This has been observed in a wide variety of enzymes, including triosephosphate isomerase (32). An important residue in this closure is serine 39, observable in Figure 1.6 (28). Site-directed mutagenesis on Ser39 has shown that it is necessary for catalysis, presumably because of its role in loop closure (33, 34). The hinges on the loop, at positions 37 and 41, are glycine residues, which presumably allow for maximal loop flexibility (28). Their location within the active site is also shown in Figure 1.6. The overall loop (35-60) extends all the way from the active site to the subunit interface, where the backbone amino moiety of residue 56 (tyrosine in mammals, tryptophan in yeast) participates in a hydrogen bond with a glutamic acid on the other monomer (3, 4, 22). Two additional flexible loops extend from the large domain. The first of these extends from residues Val153-Phe169 (12, 16, 20, 23, 28). It also appears to move upon cofactor and substrate binding, but to a much lesser extent than the active site loop (12, 16, 20, 23, 28). It connects strand S1 to strand S2 in the first few residues of the large domain (12). This loop contributes a histidine at position 159, situated at the active site (see Figure 1.6), which has been implicated in helping to maintain both catalytic site structure and loop conformation (21, 28). His159 also has been proposed as one of the residues directly participating in catalysis (35, 36). The third loop extends from residues Ser247-Gly275 (12, 28). The most mobile portion of this loop extends between Asp255-Asn266 (12, 28). Wedekind *et al.* (28) noted that approximately one half of the Ser247-Gly275 loop residues formed the hydrophobic core of the large domain, originating in the strand S3 to helix HC

loop, and extending all the way through the barrel-exposed side of helix HC, which lies between residues 275 and 288 (see Table 1.1). The positions of these loops within the overall protein structure may be viewed in Figure 1.3.

As mentioned, the loops contain approximately one half of the yeast protein's aromatic amino acid residues (30). It was observed that three of the five tryptophan residues reside in loops, as do four of the nine tyrosine residues in yeast enolase (37). The Ser247-Gly275 loop, for example, contains one tyrosine, one tryptophan, and three phenylalanine residues (30). The movement of these loops upon cofactor and substrate binding is thus accompanied by important spectral changes.

1.2.4 Subunit interface of enolase

As cited, loops play an important role in maintaining subunit interactions which occur at the dimer interface. This region is highly conserved among prokaryotic and eukaryotic organisms (12, 13, 14, 15). The interface between the subunits consists of a variety of ionic interactions and hydrogen bonds. These are summarized below in Tables 1.2 and 1.3 (22). Most of these interactions occur between strands S9 & S10 in the small domain of one monomer and helix HH in the large domain of the other monomer. The interactions at the dimer interface are mainly hydrophilic in nature, a result of the region's richness in polar side chains. In fact, the interface in enolase is much more polar than is the case in most other dimeric proteins (22, 38). The ratio of charged/hydrophobic residues at the subunit interface was found to be 1.5 for *E. coli* enolase (13), which represents more than double the average of 0.7 observed in most oligomeric proteins (38). This explains the dependency of dimerization on solvent ionic strength in *E. coli* enolase (13), as well as the

Residue A	RA(+).....(-)RB	Residue B
R8	NE-OE2	E417
R8	NH2-OE1	E417
R414	NE-OE1	E20
R414	NH2-OE2	E20

Table 1.2 Ionic interactions. Ionic bonds formed at the subunit interface. The letters in columns 1 and 3 indicate the residues involved, with their corresponding position in the protein. The interacting atoms are specified in the second column, closest to their respective residues, RA and RB (22). In this case, N represents a nitrogen atom, whereas O represents an oxygen atom. The position of these atoms with respect to the C_α of the amino acid backbone is indicated.

Residue A	RA.....H.....RB	Residue B
E417	OE2-OH	V2
N410	ND2-OE1	E379
N410	ND2-O	Y11
N410	OD1-N	Y11
E404	OE1-N	S403
E188	OE1-N	W56
H191	NE2-O	R14
S13	O-N	R402
V208	O-N	V208

Table 1.3 Hydrogen bond contacts. Subunit interface hydrogen-bonding partners are listed (22). The same convention for the specification of interacting residues and atoms as cited above is used here.

weak subunit binding observed in yeast enolase in the absence of the enzyme's natural cofactor, Mg^{2+} (22). The subunit contacts in the dimer bury 3320Å of surface in *E. coli* enolase (13), and 3740Å in lobster enolase (14, 15). This is comparable to the average buried surface of 3370Å found for most other dimeric proteins (39). Indeed, many proteins make subunit contacts over large surface areas, but the majority of the energetic contributions are often accounted for by relatively small regions of the protein interface (31), as is the case for enolase (40).

The crystal structure reported in 1990 by Stec and Lebioda (22) revealed 346 water molecules in enolase's solvation shell. Of these, 11 were considered internal, with no apparent access to the surrounding solvent bulk water. The most ordered water structures were found in the active site cavity, and in a deep cleft formed between the dimer subunits (22). The active site water molecules, as we will discuss later, have been implicated in catalysis and ligand coordination.

The intimate relationship between the structure and function of a protein prompts consideration of its catalytic mechanism.

1.3 A mechanistic overview of enolase

1.3.1 General reaction catalyzed by enolase

Enolase, also known as phosphoenolpyruvate hydratase and 2-phospho-D-glycerate hydrolyase, catalyzes the only dehydration reaction in the glycolytic pathway (41). A general representation of this is shown in Figure 1.7. The reaction involves acid/base chemistry, and is interesting from a mechanistic point of view. This is due to the fact that it catalyzes the abstraction of a relatively non-acidic proton at position C-2 (pKa of ~28-32)

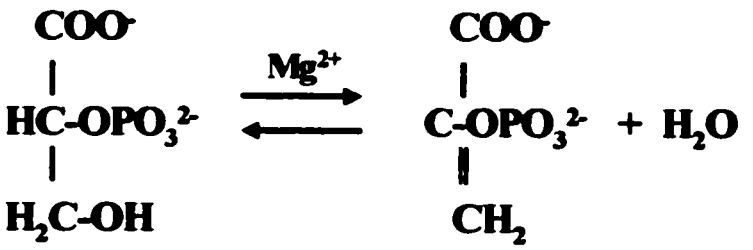

Figure 1.7 The enolase reaction. The reversible removal of H_2O from 2-PGA. The numbering convention for the 2-PGA compound is C-1 at carbonyl, C-2 at phosphonyl, and C-3 at hydroxyl.

(28), and the removal of the OH^-, a rather poor leaving group, at position C-3 (42). The reaction is accompanied by a comparatively small change in free energy (~ 1 kcal/mole) (11). Efforts were made in order to determine whether or not the abstraction of the C-2 proton and the elimination of the C-3 OH^-group occurred in a concerted fashion, or as a sequential process. Early on, it was concluded that the reaction proceeded in a step-wise manner, and that a carbanionic intermediate was formed at C-2 on 2-PGA (42, 43). This was most recently supported by Anderson *et al.* (44), who used kinetic isotope effects to probe the enolase mechanism. Therefore, the reaction begins with abstraction of the C-2 proton, resulting in carbanion formation at this position. Elimination of C-3 OH^- then precedes double bond formation between C-2 and C-3 and, finally, product release. A general scheme of the reaction was prepared by Reed *et al.* (24). Anderson *et al.* in 1994 (44) proposed that both the rate of proton abstraction and that of OH^- elimination/PEP release were rate limiting

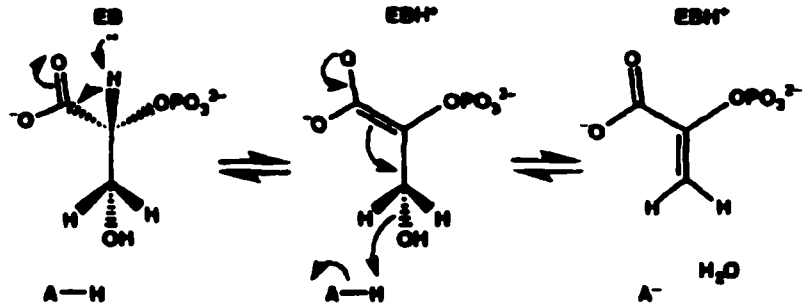

Figure 1.8 General 2-step mechanism of enolase. EB (enzymic base) abstracts H^+ at C-2. Rearrangement at C-2 forms a carbanionic intermediate. Final product release is then preceded only by OH^- elimination through the acid AH, and double bond formation between C-2 and C-3 to form PEP (24).

to the overall reaction. This was disputed by work carried out in 1996, which reported the rate limiting steps as associated with events immediately preceding product release (45). It is to be noted, however, that these studies involved different isozymes of the protein, manipulated in a non-analogous manner. Even before the earliest evidence of a step-wise chemical sequence of events, Cohn *et al.* in 1970 had determined that the elimination of H_2O from 2-PGA was specifically *anti* in its stereochemistry, whereby OH^- and H^+ left from opposite sides of the enzyme-bound substrate (46). This, in turn, meant that important catalytic residues would be situated on opposing sides of the enzyme-bound 2-PGA (47), which they indeed were found to be.

1.3.2 Mechanistic proposals

Several proposals have been put forth as to the identity of the acid/base catalysts in the enolase reaction. Of these, three have received the most attention. Lebioda and Stec in 1991 proposed a water molecule situated between Glu211 (Glu208 in *E. coli*) (13) and Glu168 as the possible catalytic base, based on the crystal structure of the enolase-Mg^{2+}-2-PGA/PEP complex (23). This possibility had first been suggested by Brewer in 1985 (48). In this view, the proton would first be transferred to a water molecule located 2.6Å away from C-2 on 2-PGA (23). The water molecule in question forms a hydrogen bond with the carboxylic groups of Glu168 and Glu211 and is ionized by these two side chains, forming OH^-, which acts as the catalytic base (23). Following abstraction, the water molecule would transfer the proton to Glu168, and, finally, to the substrate OH^- to form the departing water molecule (23). This proposed mechanism was supported by site-directed mutagenesis carried out at the Glu168 and Glu211 positions in 1993 by Brewer *et al.* (49), and in 1995 by Sangadala *et al.* (41). Both the E168Q and the E211Q mutants showed severely depressed catalytic activity, which agreed with their proposed catalytic importance (41, 49).

In 1994, a crystal structure of enolase complexed with the tight binding inhibitor phosphonoacetohydroxamate (PhAH) implicated a lysine residue at position 345 (Lys341 in *E. coli*) (13) (28). PhAH belongs to a group of very tight binding inhibitors, which mimic the structure of the enolase carboxylate reaction intermediate (50). Support for Lys345 as the catalytic base came in 1996 through the work of Poyner *et al.* (47). Their work involved site-directed mutagenesis at positions 168 (E168Q), 211 (E211Q), and 345 (K345A) (47). All three mutants possessed severely deficient rates of catalysis for the overall reaction (<1

part in 10^5 of the native protein's activity) (47). The two steps of the reaction were then studied separately. The first step of the reaction was assayed by measuring the rate of exchange of the C-2 proton on 2-PGA with the deuterons in a solution of D_2O (47). Both E168Q and E211Q catalyzed this exchange normally, whereas K345A failed to catalyze this first step of the reaction (47). This was not compatible with Brewer's ideas and earlier findings (41, 49). Poyner's results identified the catalytic base as Lys345, whereas the E168Q and E211Q variants retained a functional enzymic base (47). The second step of the reaction was studied by mimicking the addition of OH^- to the C-3 position of PEP in the reverse reaction (47). All three mutants were severely affected, in the order E211Q>>E168Q>K345A (47). They thus concluded that Glu211 functions in the second step of the reaction, catalyzing the activation of a nearby H_2O molecule for addition of OH^- on C-3 of PEP in the reverse reaction, while Lys345 ionized 2-PGA by abstracting H^+ at C-2 (47). The role assigned to Glu211 was supported further by its interaction with the C-3 OH^- group of 2-PGA, seen in Wedekind's crystal structure (28). The crystal structure published in 1994 by Wedekind *et al.* (28) showed that the intervening water molecule between Glu168 and Glu211, suggested as the catalytic base by Brewer *et al.*, was also 2.9Å away from the ε-nitrogen of His373. This was, therefore, suggested as another possible candidate for catalyzing the activation of H_2O in the reverse reaction's first step (second step of the forward reaction) (47). A summary of Poyner's proposal is shown in Figure 1.9 (47). The role of His373 was investigated by Brewer *et al.* in 1997 (29). The H373N and H373F mutants were prepared and characterized, and, although both of their activities were severely

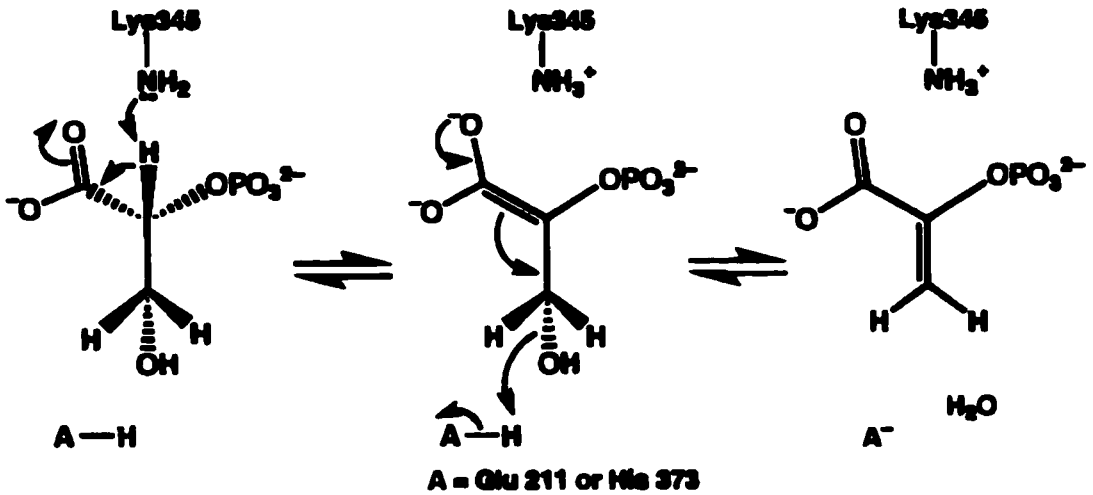

Figure 1.9 Catalytic scheme. Possible catalytic scheme, proposed by Poyner *et al.* in 1996 (47). The arrows show the movement of electrons.

reduced, it was concluded that the importance of H373 in catalysis was due to its hydrogen bonding network with Glu168, Glu211, and the intervening H_2O molecule, rather than its direct participation in the removal of OH^- (29). The role of Lys345 as the catalytic base, and that of the Glu168/Glu211/H_2O/His373 hydrogen-bonding network is further confirmed by the crystallographic work of Zhang *et al.* in 1997 (16). This model is consistent with the *anti* stereochemistry of the enolase reaction, as Lys345 is situated on the opposite side of the bound substrate analogue PhAH (28) with respect to Glu168 and Glu211, as illustrated in Figure 1.10.

The third postulated catalytic base is the imidazole group of His157 in lobster enolase (His158 in *E. coli*, His159 in yeast), crystallized by Duquerroy *et al.* in 1995 in the presence of bound inhibitor (15). The structure showed van der Waals contacts between the histidine's imidazole ring and position C-2 on the inhibitor (15). Vinarov and Nowak in

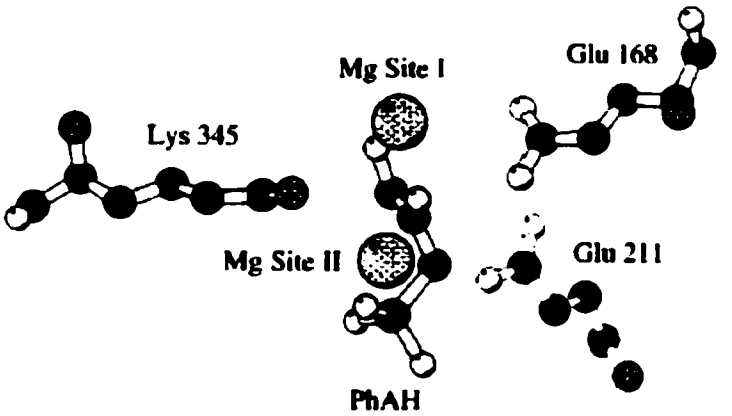

Figure 1.10 Catalytic residues. Positions of Lys345, Glu168, and Glu211 relative to PhAH. Spheres indicate bound cofactor, Mg^{2+} (47).

1999 mutated His159 in yeast to an alanine residue. They found that the mutant was unable to catalyze the ionization of 2-PGA in the first step of the reaction, thereby providing evidence for the role of His159 as the catalytic base (35). However, this was discounted by Brewer *et al.* in 2000 (36), who showed that H159A in yeast enolase possessed a significant amount of activity, and that H159 was, therefore, not the enzymic base. It is not clear, however, which of the two groups is correct in their findings.

Currently, the idea of Lys345 as the catalytic base is that which has gained the most support and approval among investigators of the enolase catalytic machinery, although many feel that results are not yet conclusive. The reaction scheme would, therefore, be best described in Figure 1.11 (24).

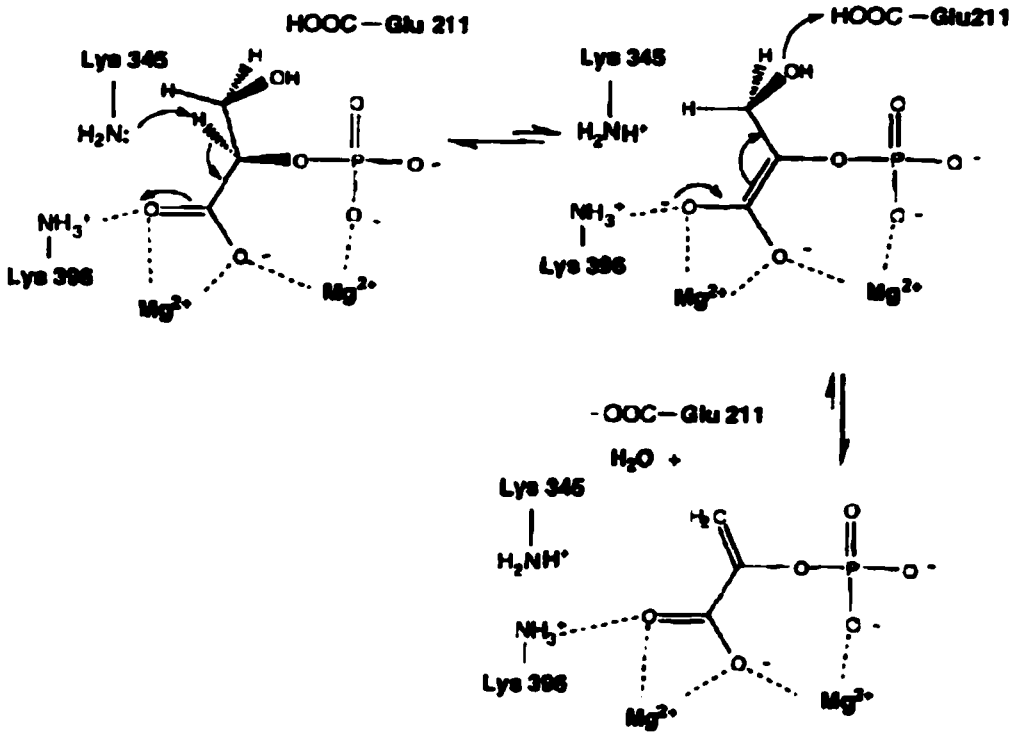

Figure 1.11 Proposed mechanism of enolase.
The roles of Lys345 and Glu211 are shown (24).

The enolase catalyzed dehydration of 2-PGA exhibits an absolute requirement for divalent metal cations. On this, most everyone agrees.

1.3.3 Enolase is a metalloenzyme

All known enolases exhibit an absolute requirement for divalent metal cations in order for catalysis to take place. Enolase's natural cofactor is magnesium, i.e., Mg^{2+} produces the highest rates of catalysis. More than 300 of the known enzymes, or roughly 15%, require metal ions (48). Mg^{2+} is the most common catalytic metal cofactor, probably since it is present in millimolar quantities in the cell, whereas Ca^{2+}, for example, is present

in micromolar quantities (48). A metal ion must be present at the active site in order for substrate/product or substrate analogue binding to occur (51). No catalysis is observed in holo-enolase upon binding this first metal ion; it simply allows substrate to bind. Substrate permits an additional metal ion to bind. This second metal ion produces catalysis, and is, therefore, known as the 'catalytic' metal ion. Catalysis only occurs in this instance if the first metal ion bound is an activating one (51).

One mole of Mg^{2+} binds per mole of enzyme subunit (51). The enzyme contains endogenous bound Mg^{2+} (23). It may be stripped of the endogenous Mg^{2+}, and almost any other ion substituted (23). A variety of other metal ions have been observed to bind at this first metal binding site, a survey of which was presented by Brewer *et al.* in 1983 (52). These included Sm^{3+}, Tb^{3+}, Co^{2+}, Ni^{2+}, Fe^{2+}, and Zn^{2+} (52). Not all of the metal ions binding at this site are activating, and no relationship is observed between affinity and activity (52). Metals which bind but do not produce activity are Ca^{2+}, Tb^{3+}, and Sm^{3+} (52). The unrelatedness of affinity and activity is exemplified by the fact that these non-activating metals actually bind to the enzyme more tightly than does Mg^{2+} (52). Their binding is so strong that it displaces bound Mg^{2+}, and even high concentrations of Mg^{2+} (>1 M) could not displace bound Tb^{3+} (52). Other activating metals have been described, including Mn^{2+} (53, 54), Cd^{2+} (55, 56), and Cu^{2+} (57). Binding of Ni^{2+} (58), Co^{2+} (59), Ca^{2+}, and Zn^{2+} (60) also has been studied. The various activating metals are classified according to the level of activity they produce when bound to enolase: $Mg^{2+}>Zn^{2+}>Mn^{2+}>Fe^{2+}>Cd^{2+}>Co^{2+}>Ni^{2+}$ (7).

Each subunit of enolase possesses one binding site for the first metal ion (51). The binding of this metal ion produces conformational changes in the overall structure of the

protein, as measured by absorption spectroscopy and circular dichroism (61, 62). The first binding metal is known as the 'conformational' metal, due to the conformational changes which take place upon its binding. As stated, almost any divalent cation may bind at this conformational site, as the metal ion affinity is not related to activation (52). The presence of this metal allows substrate to bind. The binding of substrate is accompanied by the displacement of two active site water molecules (7). Substrate allows binding of the catalytic metal ion. This step also is followed by conformational changes, a significant portion of which occur in the loop regions, as discussed in a previous section (see Section 1.2.3). Two more moles of metal ion bind per mole of enzyme. The first evidence that additional metal cations bind in the presence of substrate came in 1969 through the work of Hanlon & Westhead (63, 64). The catalytic metal ion has a lower affinity than does the conformational, and both are required for catalysis (51, 63, 64). The sequence of binding and conformational events is summarized in the eight-step mechanism seen in Figure 1.12 (45).

Figure 1.12 Binding and conformational events in the kinetic mechanism of enolase. EM=enzyme + Mg^{2+}; S=2-PGA; P=PEP; I=intermediate; *=conformational change (45).

A sufficient excess of activating metal ion inhibits the enzyme, and metal sites distinct from the previous two were postulated (65). Further studies have confirmed the presence of a third metal binding site, one which, when occupied, is inhibitory. For

example, a third site was demonstrated using Mn^{2+} as the activating metal, and binding constants were obtained for this cofactor at each site (66). High concentrations of Mg^{2+} ($\geq$ 1 mM) inhibit the enzyme by almost 50% (51), as do varying concentrations of Cu^{2+}, Zn^{2+}, Cd^{2+}, Mn^{2+}, Co^{2+}, and Ni^{2+} (65). In addition, certain monovalent cations also inhibit enolase. Na^{+} and Li^{+} (67, 68), as well as K^{+} and NH_4^{+} (68) were found to inhibit the activity of yeast enolase, although the latter two activate the enzyme at lower concentrations. The site of this inhibition is as yet unknown, but Elliott and Brewer have suggested that the inhibition may result from conformational changes upon binding at metal site (III) (65), which may disrupt the active site structure, and, therefore, impede catalysis.

1.3.4 Coordination of substrate and cofactor

Crystal structures of enolase bound to potent inhibitors and metals, for example, the crystal structure published in 1992 by Poyner & Reed (69) with bound PhAH and Mn^{2+}, have provided valuable insight into the coordination scheme of the metal ions to substrate and reaction intermediates (69). This shows a possible role for both metals in stabilizing the carbanion intermediate (69). The importance of the metals in the coordination of both substrate and product was later echoed by Zhang's crystal structure in 1997 (16).

Both Mg^{2+} ions are complexed to functional groups of the substrate/product (28). Wedekind *et al.* reported an octahedral coordination of Mg^{2+}, with a 6-fold chelation scheme for each (70). Three carboxylic ligands form the conformational metal ion binding site (28). Metal (I) coordinates to the carboxylate oxygens from the side chains of Asp246, Glu295, and Asp320, as well as to both the carboxylate oxygens of the substrate/product, and one water molecule (28). The substrate carboxylic group oxygen O1 is situated 2.9Å away from

the side chain N of Lys396, with which it interacts (16). O1 has coordination with metal (I), as does O2, which equally coordinates to metal (II) (28). The phosphoryl oxygens make hydrogen bond contacts with the amide hydrogens of Ala38, Ser39, and Ser375, as well as with the side chains of His159 and Arg374 (16, 28). Serine 39 and histidine 159 are both located in mobile loops (see Figure 1.3). The C-3 OH^- group is 3.0Å away from the NE2 atom on His373, 2.3Å away from OE2 on Glu168, and 2.4Å away from OE2 on Glu211 (16). This cluster (Glu168/Glu211/His373) functions in the second step of the reaction, where it is in close proximity to the leaving OH^- group. The proposed catalytic base, Lys345, has its side chain N atom situated 3.5Å away from the C-2 proton (16), where it can catalyze the latter's abstraction. Metal (II) coordinates to a substrate/product phosphoryl oxygen, two water molecules, as well as to both the carbonyl and hydroxyl oxygens of Ser39 from the active site loop (28). The binding of metal (II) in close proximity to the substrate phosphate group serves an important catalytic purpose. The additional positive charge on PO_4^{3-} leads to electron withdrawal from C-2, and thus facilitates proton abstraction at this position. Detailed schemes for the coordination of substrate/product and metals are shown in Figures 1.13 and 1.14.

1.3.5 Significance of loop movements

Binding of catalytic metal ion is accompanied by large movements of the loops Pro35-His43 (from the small domain), Val153-Phe169 (the most mobile part of which is Ser158-Gly162), and Ser247-Gly275 (the most mobile part of which is Asp255-Asn266). The active site loop is hinged in part by Gly37 and Gly41. These allow Ser39 to rotate into a position where its carbonyl and hydroxyl oxygens can coordinate with metal (II). Site-

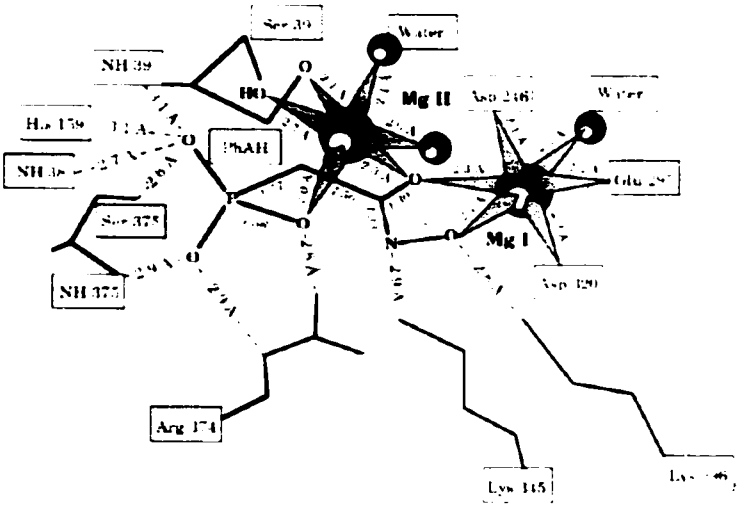

Figure 1.13 Coordination scheme of metals (I) & (II). Water molecules are shown as dark spheres (28). The coordination of both Mg^{2+} ions to both of the substrate/product carbonyl oxygens suggests an important role for the metals in stabilizing the negative charges in the carbanion intermediate (24).

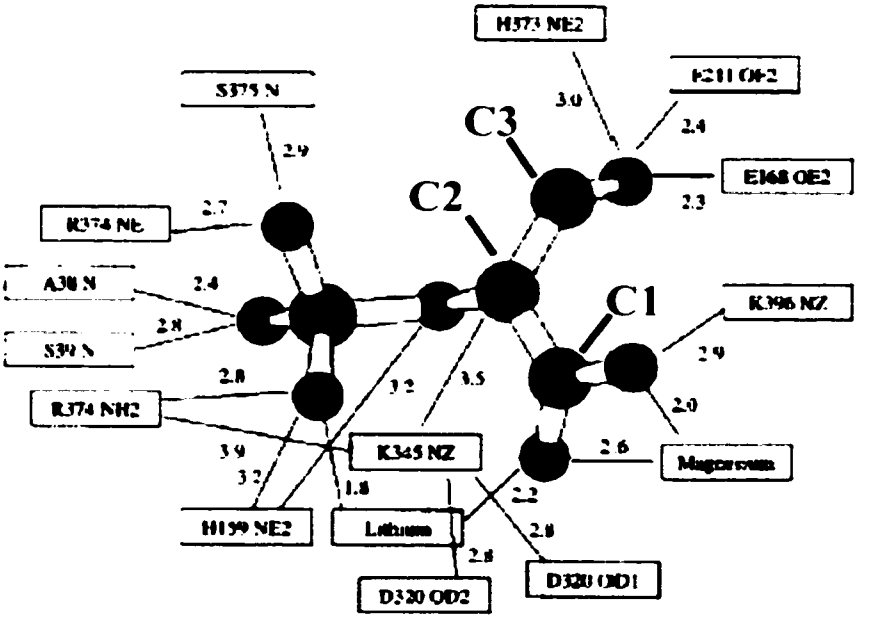

Figure 1.14 Coordination environment of 2-PGA (16). Distances are shown in Å. The substrate carbons have been highlighted.

directed mutagenesis on these positions, converting glycines to valines, has resulted in near complete loss of activity, probably due to the loop's inability to properly close (Padovani and Kornblatt, unpublished data). This demonstrates the importance of the loop closure for catalysis, and the importance of glycine in allowing room for this loop flexibility. The chelation of metal (II) to Ser39 effectively closes off the active site. Analogous loops have been studied in various other proteins, including triosephosphate isomerase (32). The loop closure in TIM may have a similar function as that in enolase. Its closure over the active site may function in protecting the reactive carbanion intermediate from solvent and electrophiles such as molecular oxygen. The loop movements in enolase are accompanied by spectral changes, due to their aromatic content, and by changes in dimer stability, due to their contributions at the subunit interface. Loops have been directly implicated in the occurrence of inactive enolase monomers (30, 37), which brings our discussion to a particularly interesting area of research on enolase.

1.4 Subunit dissociation

It long has been observed that monomers of enolase are inactive. However, each monomer possesses one completely contained active site, no part of which appears to be shared with that of the other subunit. The active site, not being formed as a result of dimerization, as is the case for certain enzymes (31), exists independently of the dimer interface and of the other monomer's active site. The question, then, of why dimerization is a prerequisite for activity in enolase is one that has prompted much attention.

Various studies have been carried out, using a number of different methods to dissociate the enolase dimer. Initially, the majority of the subunit interactions were thought

to be hydrophobic in nature (71). However, this was prior to crystallization of the enzyme, which revealed the enrichment in charged/polar residues at the dimer interface. These render the dissociation/association of the protein sensitive to solvent ionic strength.

Brewer & Weber in 1968 (72) showed that yeast enolase subunits dissociated in the absence of Mg^{2+}, in an excess of EDTA and high ionic strength (1 M KCl), are largely inactive, retaining only ~17% of their catalytic ability. The lack of bound Mg^{2+} equally resulted in loss of activity (~50-85%) at low protein concentrations (nM range), even when not pre-incubated with high KCl, as the enzyme dissociates more readily in the absence of magnesium (72). The presence of 1 M KCl, which increases the subunit K_d by ~3 orders of magnitude, did not irreversibly inactivate the enzyme in the presence of excess Mg^{2+}, although a faster rate of recovery was observed in lower ionic strength (72). The complete reversibility of the dissociation process was shown; one could therefore view the protein as existing in a state of equilibrium between monomers and dimers, with K_{eq} shifting to one or the other depending on the surrounding solvent conditions (72). Mg^{2+}, in effect, lowers the subunit dissociation constant, driving the equilibrium in favor of the dimeric form (72). The presence of 1 M KOAc was found to have a similar stabilizing effect on the enzyme's dimeric state, failing to facilitate inactivation as does an equal amount of KCl (72, 73). The associating effect of Mg^{2+}, even in high salt, was attributed to the reduction of anion binding sites when metal was bound at the active site, which was consistent with the idea that Mg^{2+} produces a more tight or compact protein structure in enolase (74). It was also suggested that the loss of activity observed in the absence of metal cofactor was due to an effect on substrate binding, presumably affecting the latter in an adverse manner (72).

Important dissociation studies have also been carried out using hydrostatic pressure as a tool to characterize the process (37, 71, 75, 76, 77). It is viewed as a relatively mild way of bringing about dissociation, and is fully reversible (77). It functions by altering the hydration state of molecular surfaces (77). Temperature has also been utilized in the study of subunit dissociation (78, 79). Differential scanning calorimetric studies have shown that the first step in the denaturation process is the dissociation of the dimer into its monomeric subunits (40). The effect of $NaClO_4$, a Hofmeister series anionic/chaotropic salt, has also been investigated (30, 80). In most cases, the monomers prepared using these techniques have been inactive, but there have been exceptions. For example, Keresztes-Nagy & Orman in 1971 (78) used temperature and low protein concentrations to dissociate the enzyme. The enzyme dissociated between 35-40°C, even while in the presence of cofactor and substrate, at enolase concentrations of less than 1 μg/ml (78). The monomers isolated in this manner were found to be active! One explanation for this occurrence is that the presence of Mg^{2+} maintains both active site structure and loop conformation, all of which are crucial for catalysis. The maintenance of specific loop conformations/movements in order for catalysis to take place normally has been discussed previously (see Section 1.3.5). A detailed coordination scheme for Mg^{2+} with both active site and loop residues also has been described (see Section 1.3.4). In addition to these, residues directly coordinated to Mg^{2+} interact with other residues in close proximity with loop regions: Asp246 forms a hydrogen bond with the backbone N of Asp248; Glu295 interacts with Lys396, and Asp320 interacts with Lys345, a proposed enzymic base (37). Each of these residues is situated near the beginning of a loop (37). Lys396 is close to the 398-403 loop, which is directly involved in subunit

interactions (37). There is, therefore, a very intricate pattern of interaction between bound Mg^{2+} and loop residues. Preparing active monomers has, therefore, posed a unique challenge. The very act of dissociating the dimer disrupts the loop conformations, which, in turn, disrupts active site structure. This results in the loss of bound Mg^{2+} at the active site, due to disruption of its coordination network with loop and active site residues. With the loss of Mg^{2+}, therefore, comes the loss of activity.

The importance of the dimer-catalysis relationship cannot be underestimated. The loop region conformations play a critical role in maintaining both. This brings us to the focal point of this discussion.

1.5 Current project

1.5.1 Thesis premise

The loops are crucial in maintaining both subunit interactions and active site architecture. They contribute residues to both the dimer interface and the site of catalysis, and play an important role in coordinating the catalytic metal ion for proper orientation at the active site. Loop structure disruption due to subunit dissociation would lead to changes in the intricate coordination scheme involved in the proper positioning of the various active site residues (see Section 1.4), and would, therefore, lead to loss of catalytic ability. One loop (Pro35-Gly60) extends all the way from the active site to the subunit interface; a smaller portion of this loop (Pro35-His43) has a crucial role to play in ensuring the closed conformation necessary for catalysis. Its particular importance in the link between dimerization and catalysis is emphasized in the present work. Its conformation would not only directly affect subunit contacts, but also active site structure and proper ligand

coordination. When the dimer is disrupted, this may conceivably lead to changes in the loop's conformation. These, in turn, lead to longer-range disruptions at the active site. The involvement of other loop residues, directly or indirectly, in the active site would result in their subsequent disruption, eventually leading to loss of Mg^{2+} due to improper coordination. This ultimately results in the loss of activity. Thus, it is postulated here that the prerequisite of dimerization for catalysis is directly mediated by the Pro35-Gly60 loop, and that all other effects of dissociation on the protein are a result of its disruption.

1.5.2 Research approach

In order to verify this postulate, the protein would have to be dissociated, or the dimer association weakened in some manner, and the effects on both structure and catalysis studied. The change would have to involve not only a subunit contact, and, therefore, a residue involved in subunit contacts, but also one which is directly involved with the Pro35-Gly60 loop.

The approach adopted to effect this change is site-directed mutagenesis. A hydrogen bond at the subunit interface became the target of this work. A glutamic acid residue at position 188 hydrogen bonds to the backbone of a tryptophan at position 56 of the opposing monomer. The interaction involves a carboxyl oxygen on E188 and the backbone N atom of Trp56, which orients its side chain into its own monomer. A depiction of this interaction is shown in Figure 1.15. Weakening this subunit contact would, therefore, be the best approach for targeting both dissociation and loop conformation. Trp56 was, therefore, changed to a phenylalanine. The change is conservative, maintaining both hydrophobicity and steric bulk at this position. The substitution was not expected to significantly weaken

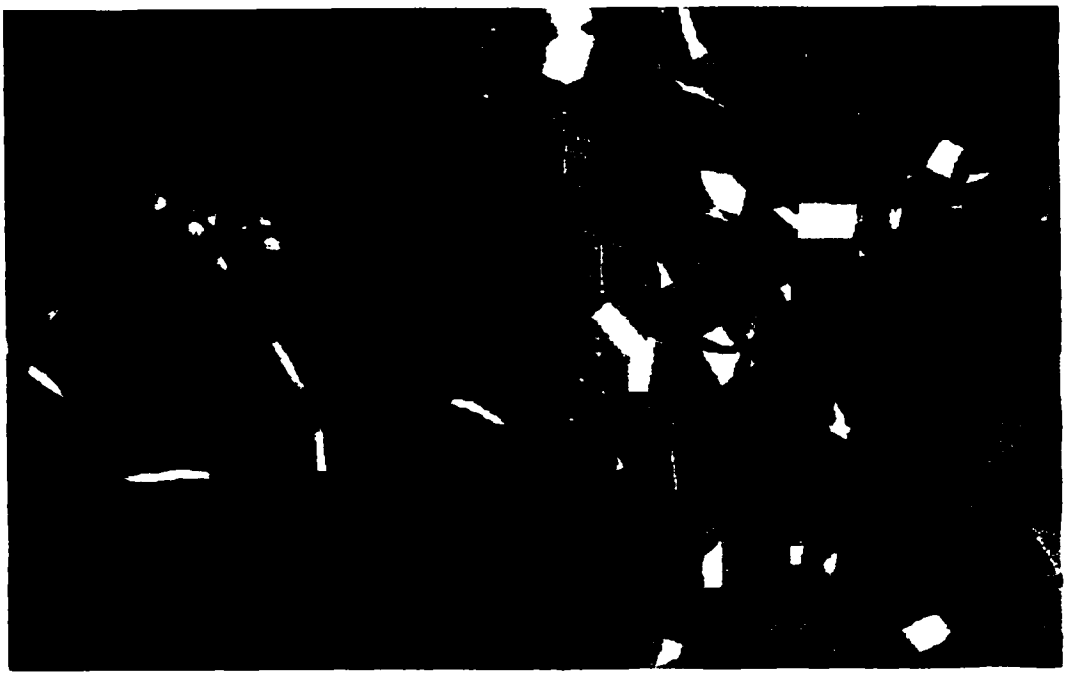

Figure 1.15 Subunit interface H-bond between Trp56 and E188. A close-up view of the H-bond between OE1 of E188 and N of W56 (see Table 1.3). Trp56 orients its side chain within its own monomer, the interaction involving its amino backbone moiety. Trp56 is shown in purple, E188 is shown in orange. The Pro35-Gly60 loop is outlined in yellow, to emphasize its trajectory over the active site (seen with bound 2-PGA (red)), and extending to the subunit interface. The position of Trp56 within this loop is clear. (Image generated using Rasmol, version 2.6, and the crystal structure deposited as 1one.pdb).

or affect the hydrogen bond, since Phe would equally be capable of participating in the interaction through its own backbone amino moiety. This is, of course, assuming that Phe will orient itself in the same manner as does Trp at this position. The side chain of Phe would not be capable of participating in any further potential hydrogen bond contacts within its monomer, as is possible for the indole ring on Trp. A mutation was also introduced at

position 188. The glutamic acid residue was replaced by an aspartic acid residue. This, again, is a rather conservative substitution, except for the fact that the Asp side chain is one methylene group shorter than that of Glu. This substitution, as a result, was expected to have a more significant weakening effect on the targeted hydrogen bond. Results, as we will discover, were both interesting and surprising.

1.5.3 Project goals

Certain goals were set for the current project, and these were as follows:

A) The enolase that would be used for this study is that from yeast. To begin, a purification scheme for recombinant yeast enolase would have to be outlined. The work previously carried out on yeast enolase in our laboratory had involved that obtained from a commercial source. In order to carry out site-directed mutagenesis and manipulate the yeast enolase gene, it would be necessary to work with recombinant yeast enzyme. A protocol for purifying the native and variant proteins would thus need to be devised and optimized.

B) The specific mutations described in section 1.5.2 would have to be prepared using the polymerase chain reaction.

C) The mutants would have to be characterized both structurally and catalytically, in order to determine in what respects and to what extent these substitutions had affected the protein. An effect on structure and function would point to the importance of the Pro35-Gly60 loop.

Chapter 2: Materials and Methods

2.1 Materials

2.1.1 Site-directed mutagenesis

Cloned *Pfu* DNA polymerase (2.5 U/μL) and 10X cloned *Pfu* buffer were purchased from Stratagene. Oligonucleotides were synthesized and obtained from BioCorp Inc. (Montreal). These had the following coding strand sequences:

W56F: 5'-GGT-GAC-AAA-**TCG**[1]-AAG-**TTC**[2]-ATG-GGT-AAG-GGT-GTT-3'

E188D: 5'-GCT-GAA-GCT-TTG-**CGT**[3]-ATT-GGT-TCC-**GAT**[4]-GTT-TAC-CAC-AAC-3'.

A 10 mM nucleotide mixture of dNTPs (2.5 mM each dNTP) was from Boehringer Mannheim Corp. Recombinant yeast enolase DNA had previously been ligated into the pET-3a vector polycloning site, between the *Nde*I and *Bam*HI restriction sites, by Isabelle Rajotte. pET-3a is a Novagen product, but was graciously supplied by Dr. Elizabeth Cadieux (Concordia University, Montreal).

---

[1] Silent mutation removing a restriction site for the enzyme *Bst*XI.

[2] Codon changed from TGG, resulting in Phe instead of Trp.

[3] Silent mutation removing a restriction site for the enzyme *Xmn*I.

[4] Codon changed from GAA, resulting in Asp instead of Glu.

2.1.2 Bacterial growth media

Tryptone (bacteriological grade), and agar were from Difco. Yeast extract powder was from Fisher Scientific. M9 salts consisted of 90 mM Na_2HPO_4, ~9 mM NaCl (biological grade), ~20 mM NH_4Cl, and ~20 mM KH_2PO_4. Unless specified otherwise, salts were A.C.S. grade. Lactose (A.C.S. certified), and ampicillin (sodium salt, BioTech grade) were from Fisher Scientific. Ampicillin was typically kept as a 100 mg/ml stock solution, having been filter sterilized through a 0.45 μm Nalgene syringe filter, and stored at -20°C. Solutions of M9 salts were prepared as 5X concentrates and autoclaved, as recommended by Sambrook *et al.* (81).

2.1.3 Bacterial strains

XL1-Blue *E. coli* was utilized for long-term storage at -86°C of pET-3a vector, containing wild type and variant forms of the yeast enolase gene insert. This strain was used for DNA manipulations involving site-directed mutagenesis. BL21(DE3) *E. coli* was used for cellular expression of the yeast recombinant proteins.

2.1.4 Extraction of DNA

Dextrose (A.C.S. grade) was from Fisher Scientific. RNAse A (from bovine pancreas) and PEG 8000 were purchased from Boehringer Mannheim. RNAse A was prepared as a 10 mg/ml solution and heat inactivated according to Sambrook *et al.* (81). PEG 8000 was prepared as a 30% stock. Both were kept frozen at -20°C. TE buffer was used to resuspend final DNA pellets, and was prepared as described by Sambrook *et al.* (81).

2.1.5 Restriction digestion

*Bam*HI (10 U/μl), *Nde*I (10 U/μl), and *Dpn*I (10 U/μl) were from Promega. *Bst*XI

(10 U/μl) was from MBI Fermentas, and *Xmn*I (20 U/μl) was from New England Biolabs. Corresponding optimal digest buffers were supplied for each restriction enzyme upon purchase, as was a 100 mg/ml solution of acetylated BSA.

2.1.6 Agarose gels

Agarose (genetic technology grade) was from ICN, and was prepared in TAE buffer upon gel casting. TAE was kept as a 50X stock solution at room temperature, as recommended by Sambrook *et al.* (81). DNA markers (*Eco*RI/*Hind*III λ-DNA digest, 500 μg/ml) were from Promega. Samples were mixed with loading dye, which was prepared as a 6X solution, and stored at 4°C. Sucrose and bromophenol blue were A.C.S certified from Fisher Scientific.

2.1.7 Glycerol stocks

Glycerin (A.C.S. certified) was from Fisher Scientific, and was kept sterile for cryogenic storage of wild type and mutant-containing pET-3a vector.

2.1.8 Cell lysate preparation

Phospho-glycolic acid, a 2-PGA substrate analogue (tri(monocyclohexyl-ammonium)salt dessicate) was from Sigma, and was kept as a 100 mM stock solution at -20°C. DNAse I (from bovine pancreas) was from Roche Molecular Biochemicals, and RNAse (from bovine pancreas) was from Boehringer Mannheim. $(NH_4)_2SO_4$ used for fractionation and purified protein storage was Ultra Pure from ICN.

2.1.9 Buffers

Trizma base (Ultra Pure grade) was from ICN. MES was from Boehringer Mannheim. $Mg(OAc)_2$ and $MnCl_2$ were A.C.S. grade from Fisher Scientific, as was

imidazole. EDTA (disodium salt dihydrate) was from Fluka, as was NaOAc (puriss., trihydrate).

2.1.10 SDS-PAGE

SDS was from Fluka, and was kept at room temperature as a 10% solution. Acrylamide (99.9%) was prepared as a 30% solution stored at 4°C, and APS (electrophoresis purity reagent) was stored at -20°C as a 10% stock solution. Both were from Bio-Rad. TEMED (electrophoresis grade) was from ICN, and glycine (tissue culture grade) was from Fisher Scientific. Bis-acrylamide (97%) was from BDH. SDS-PAGE standards (low range, 14,400-97,400) were from Bio-Rad. Coomassie brilliant blue R and 2-mercaptoethanol were from Sigma.

2.1.11 Commercial enolase and substrates

Lyophilized commercial yeast enolase (phosphoenolpyruvate hydratase, EC 4.2.1.11, 30% salt) was from Sigma, as was 2-PGA (D (+) 2-phosphoglyceric acid, sodium salt hydrate). Sigma 2-PGA was used for determinations of activity which did not necessitate metal-free conditions. Metal-free activity measurements were carried out using 2-PGA (trisodium salt crystallized) from Boehringer Mannheim. Both substrates were kept frozen at -20°C as 100 mM stock solutions.

2.1.12 $NaClO_4$ incubations

$NaClO_4$ (99%, A.C.S. grade) was from Aldrich. A 4.0 M stock solution was typically prepared and stored at room temperature.

2.1.13 Chelating reagents

Chelex 100 resin (sodium form, analytical grade) was from Bio-Rad, and nitric acid

(trace metal grade) was from Fisher Scientific.

2.1.14 Substrate determinations

NADH (grade 1, ca.100%, disodium salt), PK-L-LDH (from rabbit muscle), and ADP (monopotassium salt crystallized) were from Boehringer Mannheim. ADP (17.3 mg/ml) and NADH (3.6 mg/ml) solutions were prepared fresh each time.

2.2 Methods

2.2.1 DNA extraction

Plasmid DNA was extracted according to the alkaline lysis method (82). Suspension buffer (25 mM Tris-HCl (pH 7.5), 10 mM EDTA, 1% glucose, 50 μg/ml RNAse A) was prepared as recommended by Sambrook *et al.* (81), as was TE buffer for final DNA pellet resuspension. DNA sample concentration and purity were determined on the basis of OD_{260nm} and OD_{280nm} (81, 83).

2.2.2 Oligonucleotide synthesis

Primers were designed using the PC Gene software. Silent mutations and amino acid substitutions were introduced keeping *E. coli* codon usage statistics in mind (83). Oligonucleotides were synthesized by BioCorp Inc. (Montreal), and received in lyophilized form. Each was resuspended in 250 μl of sterile dH_2O and quantitated on the basis of $OD_{260\ nm}$, as described (83).

2.2.3 Site-directed mutagenesis

Site-directed mutagenesis was carried out by the QuickChange method (Stratagene). Briefly, 200 ng of double-stranded parental DNA were mixed with 250 ng of each complementary oligonucleotide. Each dNTP (50 μM) was added to cloned *Pfu* buffer and

sterile dH_2O, in a total reaction volume of 100 μl. Reactions were overlaid with 30 μl of mineral oil, and heated to 95°C. Cloned *Pfu* DNA polymerase (5.0 Units) were added to each, and PCR commenced. A total of 16 PCR cycles were performed in an Eppendorf Master Gradient Thermal Cycler at the following parameters:

1) Denaturation: 30 seconds at 95°C; 2) primer annealing: 1 minute at 54°C[5]; 3) primer extension: 14 minutes at 72°C[6]. Methylated and hemi-methylated parental DNA was then digested with 10 Units of *Dpn*I (1 hour, 37°C).

PCR products were transformed into XL1-Blue *E. coli* competent cells. Briefly, DNA of interest is incubated on ice for 40 minutes in the presence of the desired competent cells. Cells are grown for 1½ hours (37°C, 225 RPM) in LB medium following a 1½ minute heat shock at 42°C. Cultures were plated on LB agar (15 mg/ml) containing 100 μg/ml ampicillin for pET-3a vector selection, and grown overnight at 37°C. Six colonies per plate were picked the following day, and overnight LB liquid cultures (5 ml) were inoculated and grown as specified above. The DNA was extracted the next day as described in Section 2.2.1.

All DNA samples were double-digested with 10 Units of *Nde*I and *Bam*HI restriction enzymes. To screen for W56F, DNA was digested with 10 Units of *Bst*XI, and E188D with 20 Units of *Xmn*I. Parental DNA was also digested with *Bst*XI or *Xmn*I, for comparative purposes. All digests were at 37°C for 1 hour. Digests with *Nde*I, *Bam*HI, and *Xmn*I were

---

[5] Annealing temperature was chosen based on the results of a preliminary experiment in which a gradient of temperatures were tested.

[6] 2 minutes of extension time were allowed for each kb of plasmid/gene insert length.

supplemented with 0.1 mg/ml of acetylated BSA, as this was not a component of the supplied buffer system. Following digestion, samples were mixed with loading dye (40% sucrose, and 0.25% bromophenol blue), and loaded onto agarose gels. Both digested and undigested/uncut DNA samples were separated by electrophoresis. Agarose (1%) was prepared in TAE buffer (40 mM Tris, 20 mM acetic acid, and 1 mM EDTA), and electrophoresis was carried out for 1½-2 hours at 100 Volts. Staining took place in dilute (0.1 mg/ml) ethidium bromide (30 minutes) prior to visualization under UV-transillumination.

Mutant DNA samples were re-transformed into XL1-Blue *E. coli* competent cells. Overnight cultures were grown from the colonies, and glycerol stocks prepared the following day. Two stocks of each mutant were prepared in sterile cryogenic vials by mixing 1.7 ml of each respective bacterial culture with 0.3 ml of sterile glycerol (15%). Samples were well mixed and stored at -86°C.

2.2.4 Variant sequencing

Sequencing was carried out in the facilities of Bio S&T Inc. (Lachine, Quebec). Sequences obtained were aligned with parental DNA to ensure that the desired mutations had been introduced, and to verify that there were no additional mutations.

2.2.5 Recombinant protein expression

Wild type and variant proteins were over-expressed by the method described in Poyner *et al.* (47). DNA was transformed into BL21(DE3) *E. coli* competent cells, as described in Section 2.2.3. Colonies were picked and suspended in 5.0 ml of LB broth. The bacterial suspension was diluted 200-fold into LB medium supplemented with M9 salts, and

400 μg/ml of ampicillin. Cells were grown as described in Section 2.2.3 to an OD_{600nm} of approximately 0.5. This density was typically achieved after 2½-3½ hours of growth. Induction was then carried out by diluting the cells 100-fold into fresh growth medium supplemented with 1.6% lactose. Cells were grown in the presence of lactose overnight (12-14 hours) as specified, and harvested the next day by centrifugation (5400 g, 10 minutes) at 4°C in a Beckman J2-HS centrifuge (JA-10 rotor). The wet cell paste was weighed and stored at -20°C. Four liters of bacterial culture yielded, on average, 30 grams of wet cell paste.

2.2.6 Cell lysate preparation/protein isolation

The cell paste was resuspended in 60 ml of 50 mM Tris (pH 7.4)/1 mM $Mg(OAc)_2$/0.1 mM EDTA, and treated with ~1 mg of DNAse I and ~1 mg of RNAse. Phospho-glycolic acid, a substrate analogue, was added to the extract to a 1 mM final concentration. Cells were lysed on ice by sonication using a Branson 250 Sonifier. Six 30-second bursts were carried out per 10 grams of wet cell paste, with a 1 minute cooling period between bursts. The pH was adjusted to 7.4 using 1 M Tris, and the extract centrifuged at 4°C (20,000 g, 30 minutes). This was followed by a second centrifugation in a Beckman L5-50B ultracentrifuge at 4°C (125,000 g, 1 hour) (Ti-45 rotor). The supernatant was collected and brought to 40% $(NH_4)_2SO_4$ saturation. Contaminating proteins were collected and discarded after centrifuging as above at 4°C (20,000 g, 30 minutes). A second fractionation was carried out to 85% $(NH_4)_2SO_4$ saturation. Enolase was collected in the pellet following centrifugation. The final pellet was resuspended in 6.0 ml of the starting Tris buffer, and $(NH_4)_2SO_4$ removed by dialysis overnight against two 100-fold volume

changes of the same buffer. The extract was centrifuged to remove precipitated material, and loaded onto a 200 ml Q-Sepharose Fast Flow (Amersham) anion exchange column equilibrated in 50 mM Tris (pH 7.4)/1 mM $Mg(OAc)_2$/0.1 mM EDTA. The column was washed until no further elution of non-binding and weakly-binding proteins was observed. This typically necessitated 80 ml of wash buffer. Enolase was then eluted in a 0-0.5 M NaCl linear gradient. Fractions were collected for 10 minutes at a flow rate of approximately 0.5 ml/minute. Each was analyzed by measuring OD_{260nm} and OD_{280nm} as well as by assaying for enolase activity. Aliquots (10 μl) were also separated on SDS-PAGE. An osmolarity reading was measured for fractions containing enolase, using a Vapro Vapor Pressure Osmometer (model 5520, Mandel Scientific). Fractions were pooled based on their enolase content and purity, as assessed by calculating the ratio OD_{280nm}/OD_{260nm} and a rough estimate of specific activity. The enolase pool was precipitated in 4.23 M $(NH_4)_2SO_4$ and centrifuged. The pellet was resuspended in 3.0 ml of 20 mM MES (pH 6.0)/2 mM $Mg(OAc)_2$/0.2 mM EDTA. $(NH_4)_2SO_4$ was removed by dialysis versus two 100-fold volume changes of the same buffer. The next morning, the sample was centrifuged and loaded onto a 20 ml CM-Sepharose Fast Flow (Amersham) cation exchange column equilibrated in 20 mM MES (pH 6.0)/2 mM $Mg(OAc)_2$/0.2 mM EDTA. The column was washed with 50 ml of the equilibration buffer to remove all non-interacting and weakly-interacting proteins. Fractions were collected for 10 minutes at a 0.2 ml/minute flow-rate. Enolase was eluted by applying a 0-0.25 M KCl linear gradient. Fractions were analyzed and pooled as described. Enolase was precipitated in 4.23 M $(NH_4)_2SO_4$ and stored at 4°C as a precipitate. Throughout the course of the purification, aliquots of the samples corresponding to the

various stages of the process were saved. These were assayed for activity and for protein content, in order to monitor the progress achieved after each step. An aliquot of each was routinely electrophoresed on a 12% SDS-PAGE to assess the purity of the final enolase sample.

2.2.7 *E. coli* enolase control

A control experiment involved purification of BL21(DE3) cells not transformed with pET-3a vector, but grown in the same conditions as outlined for actual recombinant protein expression. Cells were lysed and chromatographed on Q-Sepharose as described in section 2.2.6.

2.2.8 SDS-PAGE

12% SDS gels were prepared and electrophoresed according to methods described by Laemmli (84).

2.2.9 Desalting proteins

Recombinant and commercial proteins were desalted using one of two available methods: 1) Dialysis, or 2) Nap-5 Sephadex column. BioDesign Inc. dialysis membranes were re-hydrated and stored at 4 °C in a solution of 10 mM EDTA. Dialyses were routinely carried out in the cold over a 12-14 hour period, with 2-3 buffer changes of 100 volumes each. Where appropriate, a Nap-5 column/Sephadex G-25 (DNA grade) from Pharmacia Biotech was used. The column was equilibrated with an excess of the desired buffer, and protein samples diluted in the same buffer.

2.2.10 Spectroscopic work

All spectroscopic work was carried out in 50 mM Tris (pH 7.4)/0.1 mM EDTA/

0.3 M NaOAc (+/- Mg^{2+}, +/- 2-PGA) at 20°C. The various techniques used are listed.

1) UV-visible/4th-derivative spectroscopy: Spectra were collected on a Varian Cary 1 UV-visible spectrophotometer (in 1 cm/1 ml capacity rectangular quartz cuvettes) using the following parameters: 260-305 nm range, average time 1.0 second, 0.1 nm data interval, 6.0 nm/minute scan rate, and 1.0 nm spectral bandwidth. These parameters are as suggested by Lange *et al.* (85). One single collection was carried out. The protein concentration was ~ 1 mg/ml (10.6 μM). Buffer solutions were scanned and treated in an identical manner. Samples were scanned and the baseline subtracted using the Cary WinUV software. Fourth derivatives were calculated using the equation described by Lange *et al.* (85). Peak-to-trough (r) ratios were calculated using the equation $[(A_{283nm}-A_{287nm})/(A_{291nm}-A_{295nm})]$, as described (85, 86).

2) Far-UV circular dichroic spectroscopy: Protein peptide bond signals were monitored on a Jasco 710 spectropolarimeter under continuous N_2 gas flow (3 L/hour). Spectra were collected in 0.01 cm rectangular quartz cuvettes as follows: 180-260 nm range, 0.2 nm step resolution, 50 nm/minute scan speed, 0.25 second response time, 1.0 nm bandwidth, and 15 accumulations. The protein concentration was ~1 mg/ml (10.6 μM). Spectra and baselines were subtracted using the Jasco standard analysis software.

3) Near-UV circular dichroic spectroscopy: Aromatic residue signals were monitored on the same instrument, and spectra collected in 1.0 cm rectangular quartz cuvettes (3 ml) at the following parameters: 260-360 nm range, 0.2 nm step resolution, 50 nm/minute scan speed, 0.25 second response time, 1.0 nm bandwidth, and 15 accumulations. Protein concentrations and standard spectra analysis were as above (see Far-UV CD).

4) Fluorescence spectroscopy: Fluorescence signals were monitored on an SLM-2 Aminco Bowman Luminescence spectrophotometer in 1.0 cm/3.0 ml capacity quartz cuvettes at the following parameters: 870 Volts, 300-350 nm range, λ_{ex}=280 nm (2 nm slit), λ_{em}=335 nm (2 nm slit), and 1.0 nm/second scan rate. Protein concentrations were ~0.1 mg/ml (1.06 μM).

All buffer samples were scanned in an identical manner and spectra subtracted using the appropriate software.

2.2.11 Analytical ultracentrifugation

Sedimentation velocity experiments were carried out in a Beckman Optima XL-I analytical ultracentrifuge in 1.2 cm double-sectored cells with quartz windows. Scans were collected at 20 minute intervals on 400 μl samples at 280 nm. Four scans were averaged. Protein concentrations were ~ 1 mg/ml (10.6 μM). Samples were centrifuged at a rotor speed of 42,000 RPM at 20°C. The buffer system was as described in section 2.2.10. NaOAc was present to counteract the primary charge effect phenomenon described by Ralston (87). Reference samples were identical to protein samples in buffer composition, and these were run in tandem. Prior to sedimentation, samples were routinely filtered through 2.0 ml Spin-X Costar filter tubes (0.45 μm) by centrifuging in a microcentrifuge at 13,000 RPM for a few seconds to remove particulate matter. This eventually became routine in preparation for all spectroscopic analysis. Samples were analyzed using DCDT+ (version 1.15) (Philo/VideoSoft 1995). Sedimentation coefficient values ($S_{20,w}$) were corrected for buffer density and viscosity, which were calculated with SedNTerp (version 1.06, 2001) where applicable. Buffer density and viscosity due to $NaClO_4$ and NaOAc were

taken from standard curves prepared from experimental measurements (M.J. Kornblatt, personal communication).

2.2.12 Temperature denaturation

Loss of secondary structure was monitored in the far-UV region on the Jasco 710 spectropolarimeter. The α-helix content was measured as a function of temperature in 0.1 cm quartz circular jacketed CD cells as follows: 222 nm, 20-80°C temperature range, 0.5°C/minute heating rate, 0.2°C step, 1 second response time, and 1.0 nm bandwidth. Protein concentration was ~ 1 mg/ml (10.6 μM). 200 μl samples were prepared in 50 mM MES (pH 7.4)/0.1 mM EDTA/0.3 M NaOAc +/- 1 mM Mg^{2+}.

2.2.13 Activity assays

Enolase activity was assayed by monitoring the production of PEP at 240 nm on the Varian Cary 1 UV-visible spectrophotometer in 1.0 cm quartz cuvettes. Assays were carried out at 20°C in enolase assay buffer (50 mM Imidazole (pH 7.1)/1 mM $Mg(OAc)_2$/0.1 mM EDTA/250 mM KCl and 1 mM 2-PGA). The assays were begun by addition of enzyme. The quantity of enzyme which would produce an optimal slope of ~ 0.1Δ absorbance/minute was determined empirically for each protein under the various conditions. For the $NaClO_4$ inactivation experiments (see Section 2.2.15 below), only the first 30 seconds of the assay were used in the analysis, as the enzyme slowly reactivates under the assay conditions. $NaClO_4$ incubations (see section 2.2.15) were assayed in duplicates and rates compared to that of each corresponding enzyme in 300 mM NaOAc (*i.e.*, no perchlorate).

2.2.14 Protein determinations

Protein content was determined using the Bradford method (88). The dye reagent

concentrate of Coomassie Blue was from Bio-Rad. Rough estimates were obtained using lyophilized BSA (Sigma) as a standard protein, in the range of 2-8 μg. More precise estimates were measured using wild type recombinant enolase as the standard within the same range. For spectroscopic work, protein concentration was determined at 280 nm using the molar extinction coefficient of 0.895 ml/mg/cm (6). ε_{280nm} was determined for W56F according to the near UV-absorbance method (88).

2.2.15 $NaClO_4$ incubations

Incubations were prepared maintaining constant protein concentration (1 mg/ml, 10.6 μM) and constant ionic strength (300 mM Na^+) in 50 mM Tris (pH 7.4)/0.1 mM EDTA +/- 1 mM Mg^{2+}. [ClO_4^-] was varied, and [OAc^-] adjusted accordingly. Wild type samples were prepared in 25 mM $NaClO_4$ increments to a final [ClO_4^-] of 300 mM, whereas mutant samples were prepared in 10 mM $NaClO_4$ increments to a final [ClO_4^-] of 150 mM. This was based on previous experiments, which revealed the dissociation range of each protein. Samples were incubated at 20°C for a minimum of 14 hours and subsequently assayed for activity (as in Section 2.2.13), scanned (as in Section 2.2.10), and/or sedimented in the AUC (as in Section 2.2.11).

2.2.16 Dissociation constants

K_d values were calculated at each [$NaClO_4$] using the equation

$$K_d = 4(f_m)^2\,[\text{enolase}]/f_D \quad (30, 37),$$

where f_m and f_D represent fraction of enolase monomeric and dimeric, respectively, and [enolase] is the concentration of enzyme used. Calculations were performed using activity, fourth-derivative, and sedimentation ($S_{20,w}$) data. Activity data were analyzed assuming that

dimers are active and monomers are not. The dimeric r-value for each protein was taken as that of each respective protein in the presence of 1 mM Mg^{2+}; the monomeric r-value for each was taken as that of each respective protein in high [$NaClO_4$], *i.e.*, 300 mM for wild type, and 150 mM for mutants. $S_{20,w}$ values for dimers and monomers were assumed to be identical for wild type and mutants. These were determined with wild type enzyme in 0 mM and 300 mM $NaClO_4$, respectively. A plot of $\ln K_d$ versus [$NaClO_4$] was prepared for each protein in the various conditions, and K_d extrapolated to 0 mM $NaClO_4$. $\Delta G_{(H2O)}$ was also calculated for each (89).

2.2.17 Metal-free experiments

When metal-free conditions were necessary, special procedures were utilized. All required buffers and reagents were passed through a 15 ml column of Chelex 100 resin. Plastic containers were used instead of glass, and these were soaked in a solution of 20% nitric acid for 1 hour, and then rinsed exhaustively in deionized water. Cuvettes were typically soaked overnight. Deionized water and methanol for drying cuvettes were considered metal-free.

2.2.18 Quantitation of 2-PGA

Solutions of 2-PGA were quantitated in enolase assay buffer containing 250 μM NADH, using 1 μg wild type recombinant yeast enolase. An end-point analysis using a coupled assay with pyruvate kinase and lactate dehydrogenase was performed in a 1.0 cm quartz cuvette. The assay monitored the disappearance of NADH at 340 nm in the conversion of PEP to pyruvate, which was then converted to lactate. The concentration of 2-PGA present is equal to that of the NADH used. This was calculated using $\varepsilon_{340nm(NADH)}$ of

6150 M^{-1}-cm^{-1}.

2.2.19 Kinetics

Kinetics were performed in 1.0 cm quartz cuvettes at 240 nm in 50 mM MES/50 mM Tris (pH 7.1). For experiments varying [metals], 1 mM 2-PGA (Boehringer Mannheim) was used. Stock solutions of $Mg(OAc)_2$ (0.1, 1.0, 10, 100, and 200 mM) and $MnCl_2$ (0.1, 1.0, 10, and 20 mM) were prepared and stored at -20°C. Kinetics varying [2-PGA] were in 1 mM $Mg(OAc)_2$. All assays were performed in duplicate, as was each kinetic experiment. Kinetics versus metal cofactors were analyzed on EnzFitter (BioSoft, version 1.05) using the equation for substrate inhibition, $v = (V_{max} * [S])/(K_m + [S] + ([S] * [S]/K_i))$, where [S] is concentration of Mg^{2+} or Mn^{2+}, K_i is the substrate inhibition constant, and K_m is the Michaelis constant. Experiments varying [2-PGA] were interpreted using the Michaelis-Menten equation $v = V_{max} * [S]/ K_m + [S]$. K_{cat} was calculated for each using the equation $k_{cat} = V_{max}/([enzyme]_{total} * 2)$, where 2 represents the number of catalytic sites per mole of active/dimeric enzyme. ε_{240nm} for PEP of 1.33 mM^{-1}-cm^{-1} was used. Catalytic efficiency was determined as the ratio k_{cat}/K_m, and $\Delta\Delta G$ values were obtained using the equation

$$\Delta\Delta G\ k_{cat}/K_m = -RT\ln\ [(k_{cat}/K_m)^{mutant}/(k_{cat}/K_m)^{wild\ type}]\ (31).$$

Chapter 3: Results

3.1 Protein purification

3.1.1 Screening for mutant DNA

For wild type and mutants, undigested DNA samples migrated to ~6.0 kb, as expected. *Nde*I/*Bam*HI double digests were expected to produce fragments of ~4.7 kb and ~1.3 kb, corresponding to the respective sizes of the pET-3a vector and the yeast enolase gene insert. W56F was identified on the basis of the loss of a *Bst*XI restriction site. Parental DNA *Bst*XI digests yield fragment sizes of 5000 bp, 642 bp, and 313 bp, whereas W56F mutated DNA digests yield only two of these fragments, at ~5300 bp and 642 bp. A positive W56F sample was indicated by a shift in the ~5.0 kb fragment to one migrating at ~5.3 kb. *Xmn*I digests of template DNA yielded three fragments at 2513 bp, 4934 bp, and 1464 bp. E188D mutated DNA would yield only two fragments, at 4017 bp and 1934 bp. Loss of an *Xmn*I restriction site therefore indicated a DNA sample containing the E188D mutation.

3.1.2 Purification of recombinant wild type yeast enolase

A scheme has been devised for the purification of large quantities of recombinant wild type yeast enolase. The protein was expressed and purified by adaptation of the procedures described by Wedekind *et al.* (28), and Poyner *et al.* (47). Following $(NH_4)_2SO_4$ fractionation, cell lysate preparations were purified by anion exchange on Q-Sepharose resin. Bound protein was eluted in a 0-0.5 M NaCl linear gradient, and fractions collected were analyzed for both protein and enolase activity content. A typical elution profile is illustrated

in Figure 3.1. The elution band is fairly wide, and enolase activity was detected in significant quantities in approximately 30 fractions. The protein absorbance continues to climb past the 65th fraction, as more tightly bound proteins elute late in the separation. These, however, contained little or no enolase activity. Enolase eluted at salt concentrations corresponding to 180-430 mmol/Kg in the ionic strength gradient. Fractions were examined on SDS-PAGE, a representative example of which is shown in Figure 3.2. Samples containing high activity were pooled, and prepared for further purification on CM-Sepharose cation exchange resin. Here, proteins were eluted in a 0-0.25 M KCl linear gradient. The CM-Sepharose elution profile (Figure 3.3) shows a much narrower elution band with considerably less tailing. This is also evident in SDS-PAGE results (Figure 3.4). Enolase was present in high quantities in a much smaller number of fractions, which is ideal for achieving optimal purification. Enolase eluted at salt concentrations corresponding to 100-170 mmol/Kg, which corresponds to an ionic strength of 38-52 mM KCl in the salt gradient. Results are summarized in Table 3.1, which outlines the purification achieved after each step of the process. Figure 3.5 very clearly illustrates the progress made throughout the course of the purification. The purification is evident in the removal of unwanted proteins, and the increase in both specific activity and fold purification. A significant amount of activity is lost in the procedure, although the final pool retains a high yield of both activity and protein. Protein yields of approximately 200 mg are typical of the scheme outlined, and are consistent with those published using similar expression and purification protocols, where 45 mg of protein were obtained from 1 liter of culture (47). The final protein preparation showed a single band of highly pure protein (Figure 3.5). The results shown in

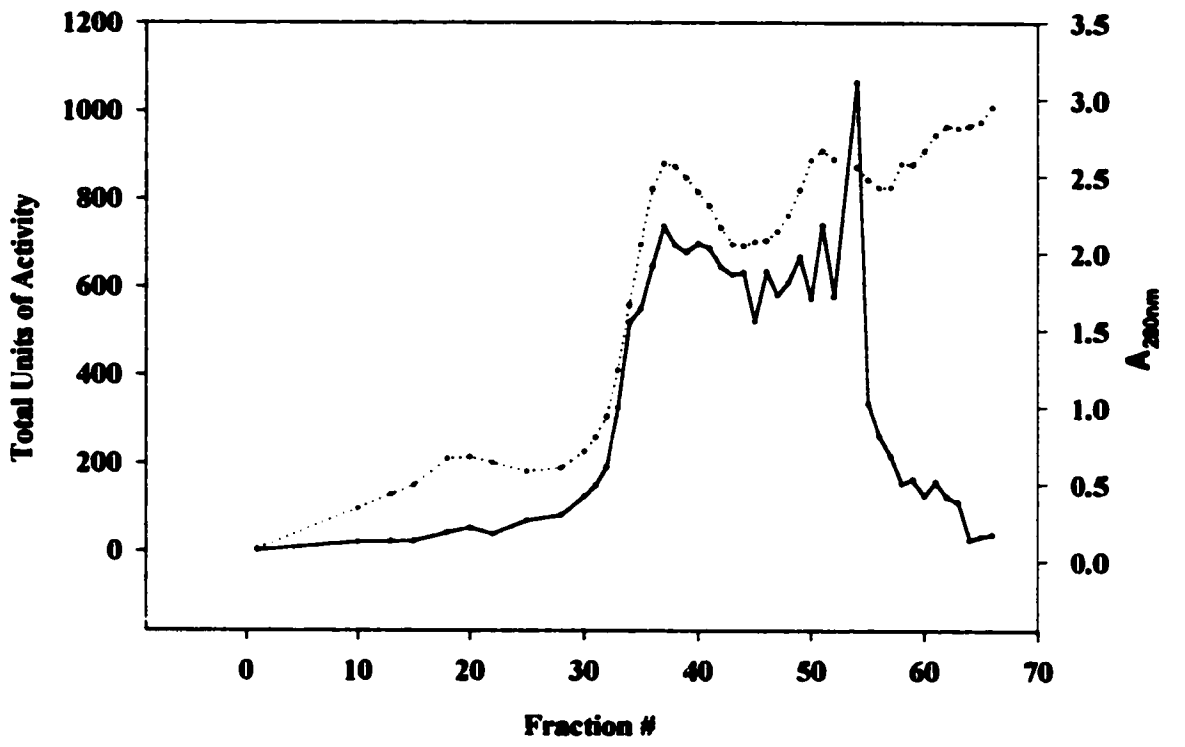

Figure 3.1 Wild type enolase eluted from Q-Sepharose. (—) Units of activity; (·····) Units of A_{280nm}.

Table 3.1 do not explicitly demonstrate the need for the second chromatographic step, in that there is no real improvement in the protein pool's specific activity. However, the CM-Sepharose significantly improved the protein sample's A_{260nm}/A_{280nm} ratio by removing material absorbing at 260 nm, which is presumed to be nucleic acid. A ratio of ≤ 0.5 is ideal for collecting protein scans and computing their fourth derivatives. Table 3.2 illustrates the purification achieved by this second ion exchange column. It is important to note that Q-Sepharose fractions were pooled based on enolase activity content, irrespective of their

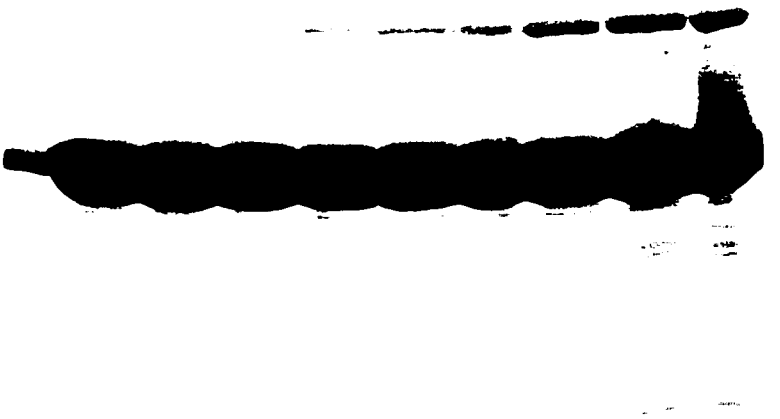

Figure 3.2 Wild type Q-Sepharose fractions. Aliquots (10 μl) of each fraction were loaded. The first lane shows the migration of native yeast enolase, obtained commercially. Samples shown are fractions 42-50, inclusively.

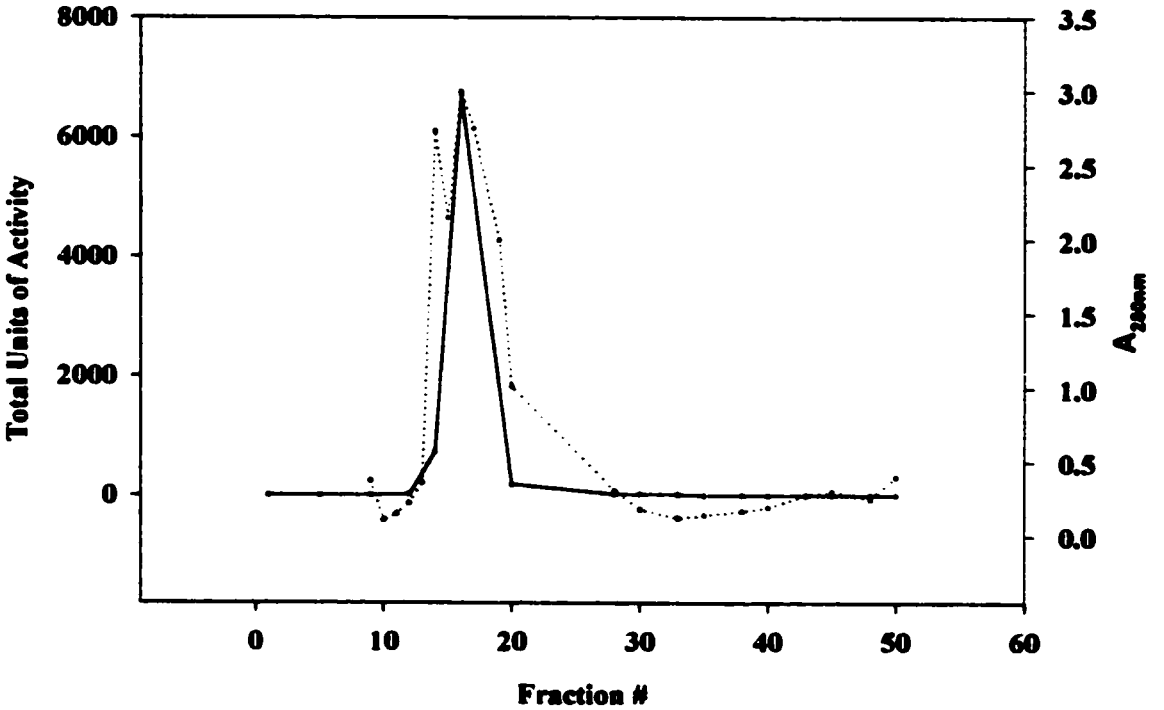

Figure 3.3 Wild type eluted from CM-Sepharose. (—) Units of activity; (····) Units of A_{280nm}.

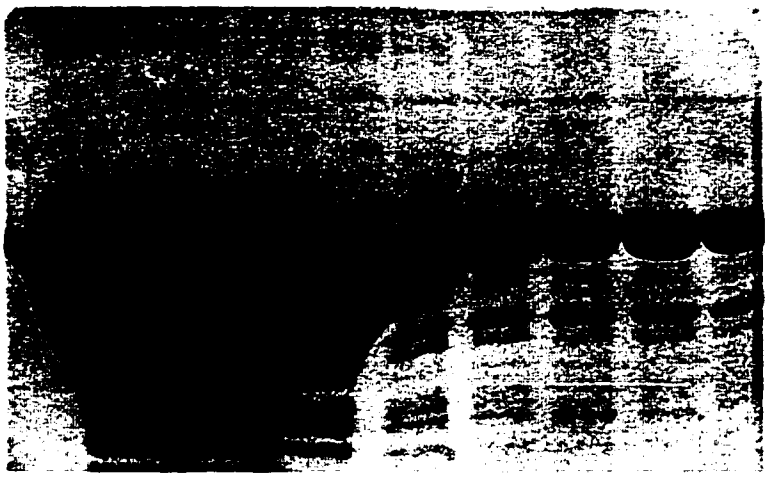

Figure 3.4 Wild type CM-Sepharose fractions. Aliquots (10 μl) of each fraction were loaded. The first sample is commercially obtained native yeast enolase; the subsequent samples are fractions 15-23, inclusively.

A_{260nm}/A_{280nm} ratios, whereas this was a crucial criterion in pooling CM-Sepharose fractions.

3.1.3 *E. coli* enolase

Basal production of enolase from the *E. coli* host strain occurs during recombinant protein expression, although it is halted somewhat. Thus, *E. coli* enolase accounts for part of the enolase activity detected in the pre-chromatographic samples. The *E. coli* protein was found to bind tightly to anion exchange resins (47). Therefore, the amount of activity lost at the Q-Sepharose chromatography step could be attributed to the fraction of *E. coli* enolase present in the starting material. In this case, approximately 7000 Units (~20%) of the total activity was lost. Yeast enolase purification would only be satisfactory once full removal of the *E. coli* protein could be accomplished and demonstrated. To this end, a control experiment was carried out. *E. coli* cells which had not been transformed with foreign DNA were allowed to grow and express proteins. The cells were lysed and prepared for Q-

Step	Volume (ml)	Total Activity (Units)	Total Protein (mg)	Activity Yield (%)	Specific Activity (Units/mg)[a]	Fold Purification[b]
Crude Extract	70.0	35000	1483	-	23.6	-
40% $(NH_4)_2SO_4$	74.0	33507	1560	95.7	21.5	0.9
85% $(NH_4)_2SO_4$	21.0	27216	1305	77.8	20.8	0.9
Q-Sepharose Pool	108.0	20444	265	58.4	77.0	3.3
CM-Sepharose Pool	13.0	17225	240	49.2	71.8	3.0

Table 3.1 Purification summary. [a] Specific activity is calculated by dividing total activity by total protein. [b] Fold purification is obtained by dividing the specific activity of a given sample by that of the starting material.

Sepharose chromatography, as outlined. The fractions contained no trace of enolase activity (data not shown), thereby confirming that the *E. coli* protein was completely removed by Q-Sepharose separation.

3.1.4 Recombinant versus native yeast enolase

Commercially available yeast enolase (minimum specific activity 60 Units/mg) was compared to the recombinant protein, in order to verify the catalytic and structural integrity of the latter. Far and near-UV circular dichroic spectra were collected for each. These revealed secondary structure and tertiary conformation, respectively. The proteins' peptide bond spectra are nearly superimposable (Figure 3.6(A)), thus showing that the recombinant

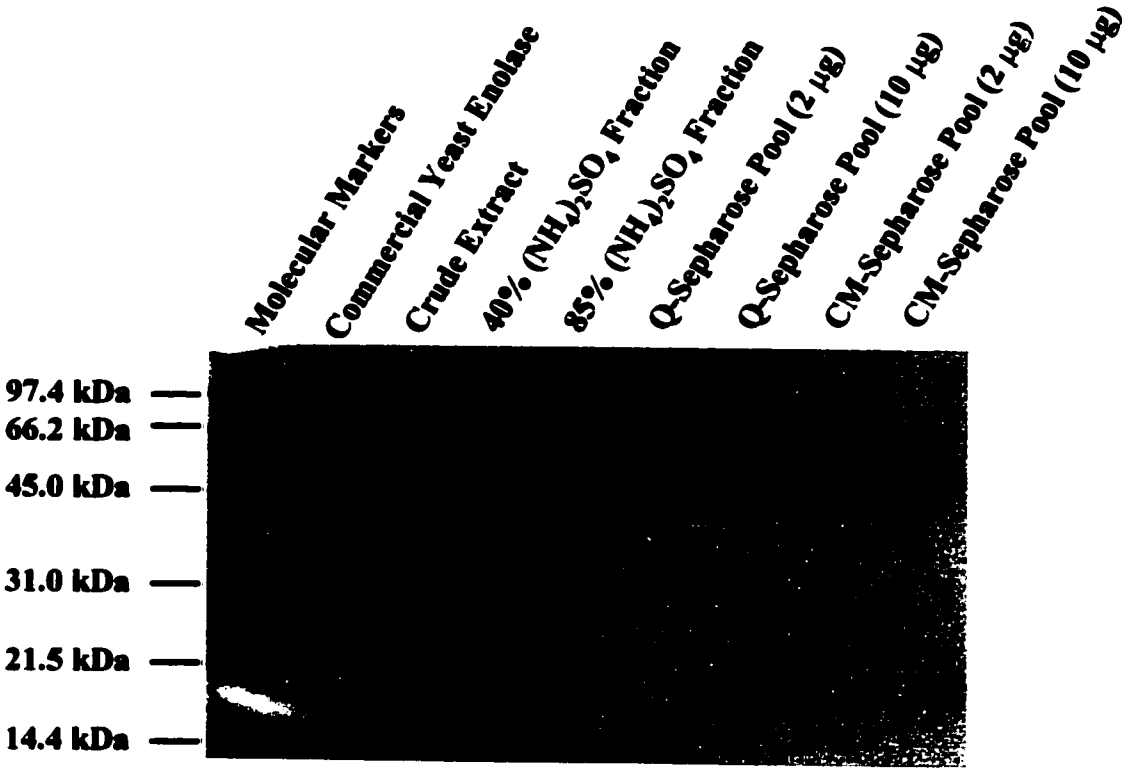

Figure 3.5 Protein purification: one step at a time. Pooled samples of both 2 μg and 10 μg were used to assess their level of purity. Total protein (10 μg) was loaded for pre-chromatographic samples.

Fraction #	A_{260nm}/A_{280nm}
32/14	1.25/0.65
36/15	0.89/0.57
40/17	0.98/0.62
44/19	0.98/0.53
48/20	0.85/0.53

Table 3.2 Removing A_{260nm} contaminant. Representative pooled fractions are shown. Q-Sepharose fractions are listed in black, and CM-Sepharose fractions are listed in red.

enzyme is properly folded. Their tertiary conformations are compared in Figure 3.6(B). Aromatic residue signals differ somewhat, although this is almost certainly due to a concentration discrepancy between the two proteins, as CD signals are highly concentration dependent. The conserved peak positions indicating tyrosyl and tryptophanyl contributions in the 275-282 nm and 288-293 nm ranges (90), respectively, point to the maintenance of proper tertiary structure in the recombinant protein.

Environment polarity (of tyrosine and tryptophan residues) also is used as a probe of tertiary conformation. Fourth derivatives were computed from zero-order near-UV protein scans. These are overlaid in Figure 3.7. The scans overlap perfectly at equimolar protein concentrations, thus revealing highly similar environments for respective Tyr and Trp residues. Characteristic peaks (283 nm and 291 nm) and troughs (287 nm and 295 nm) are used to calculate r, which can be viewed as a reflection of polarity (37, 85, 86). Ratios of 1.737 and 1.745, which differ by ~0.5%, were calculated for recombinant and commercial apo-protein, respectively.

Analytical ultracentrifugation was used to compare the sedimentation behavior of the two proteins. The coefficient describing the sedimentation of a protein is directly related to its molecular weight and inversely related to its partial specific volume, which represents the volume occupied by the protein in solution. The relationship is described by the equation

$$M=sRT/D(1-v\rho),$$

where M is the molecular weight, s is the raw sedimentation coefficient, R is the gas constant, T is the absolute temperature, D is the protein's diffusion coefficient, v is the

Figure 3.6 CD spectroscopy of native and recombinant protein samples. (A) Scans were collected for 5.3 μM protein samples. (B) Protein spectra were collected for 10.6 μM samples. All spectra were collected in 50 mM Tris (pH 7.4)/1 mM $Mg(OAc)_2$/0.1 mM EDTA. (—) Recombinant yeast enolase; (·····) commercial yeast enolase.

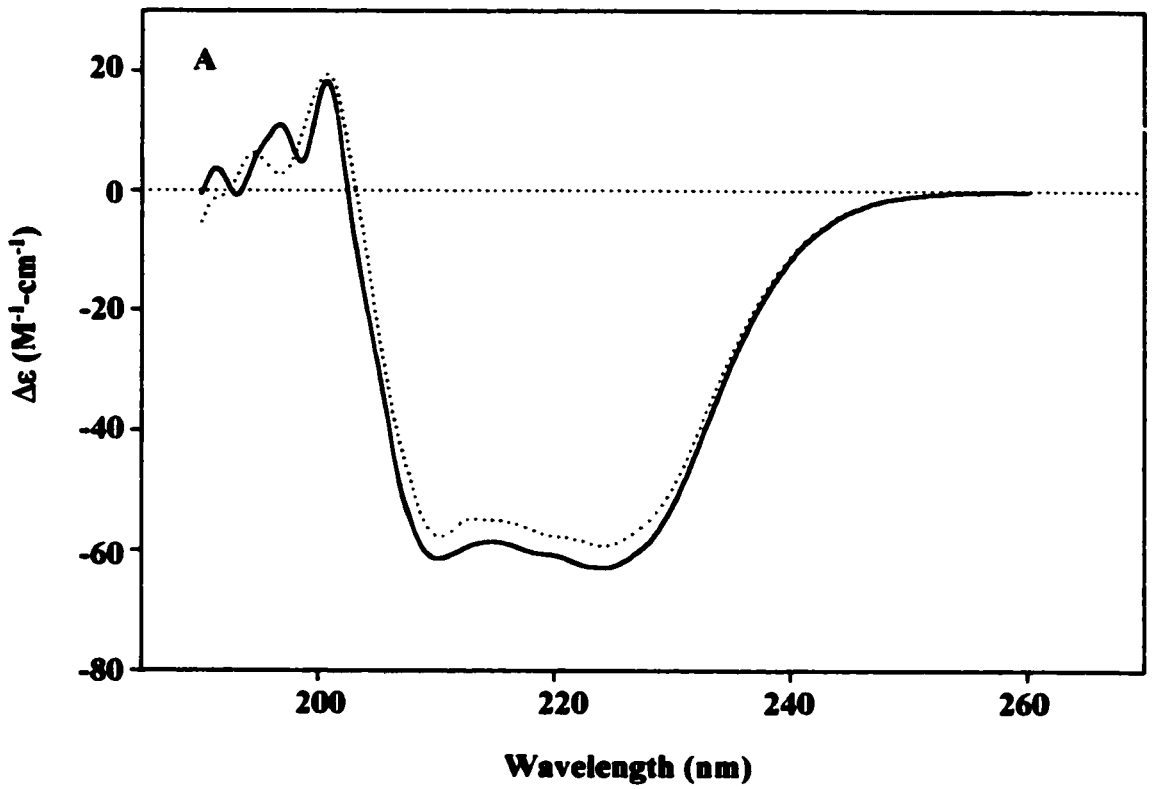
A
20
0
-20
-40
-60
-80
Δε (M-1-cm-1)
200
220
240
260
Wavelength (nm)

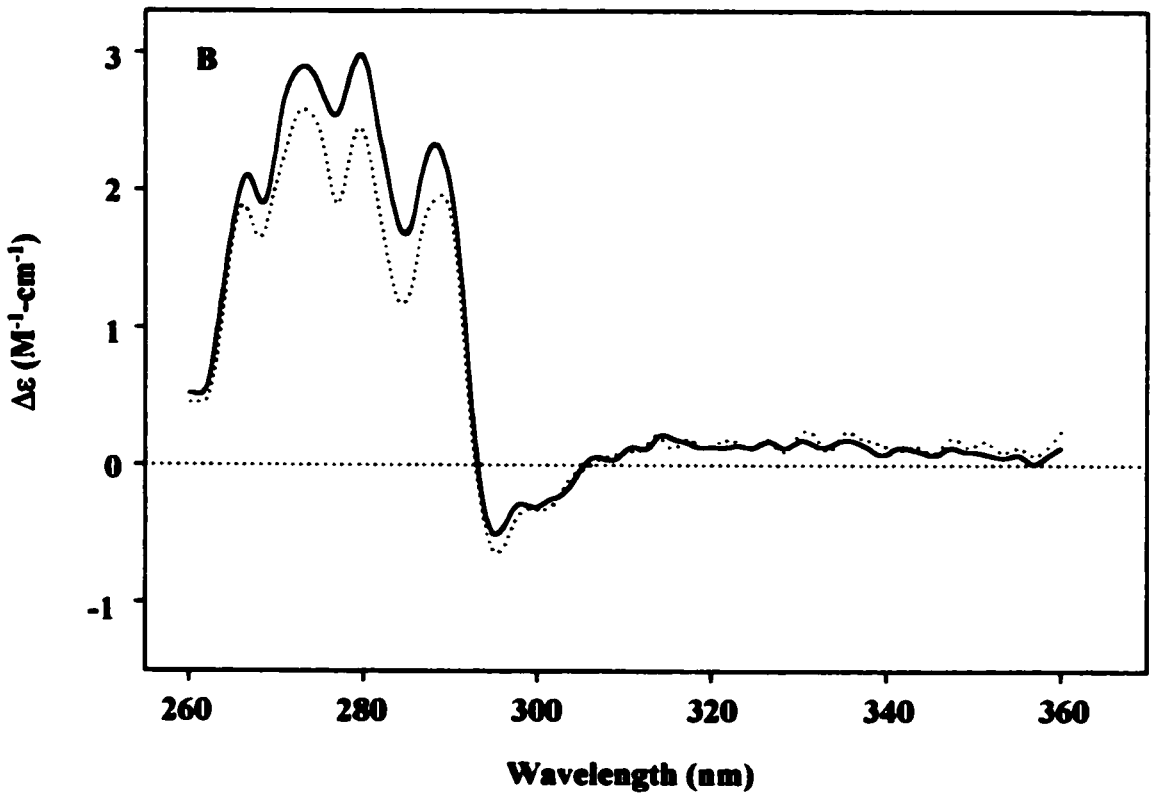
B
3
2
1
0
-1
Δε (M-1-cm-1)
260
280
300
320
340
360
Wavelength (nm)

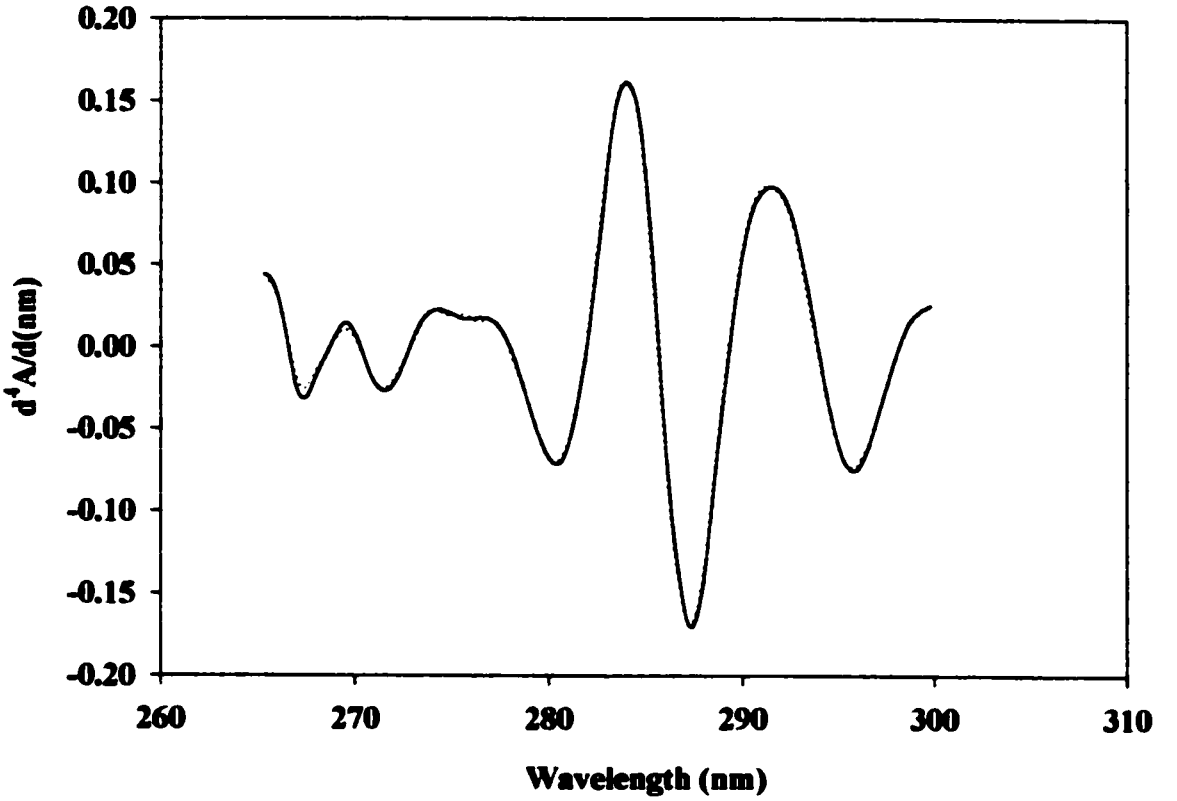

Figure 3.7 Fourth-derivative spectroscopy of native and recombinant yeast enolase. Spectra were collected for 10.6 μM protein samples in 50 mM Tris (pH 7.4)/1 mM $Mg(OAc)_2$/0.1 mM EDTA. (—) Recombinant protein; (.....) commercial protein.

partial specific volume (0.742 cc/g, (7)), and ρ is the solvent density (87). The sedimentation coefficient may be corrected for solvent density and viscosity, which both affect a protein's sedimentation. The corrected value, or $S_{20,w}$, is relative to that of the protein in water at 20°C (87). The $S_{20,w}$ coefficients for the recombinant and commercial holoproteins were determined experimentally as 5.456 S +/- 0.004 and 5.646 S +/- 0.008,

respectively, which differ by less than 4%. This indicates that the quaternary packing is very similar, if not identical, in the two proteins, thereby confirming the structural integrity of the recombinant enolase isolated.

The homogeneity of the enzyme preparations was also verified using AUC. Results could be fit to one or multiple species using the DCDT+ software, allowing for the determination of the protein sample's purity. The presence of a single moving boundary throughout the course of the experiment is evidence for a homogeneous protein sample. However, the data fit slightly better to a sample containing two species, and indicated the presence of a species larger than enolase. An overlay of the OD associated with each species revealed a 10:1 distribution of enolase:unknown species, which suggested that the preparation was >90% pure enolase. However, it is clear from the protein gel in Figure 3.5 that the level of purity is in effect substantially greater, with much less than 10% of contaminating protein bands. This was deemed acceptable for the types of studies which would later be carried out on the enzyme.

Finally, the specific activity was determined for each protein. These were 114.3 Units/mg for the commercial enzyme, and 125.9 Units/mg for the recombinant enzyme, so that recombinant enzyme appears to be fully active. The specific activity of the final protein pool reported in Table 3.1 (see Section 3.1.2) is significantly lower than 125.9 Units/mg. This is due to the presence of residual salts which, as discussed previously, have an inhibitory effect on activity (see Section 1.3.3). When properly desalted, the protein recovered full activity (data not shown).

It can, therefore, be concluded that the recombinant protein isolated in the manner

described possesses both structural and catalytic integrity with respect to its native yeast counterpart.

3.1.5 Mutant protein purification

Having confirmed that the recombinant enolase is essentially identical to that purified from yeast, mutants were prepared and subsequently purified. Site-directed mutagenesis was employed to effect amino acid substitutions at positions 56 and 188. The changes involve two hydrogen bonding partners at the subunit interface. The tryptophan at position 56 was replaced by a phenylalanine, and the glutamic acid at position 188 was substituted by an aspartic acid. Sequence analysis revealed that the desired mutations had been successfully introduced, and that no additional mutations were present. The mutants were purified as described for wild type. Q-Sepharose elution profiles for W56F and E188D are compared in Figure 3.8(A). The mutant proteins elute slightly later relative to wild type. This may be due to increased solvent exposure of charged residues which were previously either buried or only partially solvent exposed. In turn, this could indicate a more open protein conformation as a result of the mutations.

The elution profiles from CM-Sepharose (cation exchange) separations are shown in Figure 3.8(B). The mutant proteins also elute slightly later on the second column, in the same order observed as with the first. The gels are depicted in Figure 3.9(A) & (B), and the mutant purification results are summarized in Table 3.3(A) & (B). Table 3.3(A) shows significantly lower activity yields for W56F than is the case for both wild type and E188D. Protein yields, however, are high for both variants, and expression is normal. Depressed specific activity can be attributed to either of the following factors: 1) decrease in k_{cat} in

Figure 3.8 Comparing the elution profiles of wild type and mutant recombinant proteins. (A) Q-Sepharose elution profiles. (B) CM-Sepharose elution profiles. (—) Wild type; (·····) W56F; (— —) E188D.

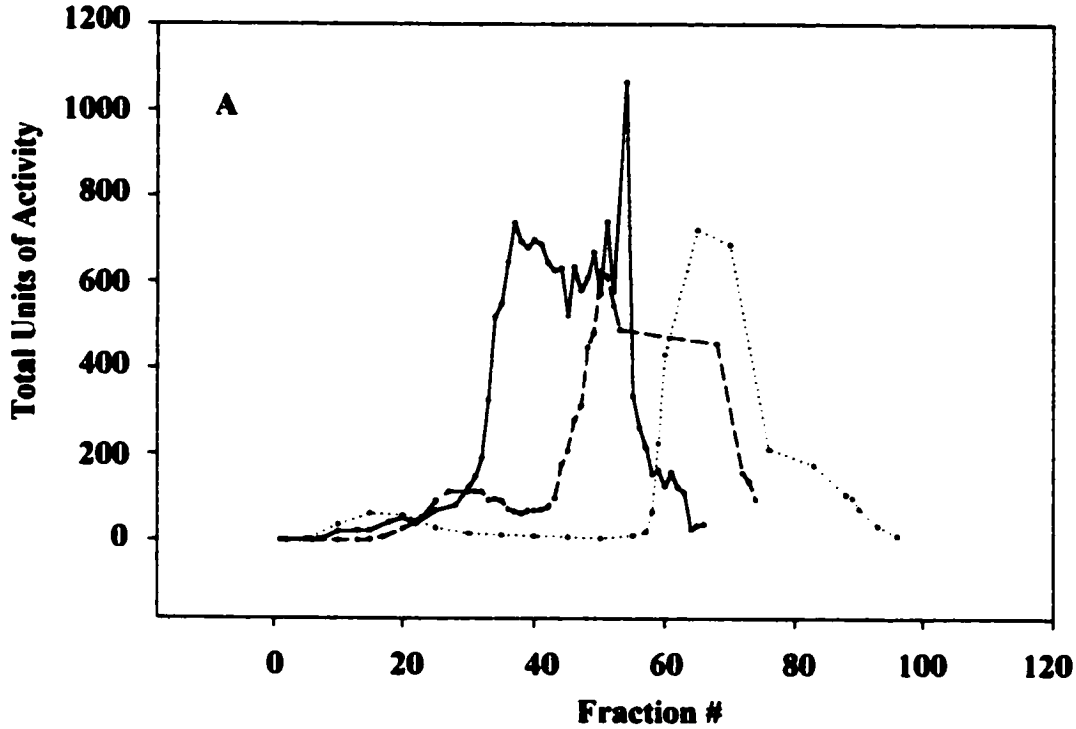
A
Total Units of Activity
1200
1000
800
600
400
200
0
0
20
40
60
80
100
120
Fraction #

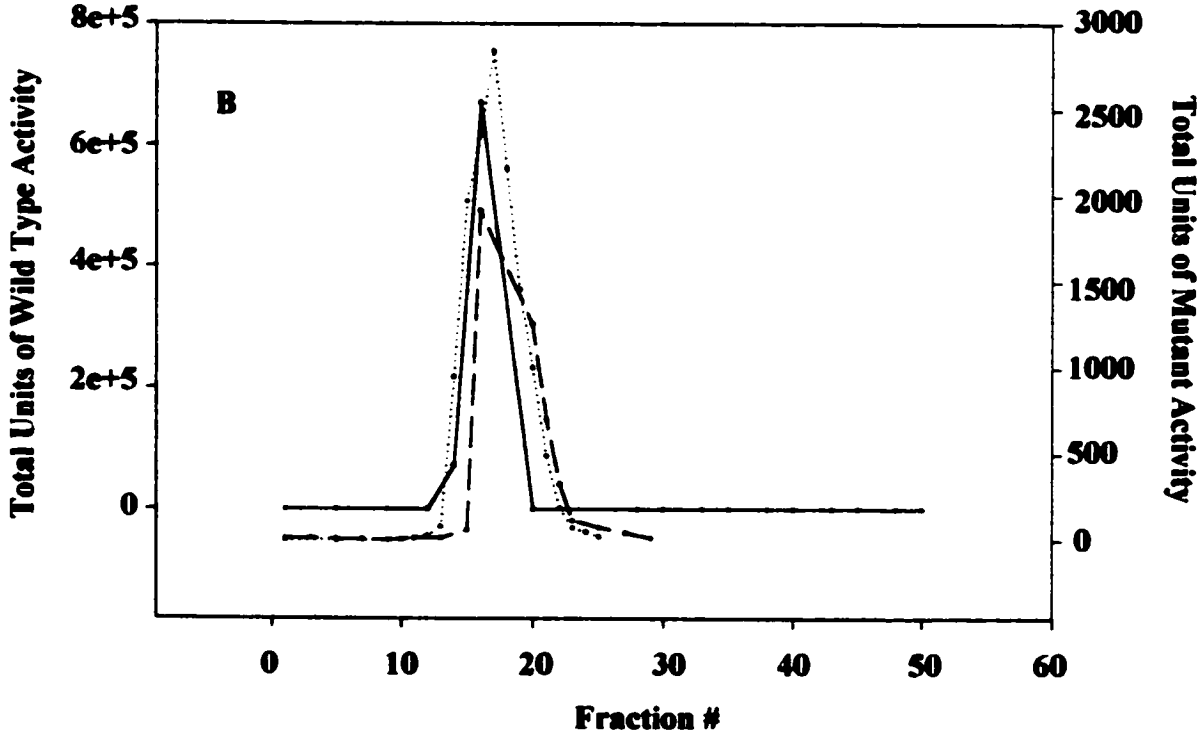
B
Total Units of Wild Type Activity
8e+5
6e+5
4e+5
2e+5
0
Total Units of Mutant Activity
3000
2500
2000
1500
1000
500
0
0
10
20
30
40
50
60
Fraction #

Figure 3.9 Electrophoresed aliquots from the purification of W56F and E188D mutant proteins. (A) W56F mutant purification; (B) E188D mutant purification. Final column pools were loaded at 2 μg and 10 μg, in order to verify the purity of the protein samples.

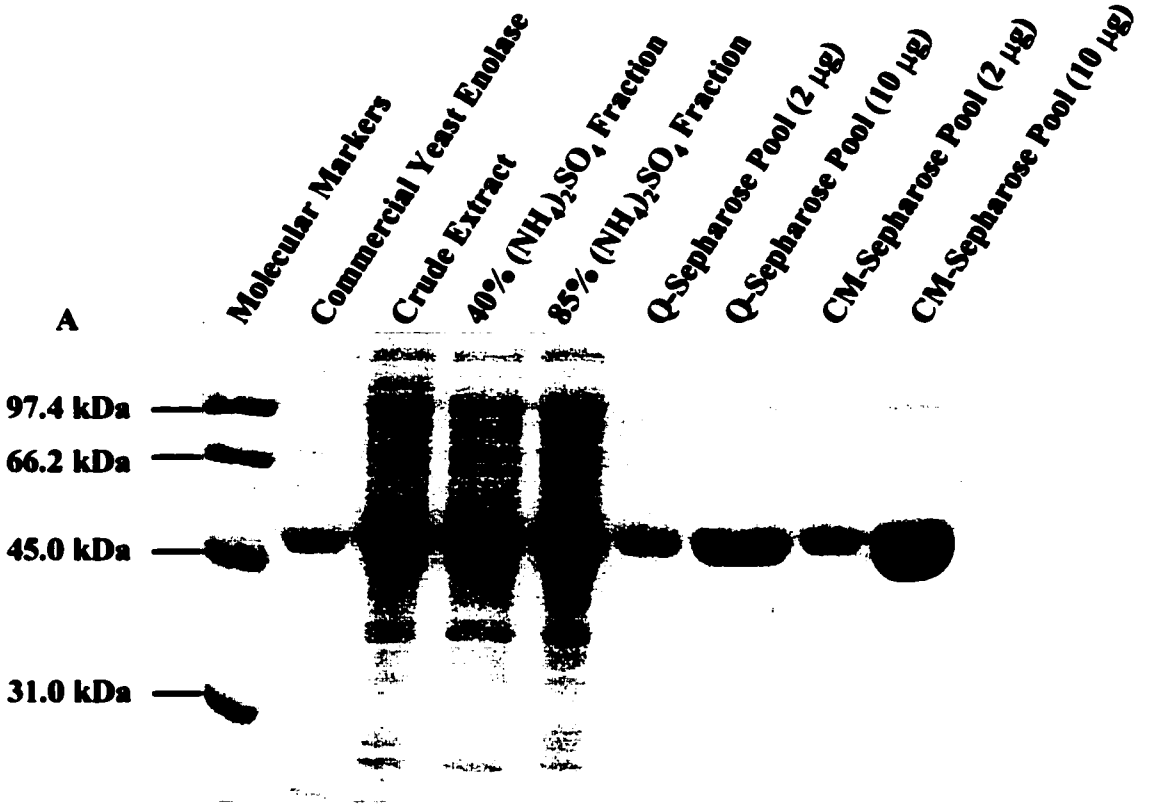
A
Molecular Markers
Commercial Yeast Enolase
Crude Extract
40% $(NH_4)_2SO_4$ Fraction
85% $(NH_4)_2SO_4$ Fraction
Q-Sepharose Pool (2 μg)
Q-Sepharose Pool (10 μg)
CM-Sepharose Pool (2 μg)
CM-Sepharose Pool (10 μg)
97.4 kDa
66.2 kDa
45.0 kDa
31.0 kDa

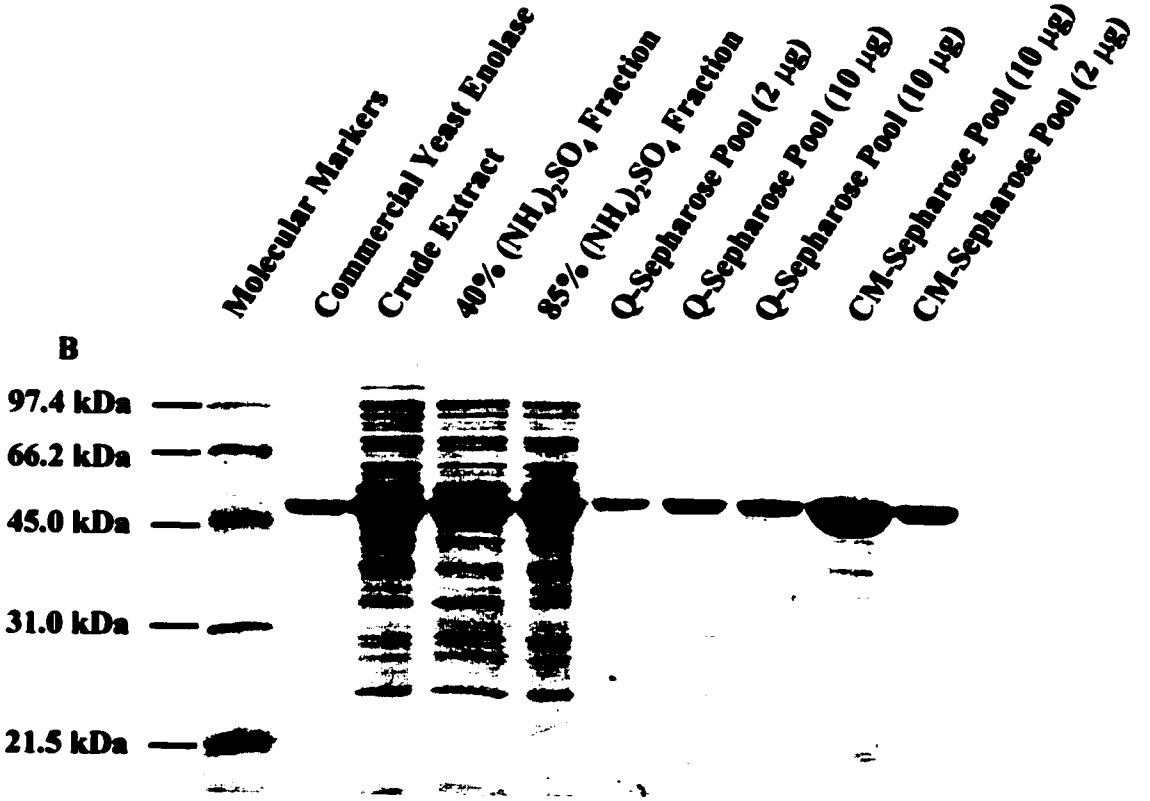
B
Molecular Markers
Commercial Yeast Enolase
Crude Extract
40% $(NH_4)_2SO_4$ Fraction
85% $(NH_4)_2SO_4$ Fraction
Q-Sepharose Pool (2 μg)
Q-Sepharose Pool (10 μg)
Q-Sepharose Pool (10 μg)
CM-Sepharose Pool (10 μg)
CM-Sepharose Pool (2 μg)
97.4 kDa
66.2 kDa
45.0 kDa
31.0 kDa
21.5 kDa

(A)

Step	Volume (ml)	Total Activity (Units)	Total Protein (mg)	Activity Yield (%)	Specific Activity (Units/mg)	Fold Purification
Crude Extract	73.5	9555	3374	-	2.8	-
40% $(NH_4)_2SO_4$	76.0	14668	3124	100	4.7	1.7
85% $(NH_4)_2SO_4$	22.5	11992	2232	81.8	5.4	1.9
Q-Sepharose Pool	12.5	10912	791	74.4	13.8	4.9
CM-Sepharose Pool	13.0	6045	569	41.2	10.6	3.8

(B)

Step	Volume (ml)	Total Activity (Units)	Total Protein (mg)	Activity Yield (%)	Specific Activity (Units/mg)	Fold Purification
Crude Extract	74.0	60458	3536	-	17.1	-
40% $(NH_4)_2SO_4$	76.0	55936	2862	92.5	19.5	1.1
85% $(NH_4)_2SO_4$	29.5	45784	2529	75.7	18.1	1.1
Q-Sepharose Pool	14.5	38309	863	63.4	44.4	2.6
CM-Sepharose Pool	11.5	31993	484	52.9	66.1	3.9

Table 3.3 Purification summary for the mutants. (A) W56F; (B) E188D.

dimeric W56F, indicative of changes in the protein's kinetic properties; or 2) decreased fraction of the dimeric form resulting from dissociation into monomers, which are assumed to be inactive. It was not possible, at this early stage, to determine which of these was indeed the case. Final protein preparations obtained were highly pure, as evidenced in Figure 3.9(A) & (B). AUC assessment of sample homogeneity showed that both preparations contained a small amount of contaminant. Proteins were >90% pure, as a 62:1 enolase:contaminant ratio was observed for E188D, and a ratio of 17:1 for W56F.

3.2 Structural studies on apo-proteins: Probing changes in the W56F and E188D variants

ε_{280nm} was determined experimentally for W56F, due to the loss of one tryptophanyl residue. ε_{280nm} of 0.897 ml-mg^{-1}-cm^{-1} was obtained for wild type, in excellent agreement with the published value of 0.895 ml-mg^{-1}-cm^{-1} (6, 7). ε_{280nm} was determined for W56F as 0.624 ml-mg^{-1}-cm^{-1}. This allowed for rapid and convenient W56F protein quantitation using the enzyme's A_{280nm}.

3.2.1 Examining secondary structural features

Mutant protein secondary structure was compared to wild type's using peptide bond (far-UV) region circular dichroism. The region monitored corresponds to absorption of circularly polarized light due to amide-amide interactions in the protein's peptide backbone (96). The various elements of secondary structure, such as α-helices, β-sheets, and β-turns, each possess a distinctive pattern and number of such amide-amide interactions, thus producing characteristic CD spectra. The main secondary structure elements of enolase are α-helices and β-strands (see Section 1.2.1). The CD scans for wild type and mutant proteins are compared in Figure 3.10. It is to be noted that most studies were carried out in 300 mM

NaOAc, necessary for analytical ultracentrifugation (see Section 3.2.5) and K_d determinations using $NaClO_4$ (see Section 3.4). However, this salt was not used for CD scanning in the peptide bond region, as it severely lowered the signal-to-noise ratio at ≤200 nm in preliminary experiments. In so doing, it obscured the α-helix peak at 192 nm, and rendered the scans noisier even at somewhat longer wavelengths. NaOAc did not, however, affect the peaks observed at 208 nm and 222 nm. The signal due to α-helix content dominates in the region between 200 nm and 240 nm, with two reasonably intense negative bands at 208 nm and 222 nm (96). A third characteristic band occurs below 200 nm, at 192 nm, and has an intense positive signal. Both mutant proteins display these distinct spectral features, having peptide bond CD spectra which are close to that of the wild type. They display conserved characteristic α-helix signals on a qualitative scale, and signal intensities, at equimolar concentrations, on a quantitative one. Thus, secondary structure has been maintained in the mutant proteins, suggesting that they are correctly folded.

3.2.2 Near-UV circular dichroism

The tertiary conformation of the mutant proteins, compared to wild type, was assessed using a variety of biophysical methods. Circular dichroic spectra were obtained in the near-UV region, where absorption is due to aromatic amino acids, *i.e.*, phenylalanine, tyrosine, and tryptophan. The absorption bands characteristic of each of these are sensitive to changes in the aromatic environments, both in intensity and in wavelength of maximum absorption. These, in turn, provide information about the overall conformation of the protein. Figure 3.11 displays an overlay of the results obtained for the three apo-proteins. The spectra depicted in blue illustrate data obtained for the apo-wild type recombinant

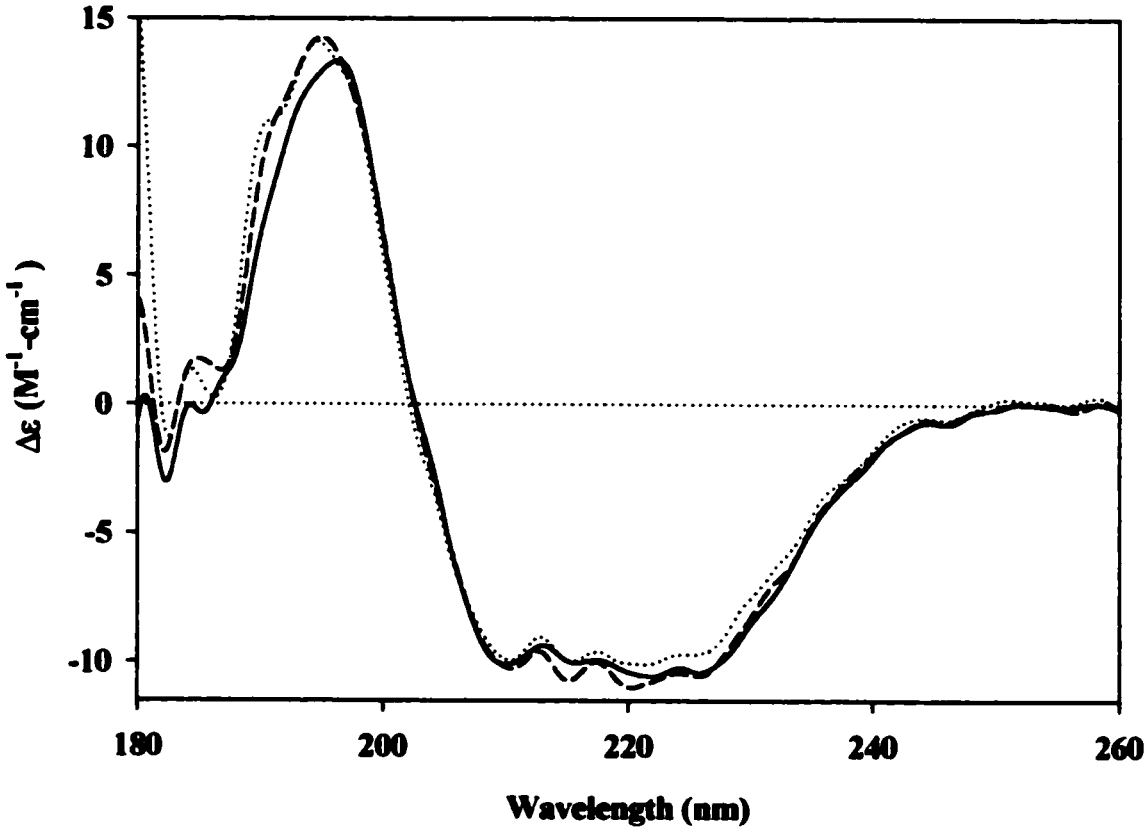

Figure 3.10 CD spectra of wild type and mutant enolases. Protein samples (10.6 μM) were scanned in 0.01 cm cells at equimolar concentrations in 50 mM Tris (pH 7.4)/0.1 mM EDTA. All proteins are apo. (—) Wild type; (·····) W56F; (— —) E188D.

enzyme. The phenylalanyl residues exhibit characteristic absorption bands in the range of 255-270 nm (90). A small positive peak at ~266 nm is due to phenylalanine. Tyrosyl bands occur between 275 nm and 282 nm (90). Two sharp peaks at 275 nm and ~279 nm may therefore be due to tyrosine side chains. Tryptophanyl contributions typically occur at wavelengths above 280 nm (90). The tryptophan residues in the native enzyme may therefore contribute bands at ~284 nm and 294 nm, each of which is both sharp and

Figure 3.11 Near-UV CD of wild type and mutant apo-proteins. Equimolar (10.6 μM) comparison of apo-proteins. (A) Wild type (—) and W56F (– – –); (B) Wild type (—) and E188D (– – –). Samples were scanned in 50 mM Tris (pH 7.4)/300 mM NaOAc/0.1 mM EDTA. 15 accumulations at 20°C/1 cm pathlength.

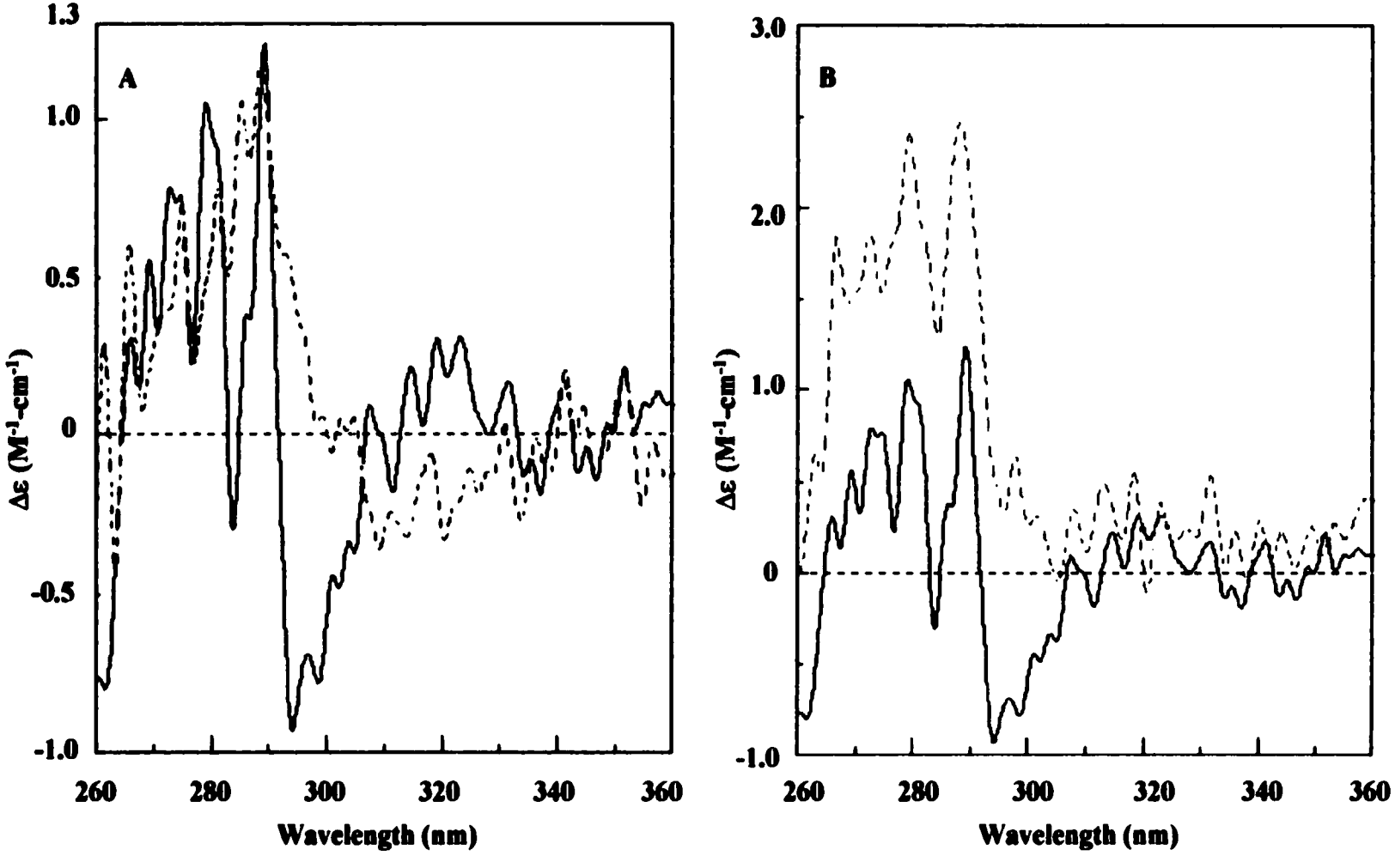
A
B
1.3
1.0
0.5
0
-0.5
-1.0
3.0
2.0
1.0
0
-1.0
Δε (M-1-cm-1)
260
280
300
320
340
360
Wavelength (nm)

negative. Positive tryptophanyl signals also occur at ~289 nm, in particular, and at 281 nm and ~286 nm as shoulders. The two shoulders, approximately 5 nm apart, are characteristic of tryptophan (90). The spectral features outlined above mirror findings from previous CD studies on apo-yeast enolase (62). It is important to note that these peak assignments can be called into question, in that some peaks may be due to one or more type of side chain. For example, the peak at 275 nm assigned to tyrosine can theoretically be due to tyrosine and/or phenylalanine residues, just as that at ~284 nm can be attributed to tyrosyl and/or tryptophanyl residues (62). However, the signal intensity observed at 275 nm ($\Delta\varepsilon$=+0.77) is of a magnitude uncommon to phenylalanine residues (typically, $\Delta\varepsilon$=+/- 0.3), and so the tyrosyl assignment of this peak is most likely correct (90). As can be noted in this comparison, the changes in aromatic environments upon effecting the described mutations are substantial. In the case of W56F, the notable changes in signals due to tryptophans and phenylalanines are to be expected. The phenylalanine signal at ~266 nm increases in intensity and becomes more prominent. This is due to the additional Phe residue. The loss of one tryptophan is evident in a number of areas. Negative peaks at ~284 nm and 294 nm are lost, becoming a positive trough at ~283 nm and a small shoulder at ~295 nm, respectively. In addition, a characteristic shoulder at 281 nm and one at ~286 nm are both lost. The tyrosine environments have also changed, as seen by the decrease in intensity of the strong peak at ~279 nm.

Important changes have also taken place in E188D. The overall increase in signal and the loss of key negative peaks is evident. In particular, the Phe signal at ~266 nm has increased sharply in $\Delta\varepsilon$, with a small 0.7 nm shift to the red. Signals due to tyrosine at 275

nm and 279 nm have also increased substantially, as do tryptophan signals at 281 nm and 289 nm. This increased intensity obscures detail associated with Trp signals, such as that of a shoulder at ~286 nm, and leads to the loss of strong negative bands at ~284 nm and 294 nm, which are typical of the yeast enzyme (62).

3.2.3 Fluorescence spectroscopy

Fluorescence emission spectra were collected on samples of apo-enzymes excited at 280 nm. The $(\lambda)_{excitation}$ used allows for both tyrosyl and tryptophanyl signals to be monitored. Fluorescence signals can be sensitive to a number of factors, including ligand binding, protein-protein association/dissociation, and denaturation (91). This results from shifts in the environment of aromatic side chains, which can produce altered polarity, fluorescence quenching, and changes in the extent of solvent exposure. The apo-proteins' spectra are compared in Figure 3.12, with λ_{max} (emission) and intensities shown in Table 3.4. The differences in signal intensities are marked, especially in the case of W56F in which ~60% of the signal is lost. Approximately 30% of the intensity is lost in E188D. The W56F spectrum reflects altered environments of aromatic residues, also the case for E188D, and loss of the contribution from a single tryptophan residue. A small amount of red-shifting, *i.e.*, shift in λ_{max} to longer wavelengths, has also taken place in both mutants (Table 3.4). The shift is slightly more pronounced in E188D. The drop in intensity suggests increased solvent accessibility of buried surfaces, which can lead to signal quenching. This, and the red-shift in λ_{max} (emission), is suggestive of dissociation, or, at the very least, of less compact tertiary and quaternary protein structures.

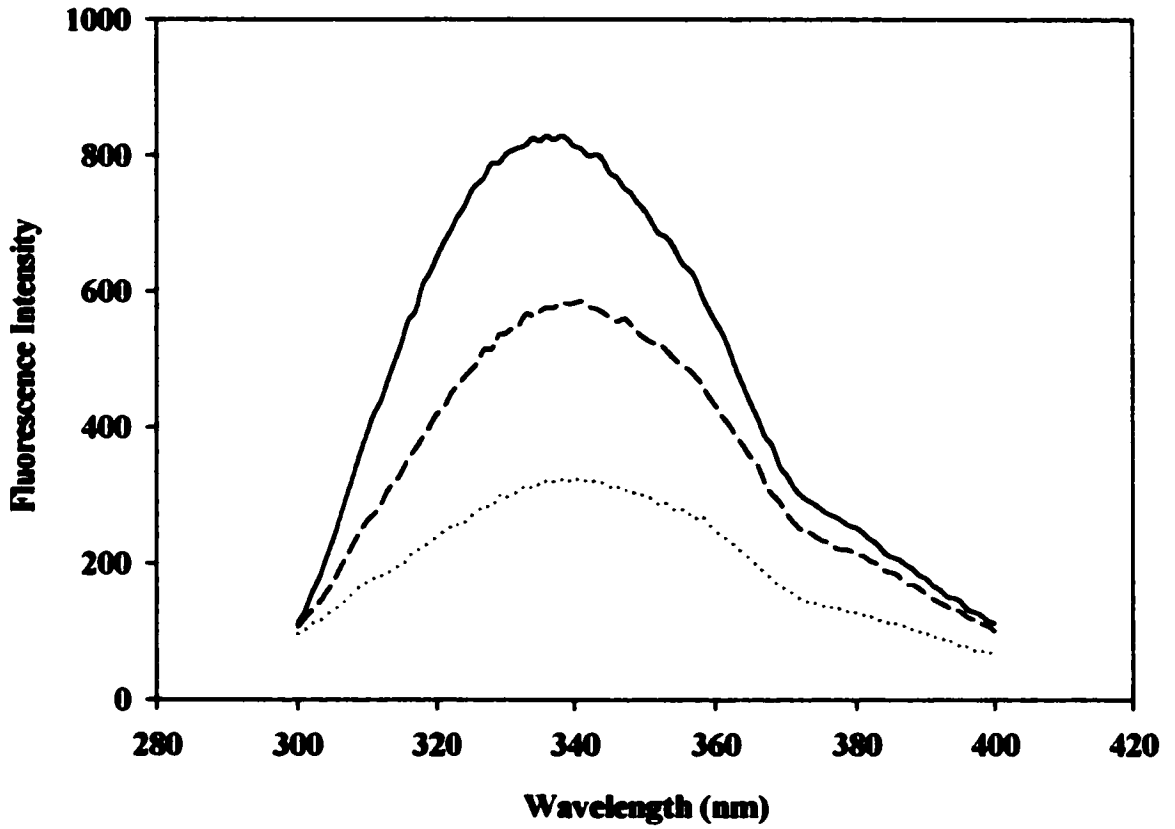

Figure 3.12 Fluorescence emission spectra of wild type and mutant apo-proteins. Protein samples (1.06 μM) were scanned at 20°C/1.0 cm pathlength in 50 mM Tris (pH 7.4)/300 mM NaOAc/0.1 mM EDTA. $\lambda_{(excitation)}$=280 nm; 2 nm band width for emission and excitation. (—) Wild type; (·····) W56F; (— —) E188D.

3.2.4 Fourth derivative spectroscopy

UV absorbance spectra of apo-protein samples were scanned, and their fourth derivatives calculated from respective zero-order spectra, according to the mathematical equation described by Lange *et al.* (85). Characteristic peak and trough positions are obtained with native yeast enolase, as illustrated in Figure 3.13. The position and height of each peak and trough provides information regarding the environment polarity of aromatic

Apo-Protein	λ_{max} (emission) (nm)	Fluorescence Intensity
Wild Type	336	828.6
W56F	338	323.0
E188D	341	585.1

Table 3.4 Summary of fluorescence spectra.
Data for spectra shown in Figure 3.12.

residues. Zero-order data were transformed here using a window of 2.6 nm, which is optimized for studying tyrosyl environments, while also providing insight into tryptophanyl environments. Its significance is discussed in work presented by Lange *et al.* (85). Spectral changes may be quantitated by calculating the ratio of peak-to-trough distances, or

$$r=[(A_{283nm} - A_{287nm})/(A_{291nm}-A_{295nm})].$$

Respective r values were calculated as 1.744 for wild type, 1.063 for W56F, and 1.444 for E188D. In general, dissociation and changes in protein packing are accompanied by a decrease in the protein's r value, usually a sign of increased solvent accessibility. As will be discussed further, dissociation in yeast enolase is accompanied by a decrease in the A_{283nm}/A_{287nm} peak-to-trough distance, along with an increase in the A_{291nm}/A_{295nm} peak-to-trough distance, leading to a decrease in the overall ratio. Both peak-to-trough distances have decreased in W56F, most likely due to the loss of one tryptophan. However, the change may be viewed as indicative of dissociation, or, again, of a change in protein packing, as the loss of peak sharpness can result from increased side-chain mobility (92). The changes in E188D are not as great as with W56F, but a notable increase in the A_{291nm}/A_{295nm} peak-to-

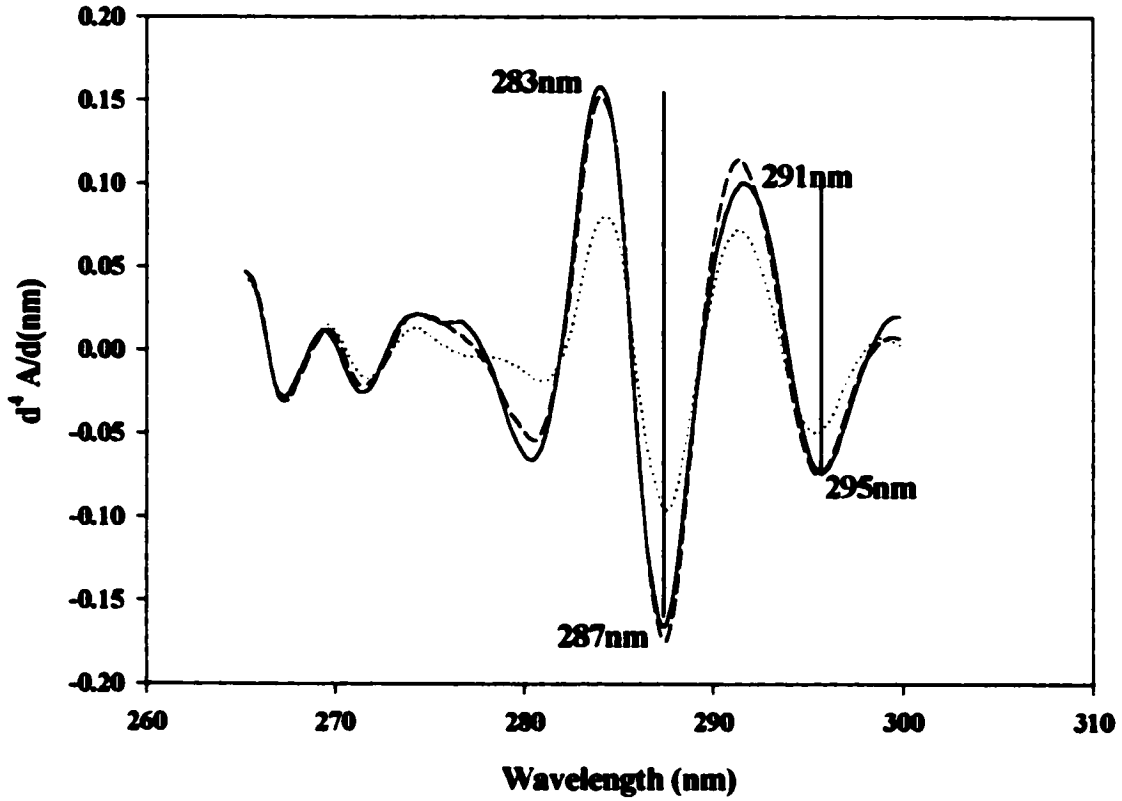

Figure 3.13 Fourth derivative spectra of native and mutant enolases. Protein samples (10.6 μM) were scanned at 20°C/1.0 cm pathlength in 50 mM Tris (pH 7.4)/300 mM NaOAc/0.1 mM EDTA. When concentrations were not equimolar, the mutants' spectra were normalized accordingly. Characteristic peak and trough positions are highlighted for wild type, with peak-to-trough distances depicted by vertical bars. (—) Wild type; (·····) W56F; (— —) E188D.

trough distance (dashed line, Figure 3.13) and the resulting decrease in r, are indicative of changes in the protein's quaternary structure. Although small, the spectral changes observed show that aromatic environments in E188D are of lower polarity. No wavelength shifts in peak and trough positions for either protein were noted.

Finally, by subtracting the spectrum of W56F, which contains four tryptophans, from

that of wild type, which contains five tryptophans, the spectrum of W56, as it occurs in the native enzyme, could be obtained. This result is provided in Figure 3.14.

As will be discussed further, the difference spectrum of W56 may be used to examine the change in environment at this particular location when the native protein dissociates.

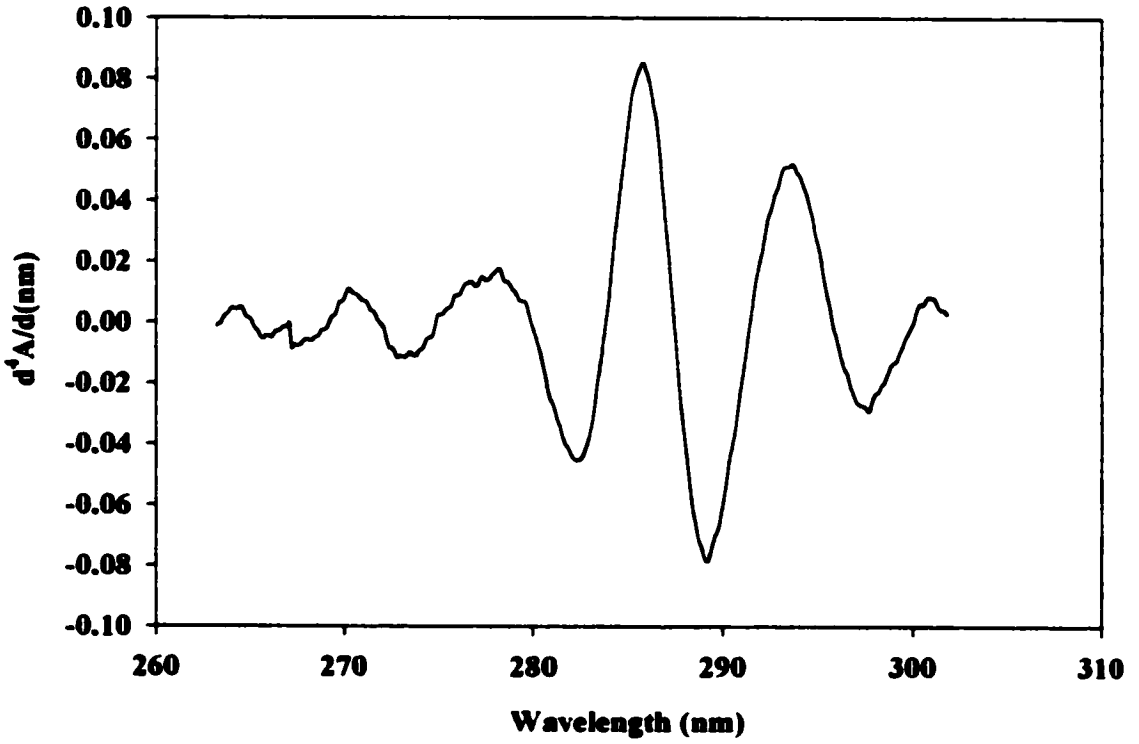

Figure 3.14 Fourth derivative UV spectrum of W56. The difference spectrum was calculated by subtracting an equimolar normalized W56F spectrum from that of wild type at 10.6 μM.

3.2.5 Analytical ultracentrifugation: Dissociating system

Having observed evidence for possible dissociation, the mutants were subjected to

high velocity centrifugation in an analytical ultracentrifuge, and their sedimentation behaviors compared with that of wild type. Although spectroscopy suggests that dissociation occurred, more rigorous and quantitative methods are needed to confirm and assess the extent of dissociation for each. AUC is such a method. The sedimentation coefficients, or $S_{20,w}$, are proportional to the average molecular weight of species present in the sample. The term, describing the velocity of a particle per unit gravitational acceleration, provides information about the quaternary structure of a protein, and can be used to assess if dissociation has taken place (87). Near equimolar amounts (~10.6 μM) of protein were centrifuged; the results shown in Figure 3.15 provide a snap-shot look into the proteins' comparative sedimentation at particular times during the run. Samples were run in the presence of 300 mM NaOAc. Addition of salt is necessary in order to prevent primary charge effects, which can impede or slow the sedimentation of a protein (87). Chloride salts are often used, but these destabilize the enolase dimer (40). An acetate salt was used instead, as this has a stabilizing effect on the protein (40, 73). As a result, and in order to ensure that all studies were comparable, all experiments, including spectroscopic work and kinetics, were carried out in the presence of NaOAc when possible. The occurrence of a single boundary for each sample (see arrows in Figure 3.15) indicates the presence of a single and relatively pure species. The position of each boundary shows how far down the cell each protein has sedimented. It is evident that the mutants lag behind wild type during sedimentation. The sedimentation coefficient values are shown in Table 3.5; these were corrected for both solvent density and viscosity. The data confirm those previously obtained using the various spectroscopic methods described, by providing direct evidence of

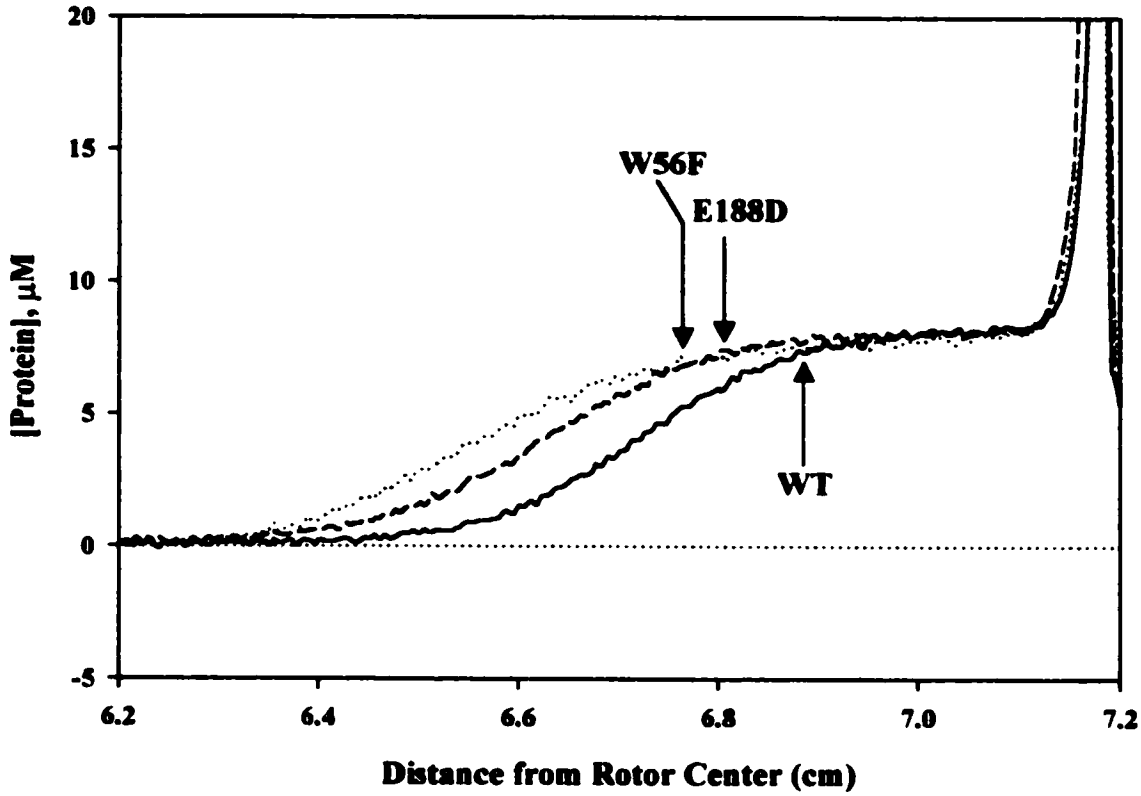

Figure 3.15 Sedimentation velocity. Each protein (10.6 μM) was centrifuged at 42,000 RPM/20°C in 1.2 cm quartz double compartment cells. Samples were in 50 mM Tris (pH 7.4)/300 mM NaOAc/0.1 mM EDTA. Data represents scan # 40 in the run. (—) Wild type; (·····) W56F; (— —) E188D. A_{280nm} were converted to protein concentrations using appropriate ε_{280nm}.

dissociation. A sample of fully dissociated native enzyme (monomeric enolase) was determined to have a coefficient of 3.274 S +/- 0.004. By comparing the sample of interest (mutants) with dimeric and monomeric forms of wild type protein, the fraction of mutant enzyme in both forms could be established, using the equation

$$f_{monomeric}=[(S_{20,W(Dimeric)} - S_{20,W(Sample)})/(S_{20,W(Dimeric)} - S_{20,W(Monomeric)})].$$

Apo-Protein Sample	$S_{20,w}$ (S)
Wild Type	5.217
W56F	4.286
E188D	4.817

Table 3.5 Sedimentation coefficients. Values were obtained using DCDT+ software (version 1.15). $S_{20,W}$ are in units of Svedbergs (S).

From this, W56F was found to be ~52% dissociated, and E188D was found to be ~26% dissociated. It is important to note that this quantitation of dissociation actually represents the population estimates of each respective apo-enzyme in the monomeric and dimeric states. The mutations effected at the subunit interface have, therefore, shifted the equilibrium in favor of the monomer by the calculated amounts.

A concentration dependence study of $S_{20,w}$ was also carried out, and these results are also consistent with a dissociating system. These experiments assume that a self-associating system will show $S_{20,w}$ values which are dependent on protein concentration. In the case of a monomer-dimer equilibrium, as is the case with enolase, the increase in concentration is reflective of an increased proportion of the dimer in solution, as association is promoted with increasing concentration, whereas dissociation is promoted in the reverse situation (87). The results obtained showed that the apo-mutant proteins were undergoing dissociation. Apo-W56F enzyme was significantly dissociated by ~0.3 mg/ml, whereas apo-E188D showed only slight dissociation at ~0.5 mg/ml. However, further decrease in concentration (to ~0.1 mg/ml) showed a significant decrease in $S_{20,w}$. These results show that the apo-W56F equilibrium is more readily shifted by lowering protein concentration than is the apo-

E188D equilibrium.

The AUC results provide definitive evidence that the apo-mutant proteins are partially dissociated, supporting the preliminary conclusions from the spectroscopic investigations.

3.2.6 Temperature-induced denaturation of wild type and mutant proteins

In order to compare the proteins' thermostabilities, temperature-induced denaturation curves were obtained by monitoring the α-helical signal at 222 nm as a function of increasing temperature using circular dichroic spectroscopy. As denaturation takes place, a progressive loss of secondary structure occurs. The melting temperature of denaturation indicates the temperature at which 50% of the protein sample is denatured. The denaturation curves obtained are compared in Figure 3.16. Samples were prepared in 50 mM MES rather than in Tris buffer, as the latter's pK_a shows greater variability than MES when subjected to heat. The curves show a single, sharp transition involving two species, *i.e.*, native and denatured proteins, as reported for wild type (40). Differential scanning calorimetric studies have shown that denaturation is preceded by dissociation, which, as discussed in Section 3.4.1, does not in itself produce denaturation. It is clear that the mutants are denaturing at slightly lower temperatures than wild type (Figure 3.16). This may suggest dissociation, a view which would be in agreement with the model for denaturation proposed by Brewer, wherein dimer→monomer→loss of secondary structure (40). Since the mutants are already partially dissociated, denaturation begins at lower temperatures. The midpoint of the steep transition yields the melting temperature, or T_m, which was 43.4°C for

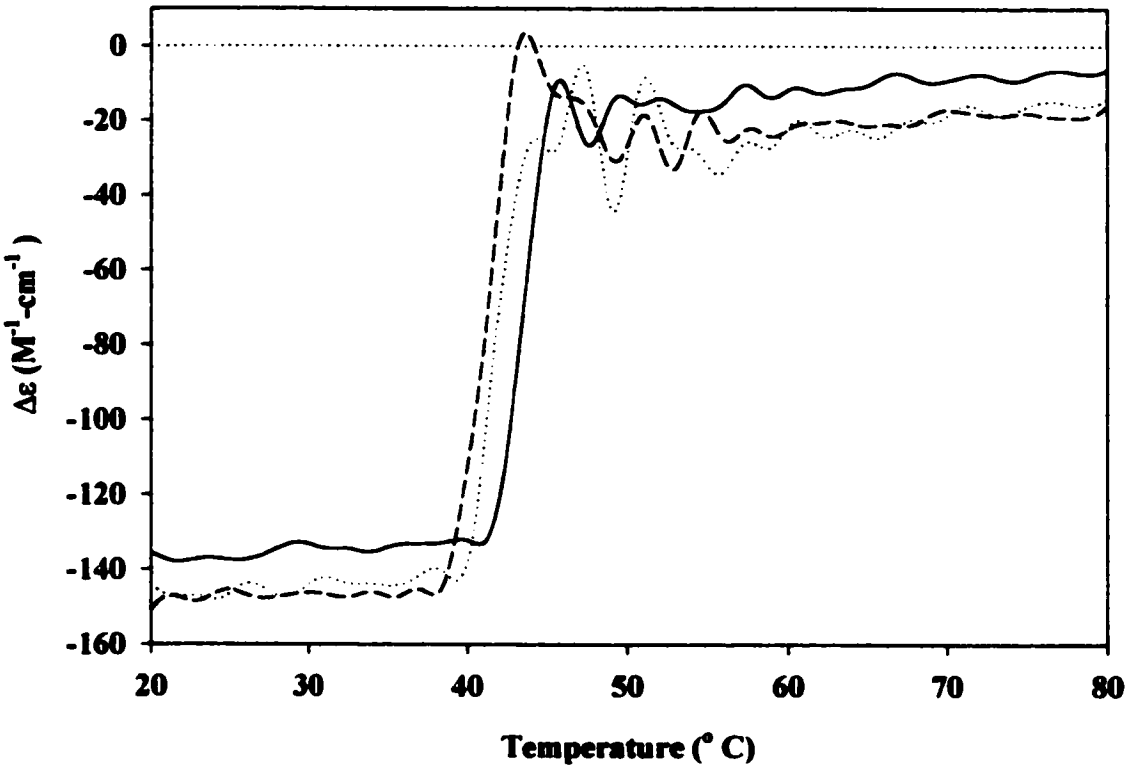

Figure 3.16 Denaturation with temperature. Each protein (10.6 μM) was heated between 20°C-80°C, at a rate of 0.5 °C/minute. Samples were in 50 mM MES (pH 7.4)/300 mM NaOAc/0.1 mM EDTA, and parameters were as indicated in Section 2.2.12. (—) Wild type; (·····) W56F; (— —) E188D.

wild type, 41.6°C for W56F, and 41.2°C for E188D. The denaturation of enolase with increasing temperature is irreversible, and results in protein precipitation. As a consequence, denaturation data could not be used to determine K_d.

3.3 Binding of Mg^{2+} at Metal site 1: Re-association of the variant proteins

3.3.1 Evidence of dimerization

Using analytical ultracentrifugation, it was established that the mutants, in their apo-forms, were partially dissociated. Having determined $S_{20,W}$ for dimeric and monomeric forms of the wild type enzyme, the extent of dissociation was calculated for each (see Section 3.2.5). However, determinations of K_d require that all proteins start out in identical conditions before applying dissociative forces, *i.e.*, the mutants would have to be in their dimeric state in order to compare them with wild type. The first attempt to drive the mutants' K_{eq} toward the dimeric state was successful. It involved incubating the proteins in a saturating amount (1 mM) of Mg^2. As discussed earlier, previous studies have already shown that Mg^{2+} lowers the subunit dissociation constant, effectively driving the equilibrium in favor of the dimeric state (see Section 1.4). This result was obtained with wild type, and re-association was then observed with the variant proteins as well, demonstrating that cofactor binding at metal site (1) in W56F and E188D produces comparable structural shifts to tighter, more compact polypeptide assemblies. Samples were run in the analytical ultracentrifuge, as described. Results are shown as a series of panels in Figure 3.17, each of which illustrates the associative effect of Mg^{2+} on one of the proteins. In each case, the apo-protein's sedimentation lags behind that of the holo-protein. This is especially evident for the mutants, which undergo extensive re-association in the presence of Mg^{2+}. The solvent corrected $S_{20,W}$ coefficients for the holo-mutants are virtually equal to that of holo-wild type protein, demonstrating that W56F and E188D are dimeric in the presence of 1 mM

Figure 3.17 Sedimentation of wild type and mutant proteins in the presence and absence of 1 mM Mg^{2+}. A) Wild type; B) W56F; and C) E188D. (—) Apo-proteins; (·····) holo-proteins. Respective $S_{20,W}$ coefficients are provided alongside corresponding scans. Each panel shows data from one single comparative run; the three sets of data reflect different time points in the sedimentation run. Each scan is the 63rd of its respective run. Concentrations are normalized to 10.6 μM, according to [wild type].

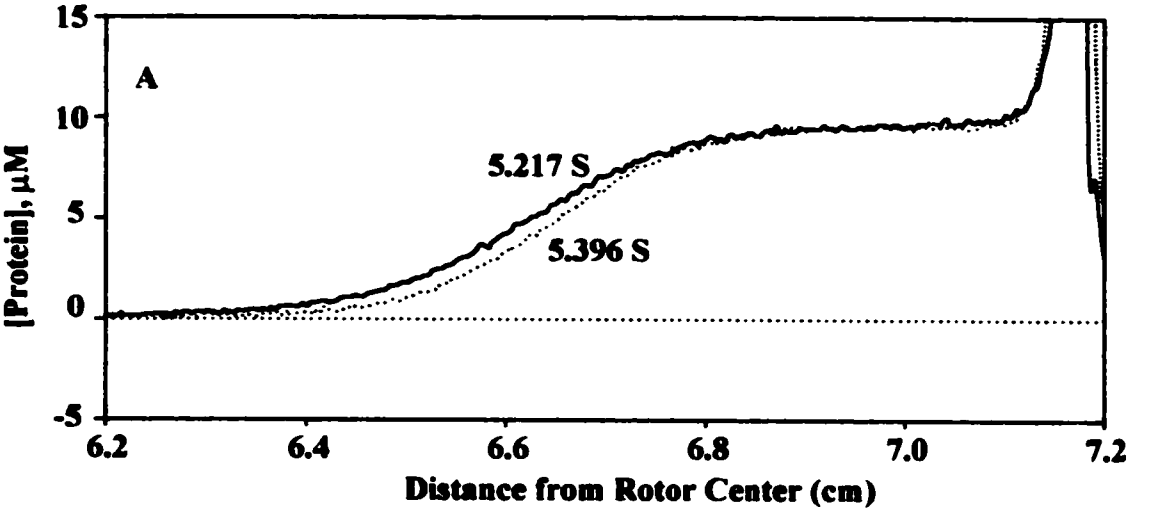
A
5.217 S
5.396 S
[Protein], μM
Distance from Rotor Center (cm)

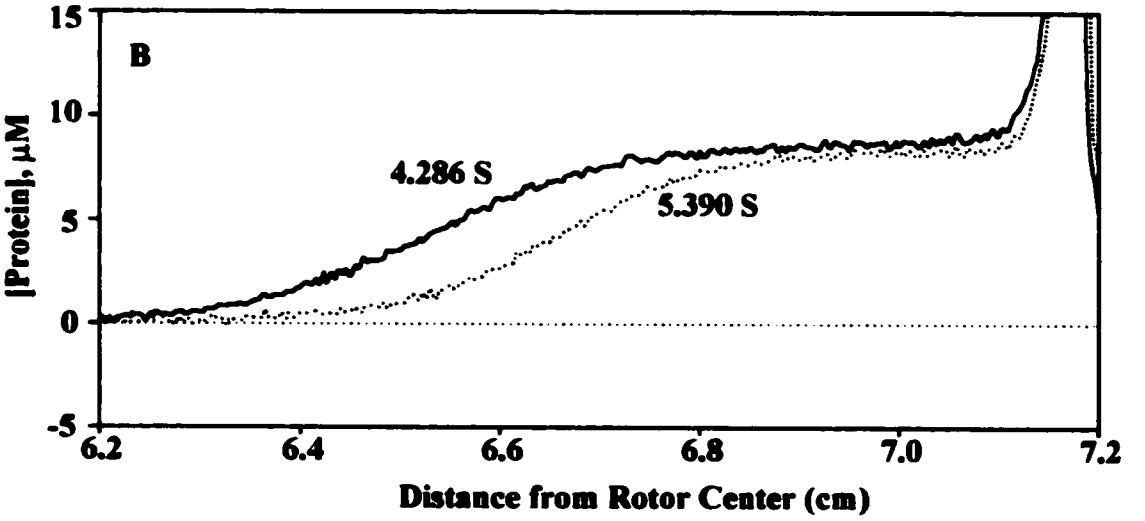
B
4.286 S
5.390 S
[Protein], μM
Distance from Rotor Center (cm)

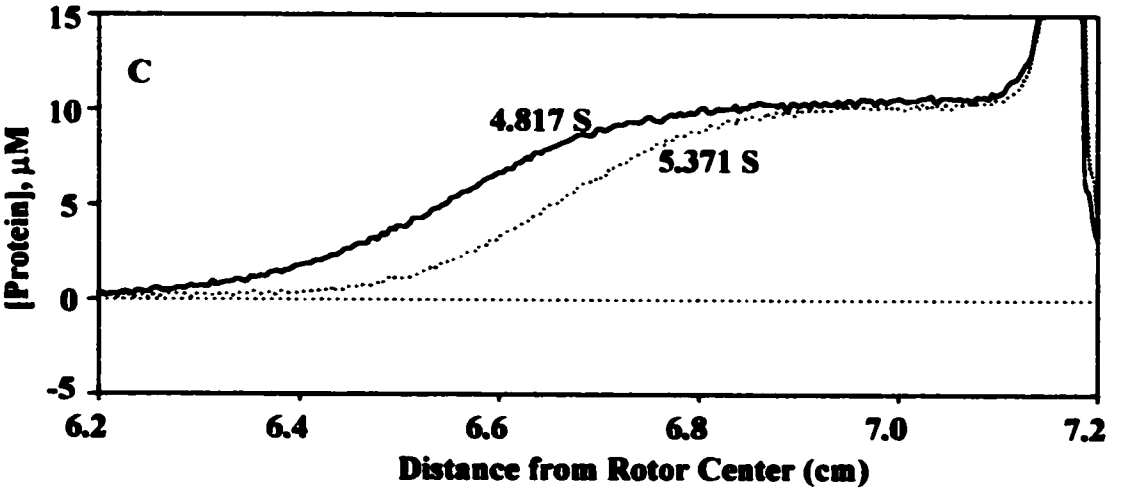
C
4.817 S
5.371 S
[Protein], μM
Distance from Rotor Center (cm)

Mg^{2+}.

3.3.2 Fourth derivative spectroscopy of holo-mutants

UV-visible spectra were acquired for the proteins in their holo-forms, and the fourth derivative of each was computed. Fourth derivative spectral changes upon binding of magnesium are illustrated in Figure 3.18 for all three proteins. The binding of Mg^{2+} produces changes in the fourth derivative spectra which are consistent with a shift in aromatic environment into one of greater polarity. This is seen as decreases in the principal peak-to-trough distances, *i.e.*, A_{283nm}-A_{287nm} and A_{291nm}-A_{295nm}. This is consistent with tighter subunit association, due to the presence of a water-filled cleft at the monomer-monomer interface. The difference is small with wild type, as it is already largely dimeric in the apo-form. This is illustrated by the relatively similar $S_{20,W}$ values obtained for apo and holo-wild type protein (see Figure 3.17(A), Section 3.3.1). Mg^{2+}, however, tightens the overall dimeric structure by strengthening dimer association, leading to a more compact protein. This is observed with sedimentation velocity, where the hold-enzyme sediments slightly more quickly due to its more compact structure. Figure 3.17(B) & (C) clearly illustrates that the mutants re-associate in the presence of the metal cofactor, thereby producing significant changes in their fourth derivative spectra (Figure 3.18 (B) & (C). Each undergoes spectral shifts consistent with re-association, but to varying extents relative to wild type, as the mutants are partially dissociated in their apo-form. The r corresponding to each mutant's spectrum also increases, with that of E188D becoming virtually identical to the r of holo-wild type. The changes in spectrum and in r are particularly revealing in the case of W56F. The latter's apo-spectrum is not easily interpretable, as differences almost certainly arise

Figure 3.18 Fourth derivative spectroscopy of wild type and mutant enolases in the presence and absence of 1 mM Mg^{2+}. A) Wild type; B) W56F; and C) E188D. (—) Apo-proteins; (·····) holo-proteins. All [protein]=10.6 μM, with W56F and E188D concentrations having been normalized according to [wild type]. Corresponding r are shown beside each spectrum.

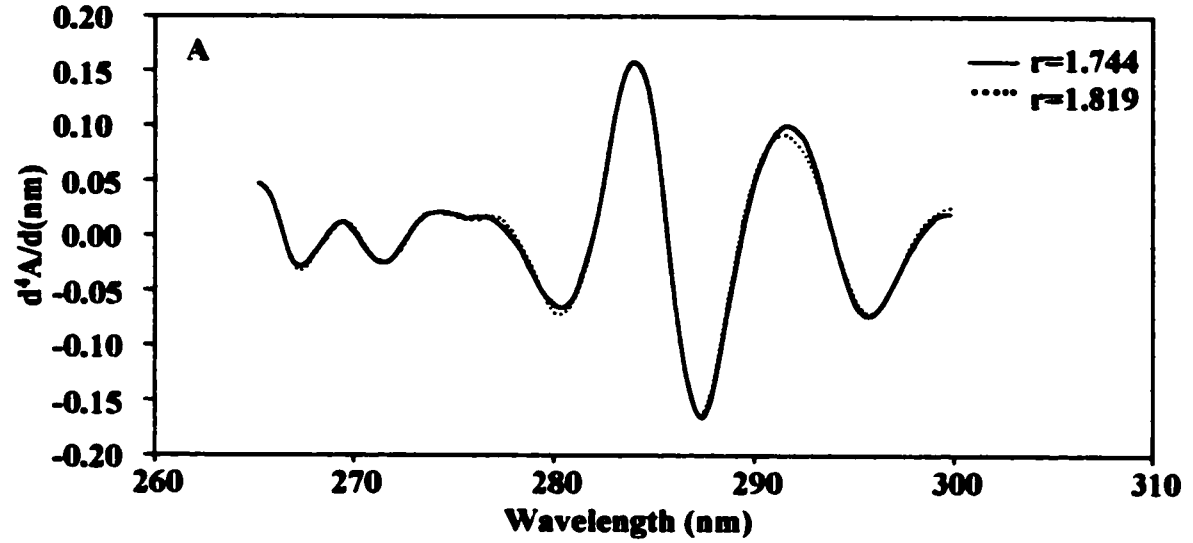
A
r=1.744
r=1.819
d⁴A/d(nm)
Wavelength (nm)

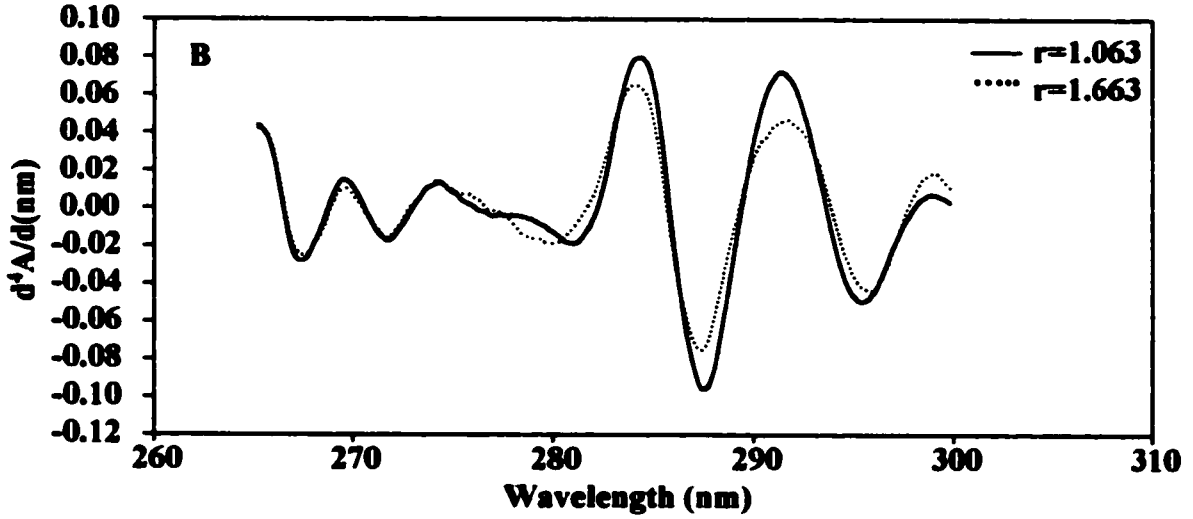
B
r=1.063
r=1.663
d⁴A/d(nm)
Wavelength (nm)

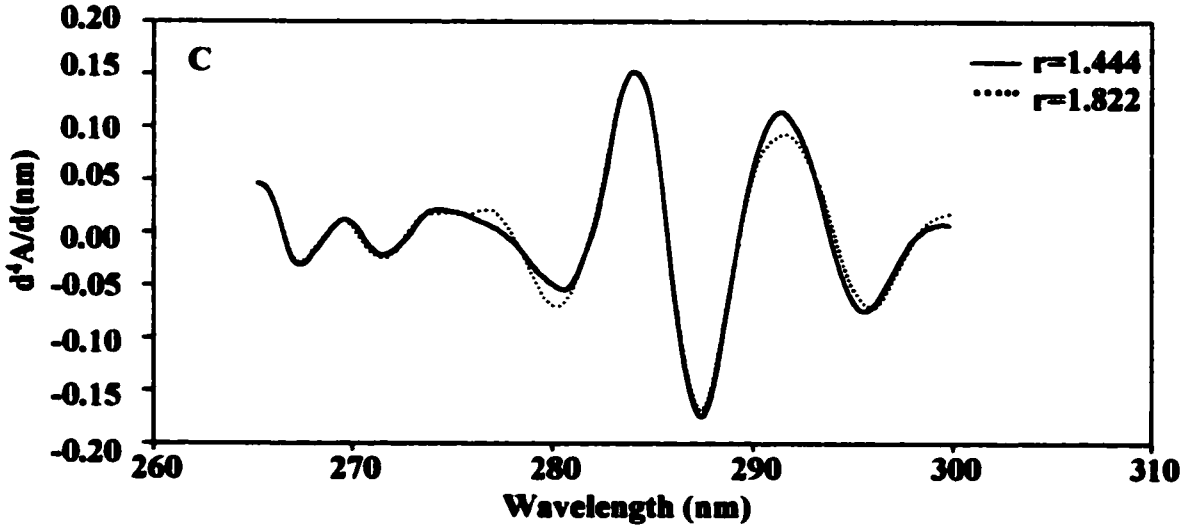
C
r=1.444
r=1.822
d⁴A/d(nm)
Wavelength (nm)

from both dissociation and the loss of a contributing tryptophan, and these are difficult to separate. The r for dimeric W56F is still notably lower than that of wild type, and this by a little over 8.5%. However, r has increased by a little more than 56.5% upon binding magnesium, which is in relatively good agreement with sedimentation data which showed apo-W56F to be ~52% dissociated (see data in Section 3.2.5). This confirms that the spectral changes observed are due to both factors outlined above, and allows for the quantitation of each factor's respective effect on the protein's spectra. It also provides insight into the extent to which the single tryptophan at position 56 contributes to the overall protein's spectrum in wild type. E188D sees just over 26% improvement in r in its holo-state, which is also in excellent agreement with the earlier assessment of its level of dissociation (~26% dissociation, see Section 3.2.5). Figure 3.19 shows an overlay of fourth derivative spectra of the holo-proteins. E188D is undistinguishable from wild type, and W56F illustrates the extent of Trp56's contribution. The difference in the dimeric W56F spectrum may be due to increased side chain mobility, indicative of the more loosely-held hydrogen bond at the interface. This, in turn, indicates that the mutant dimer possibly has an elevated K_d. This would be coupled to the loss of one Trp residue.

3.3.3 Fluorescence difference spectra

Fluorescence spectra were also obtained for holo-proteins (in 1 mM Mg^{2+}), and difference spectra were computed. The apo-protein spectrum was subtracted from its corresponding holo-protein spectrum. The difference corresponds to the changes that occurred in the protein upon binding Mg^{2+}. An overlay of these difference spectra is provided in Figure 3.20. A small increase in fluorescence intensity accompanies the binding

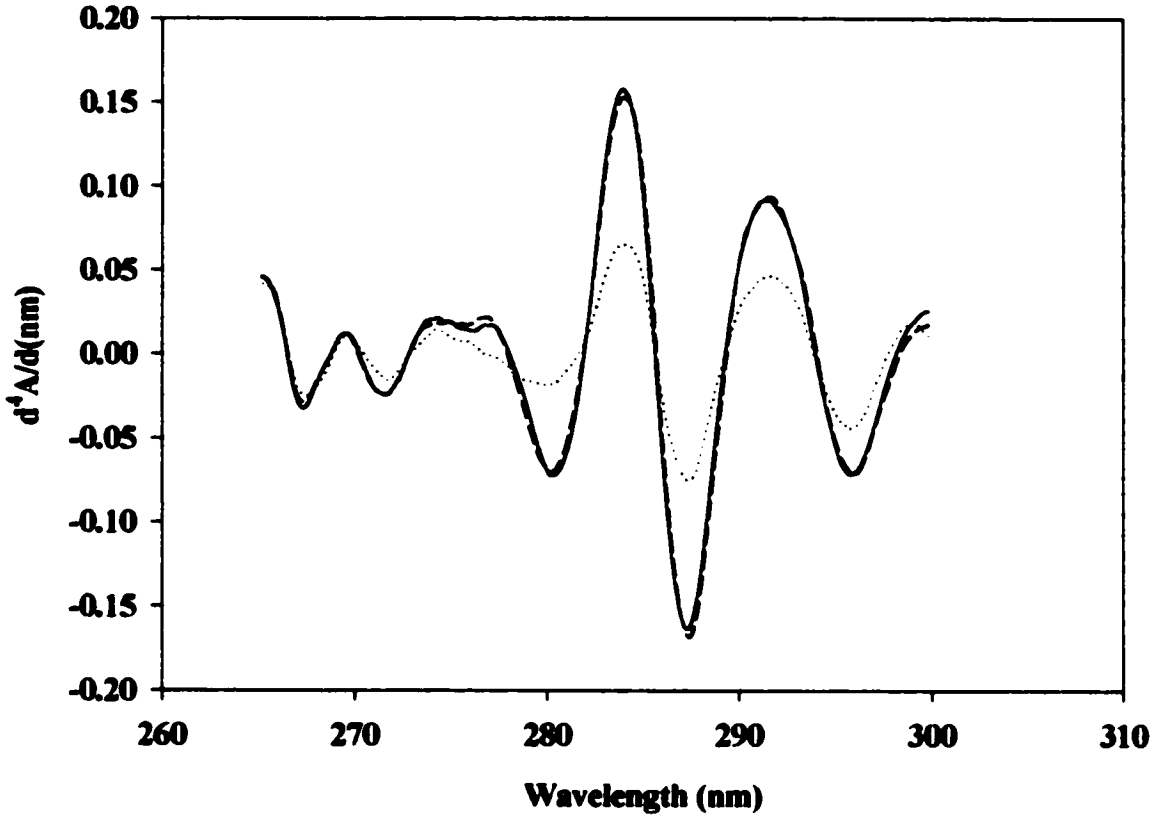

Figure 3.19 Overlay of the fourth derivative spectra of holo-proteins. (—) Wild type; (·····) W56F; (— —) E188D. Protein concentrations are normalized to 10.6 μM, according to [wild type].

of Mg^{2+} to apo-wild type protein, in keeping with the overall tightening effect of the cofactor, which very likely shifts aromatics into a much more rigid and less solvent accessible environment. The increase in fluorescence with Mg^{2+} binding has been previously reported (72). W56F and E188D undergo far more extensive shifts in respective aromatic environments, due to their re-association when cofactor binds. The significant

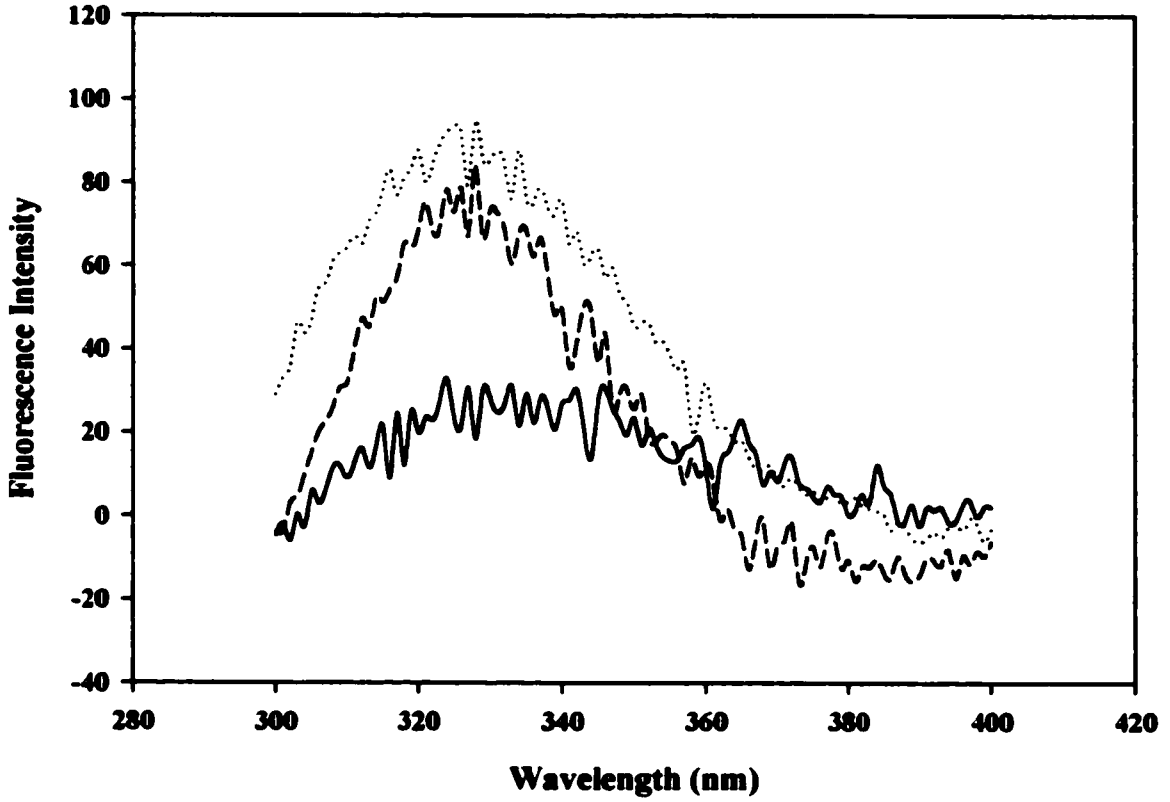

Figure 3.20 Fluorescence difference spectra of apo versus holo-proteins upon binding Mg^{2+}. 1.06 μM holo-protein spectra were subtracted from the corresponding equimolar apo-protein spectra. (—) Wild type; (·····) W56F; (— —) E188D.

increase in the intensity of fluorescence signals shows that although the mutants behave in an analogous manner upon binding Mg^{2+}, they do so on a much larger scale. Whereas wild type displays just over 3% in signal increase, W56F's signal increases in intensity by ~23.5%, and that of E188D by just under 10%. Despite these substantial differences, the holo-mutant proteins' aromatics remain in a much more quenched environment with respect

to wild type, as substantiated by the data shown in Figure 3.21. As is most often the case, this is particularly true of W56F. Aromatics within W56F and E188D proteins are likely in much less rigidly held positions due to the changes at the subunit interface. The mutations could have produced weakened subunit association, which, as discussed earlier (see Chapter 1, Sections 1.2.3, 1.3.5, 1.4, and 1.5), could lead to changes in the conformations of loops. The presence of W56/F56 within one of these loops (Pro35-Gly60) could provide an explanation for the particularly depressed signals observed with W56F.

3.3.4 Stabilization against denaturation

Holo-proteins were subjected to heat as described for apo-proteins (see Section 3.2.6). The stabilization provided by excess Mg^{2+} to wild type and mutant proteins is clearly evident in Figure 3.22. The most appreciable degree of stabilization occurs with wild type, in which case T_m increases by 8.6°C. W56F and E188D are stabilized by 4.2°C and 6.2°C, respectively. Even in their dimeric forms, the variant proteins maintain substantially lower T_m values. The associating effect of Mg^{2+} renders all three proteins more stable against denaturation, as more energy is needed to fully dissociate the dimer. Dissociation precedes denaturation, in which the monomers subsequently undergo unfolding (see Section 3.2.6). Stability is improved in the case of wild type in the presence of Mg^{2+}. The mutants are not stabilized to the same extent, even though they re-associate. Decreased T_m values indicate that both W56F and E188D are more readily dissociable and thus have elevated K_d relative to wild type. For this reason, denaturation commences at lower temperatures.

These results agree with fluorescence data obtained for the holo-proteins, where the dimeric mutants retain significantly quenched signal intensities (see Section 3.3.3). Both

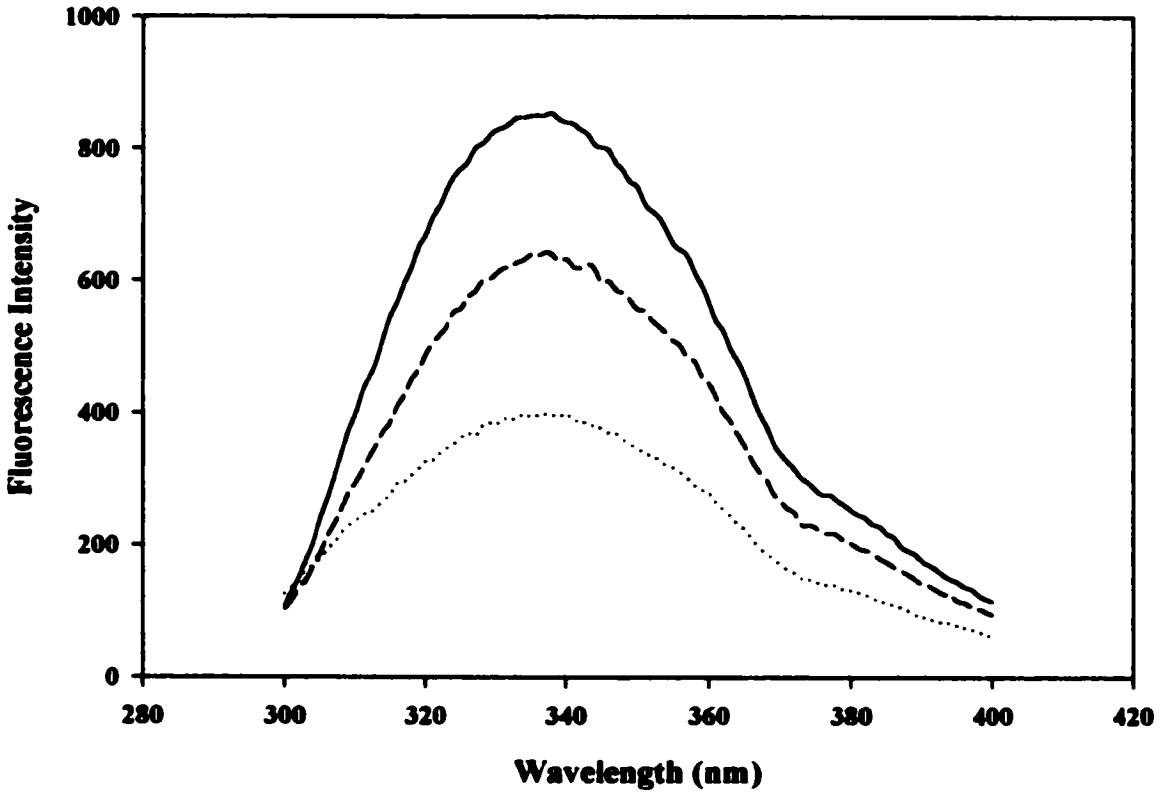

Figure 3.21 Fluorescence of holo-proteins. Proteins, 1.06 μM of wild type (—), W56F (·····), or E188D (— —). Scans were collected as previously described.

data sets thus support the contention that the subunit interface hydrogen bond between Trp56 and Glu188 was successfully weakened.

3.4 Dissociation of yeast enolase in $NaClO_4$

Dissociation experiments were carried out using $NaClO_4$, a Hofmeister series chaotropic salt. $NaClO_4$ has been used in a number of enolase studies (30, 80, 93, 94). It destabilizes protein structures by weakening hydrophobic interactions, thereby leading to the hydration of buried protein surfaces. Chaotropic salts, therefore, destabilize proteins by

Figure 3.22 Temperature-induced denaturation of wild type and mutant enolases in the presence and absence of 1 mM Mg^{2+}. A) Wild type; B) W56F; C) E188D. (—) Apo-proteins; (·····) holo-proteins, pre-incubated with 1 mM $Mg(OAc)_2$ at 20°C. All proteins were in 50 mM MES (pH 7.4)/300 mM NaOAc/0.1 mM EDTA, at 10.6 μM. Corresponding T_m values are indicated for each denaturation curve. CD parameters were as outlined for apo-protein experiments (see Section 3.2.6).

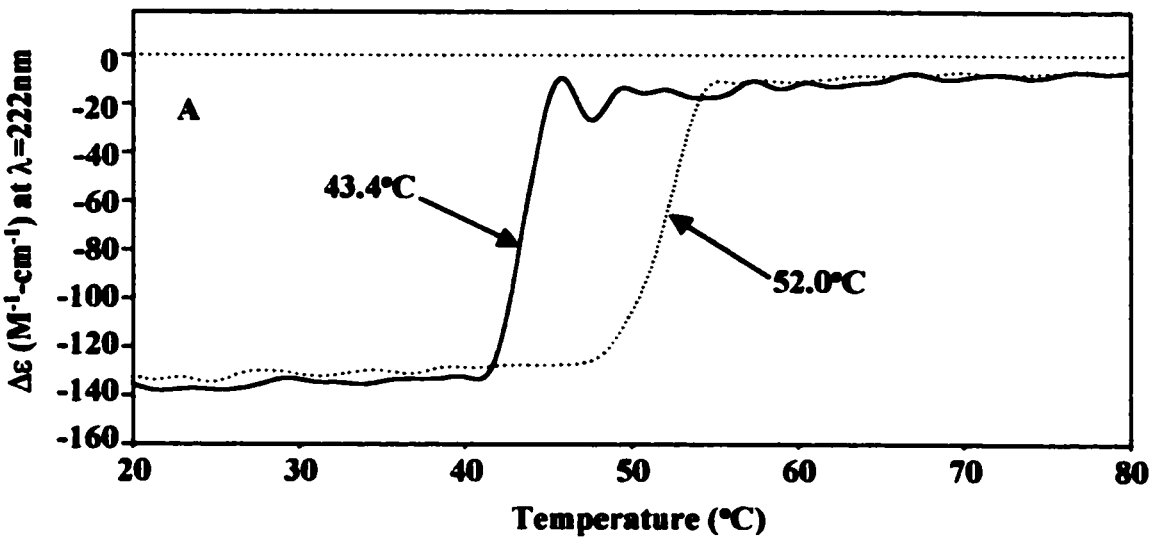
A
43.4°C
52.0°C
Δε (M-1-cm-1) at λ=222nm
Temperature (°C)

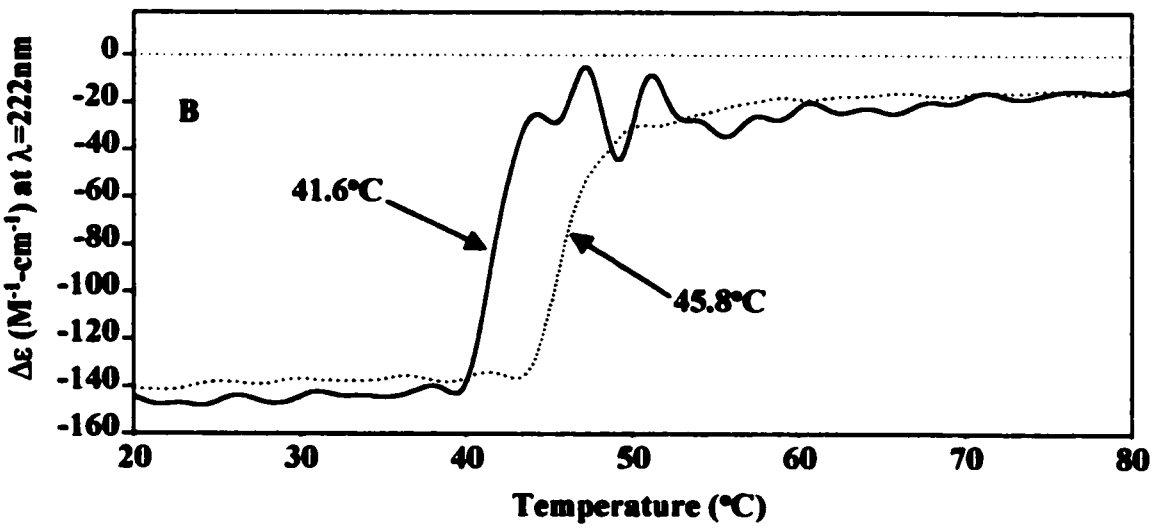
B
41.6°C
45.8°C
Δε (M-1-cm-1) at λ=222nm
Temperature (°C)

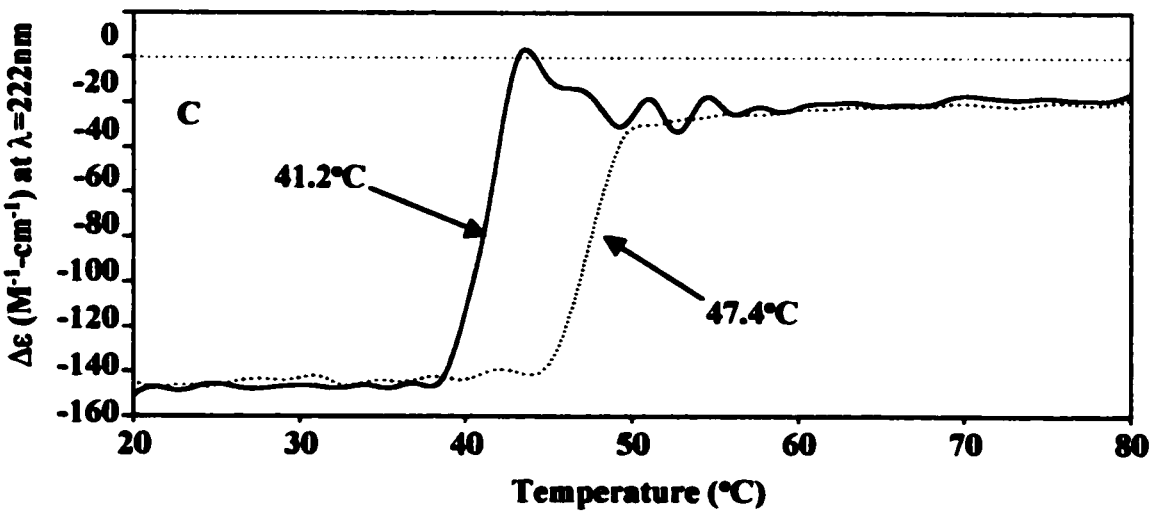
C
41.2°C
47.4°C
Δε (M-1-cm-1) at λ=222nm
Temperature (°C)

favoring the form with the largest surface area (95). $NaClO_4$ was used to establish and compare the dissociation constants of wild type and mutant proteins in varying conditions. Proteins (usually 10.6 μM) were incubated in varying [$NaClO_4$], to a maximum concentration of 300 mM. Published results have shown that ≤300 mM $NaClO_4$ is required for complete loss of enzymatic activity in wild type (30). [Na^+] was kept constant by compensating the concentration of $NaClO_4$ with the required [NaOAc] to 300 mM. This was necessary due to the adverse effect of Na^+ on activity (see Chapter 1, Section 1.3.3). Keeping [Na^+] constant eliminates changes in activity due to factors other than ClO_4^- ions. Constant ionic strength is also required, as it has been shown to affect dimer association/dissociation (see Chapter 1, Section 1.4) (13).

3.4.1 Effect of $NaClO_4$ on wild type

$NaClO_4$ produces spectral shifts and loss of activity in enolase (30, 80, 93, 94). It was assumed that these effects were due to dissociation, however, they did not, in themselves, provide conclusive and definitive evidence that the underlying cause was dissociation. This is because spectral changes and loss of activity do not constitute a direct means of monitoring the association/dissociation process. Dissociation due to $NaClO_4$ was confirmed using analytical ultracentrifugation, which monitored the sedimentation of the protein as a function of [$NaClO_4$], providing a direct probe of the enzyme's quaternary structure. Effects of $NaClO_4$ on fourth derivative UV spectra, activity, and $S_{20,w}$ are shown in Figure 3.23. Increased [$NaClO_4$] leads to progressive loss of enzymatic activity, decrease in r, and decrease in sedimentation coefficient. It can, therefore, be asserted that $NaClO_4$ is indeed dissociating the enzyme, thus causing the other monitored effects. The spectral

Figure 3.23 Effects of $NaClO_4$ on the enzymatic activity and structure of wild type yeast enolase. A) Activity data; B) fourth derivative data; C) $S_{20,w}$ data. Activity data is shown as fraction active, equated with fraction of dimeric protein, versus [$NaClO_4$]; fourth derivatives show an overlay of spectra in differing [$NaClO_4$]; and $S_{20,w}$ are shown as a function of [$NaClO_4$]. All protein samples were apo at ~10.6 μM. Protein was pre-incubated in $NaClO_4$ at 20°C overnight. Fourth derivatives are accompanied by corresponding r.

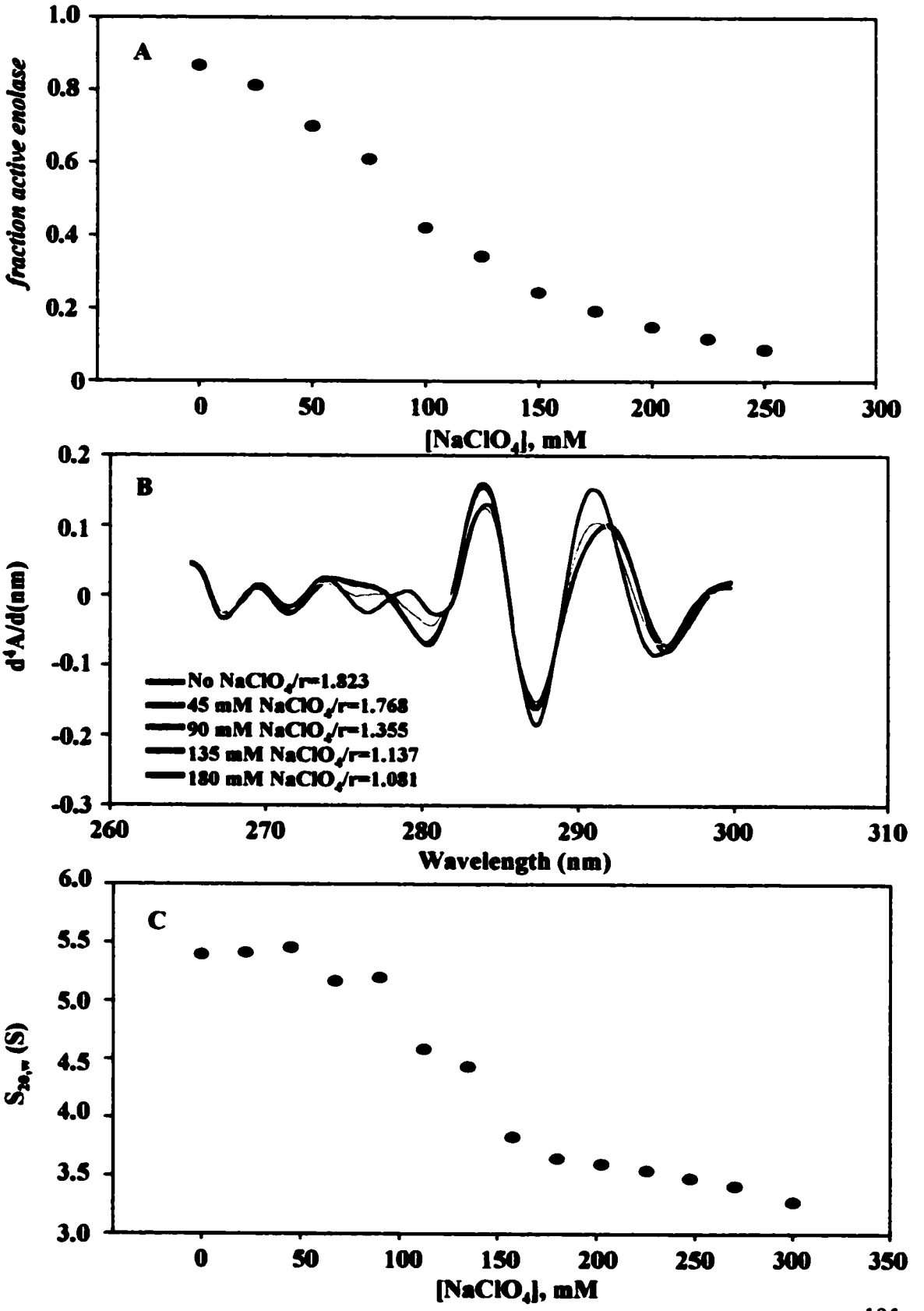
A
fraction active enolase
1.0
0.8
0.6
0.4
0.2
0
0
50
100
150
200
250
300
[NaClO4], mM
B
d4A/d(nm)
0.2
0.1
0
-0.1
-0.2
-0.3
No NaClO4/r=1.823
45 mM NaClO4/r=1.768
90 mM NaClO4/r=1.355
135 mM NaClO4/r=1.137
180 mM NaClO4/r=1.081
260
270
280
290
300
310
Wavelength (nm)
C
S20,w (S)
6.0
5.5
5.0
4.5
4.0
3.5
3.0
0
50
100
150
200
250
300
350
[NaClO4], mM

changes observed show an increase in the A_{291nm}-A_{295nm} peak-to-trough distance, while that between A_{283nm}-A_{287nm} decreases. This ultimately results in the lower r obtained. Within the concentration range of $NaClO_4$ used, there is no evidence for loss of secondary structure, as reported (30). This is substantiated in Figure 3.24. Experiments using $NaClO_4$ are used here to determine and compare wild type and mutant dissociation constants. At each [$NaClO_4$], the fraction of dimeric enzyme was calculated. Activity, spectral changes, and sedimentation coefficients were used as probes of the enzyme's level of dissociation. This was accomplished by comparing the percent activity, r, and $S_{20,w}$ associated with a given [$NaClO_4$] to those obtained for dimeric and monomeric enzyme. A comparison of results from the different structural and catalytic probes is shown in Figure 3.25. The figure illustrates that changes occurring in activity, tertiary structure, and quaternary structure as a function of [$NaClO_4$] parallel one another, thus proving that the same event is being monitored in all cases.

3.4.2 Calculation of dissociation constants

For each concentration of $NaClO_4$ in which the enzymes were incubated, a K_d value was obtained. K_d was computed as described (see Section 2.2.16). A linear relationship between K_d and [$NaClO_4$] is established by plotting $\ln K_d$ versus [$NaClO_4$], as shown in Figure 3.26(A). Extrapolation to 0 mM $NaClO_4$ allows for the determination of the dimer's dissociation constant in the absence of $NaClO_4$. Using $\ln K_d$ at each [$NaClO_4$], ΔG was obtained and plotted, as illustrated in Figure 3.26(B). Extrapolation to 0 mM $NaClO_4$ in this instance yields information on the protein's conformational stability, or $\Delta G_{(H2O)}$ (89). Table 3.6 shows dissociation constants obtained for apo-wild type protein using activity, fourth

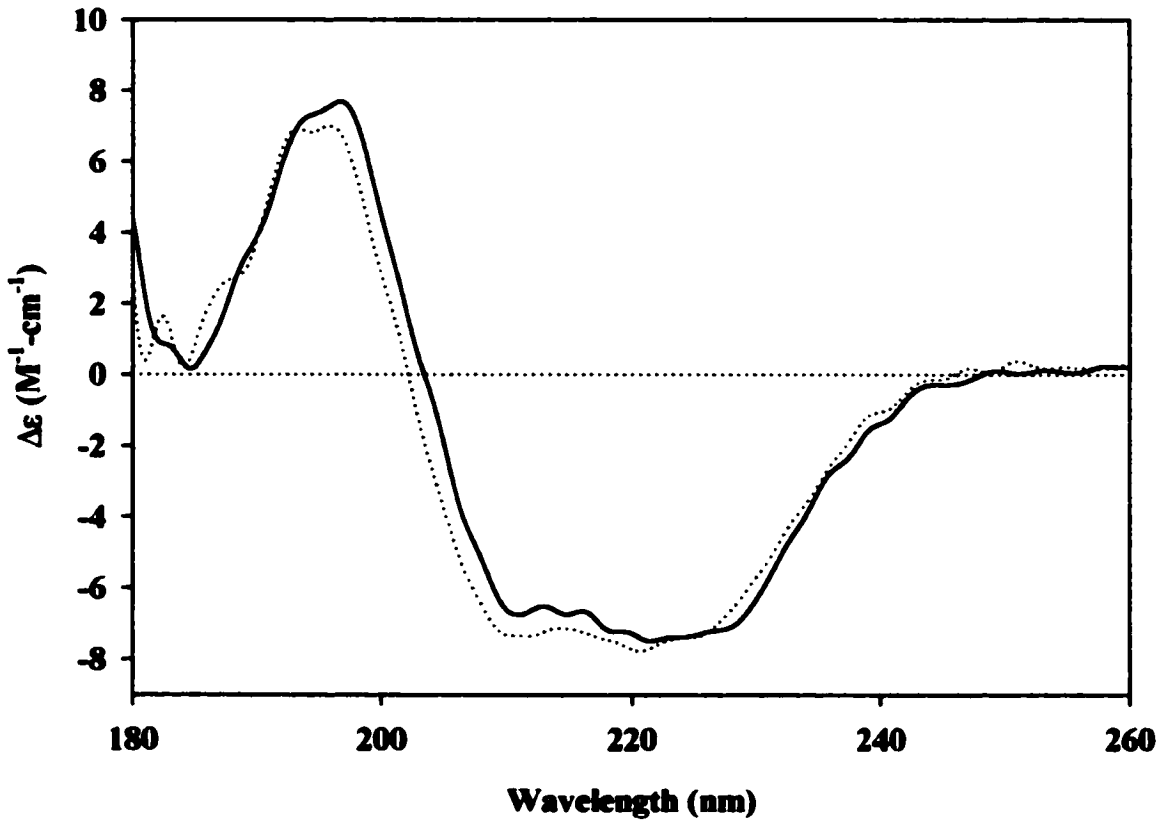

Figure 3.24 Peptide bond CD signal of wild type yeast enolase in 300 mM $NaClO_4$. Protein samples (10.6 μM) of apo-wild type scanned in 0 mM $NaClO_4$ (—), and in 300 mM $NaClO_4$ (·····). Parameters and buffer conditions were as described in Section 3.2.1.

derivative spectra r values, and $S_{20,w}$ values as probes of the effect of $NaClO_4$ on the enzyme. In general, results obtained are in reasonably good agreement. The agreement between activity and fourth derivative data is particularly good, with dissociation constants ca. 150 nM. AUC results vary somewhat, as fewer [$NaClO_4$] points were used, which resulted in larger standard errors. This probe yielded a K_d ca. 40 nM, which is comparable.

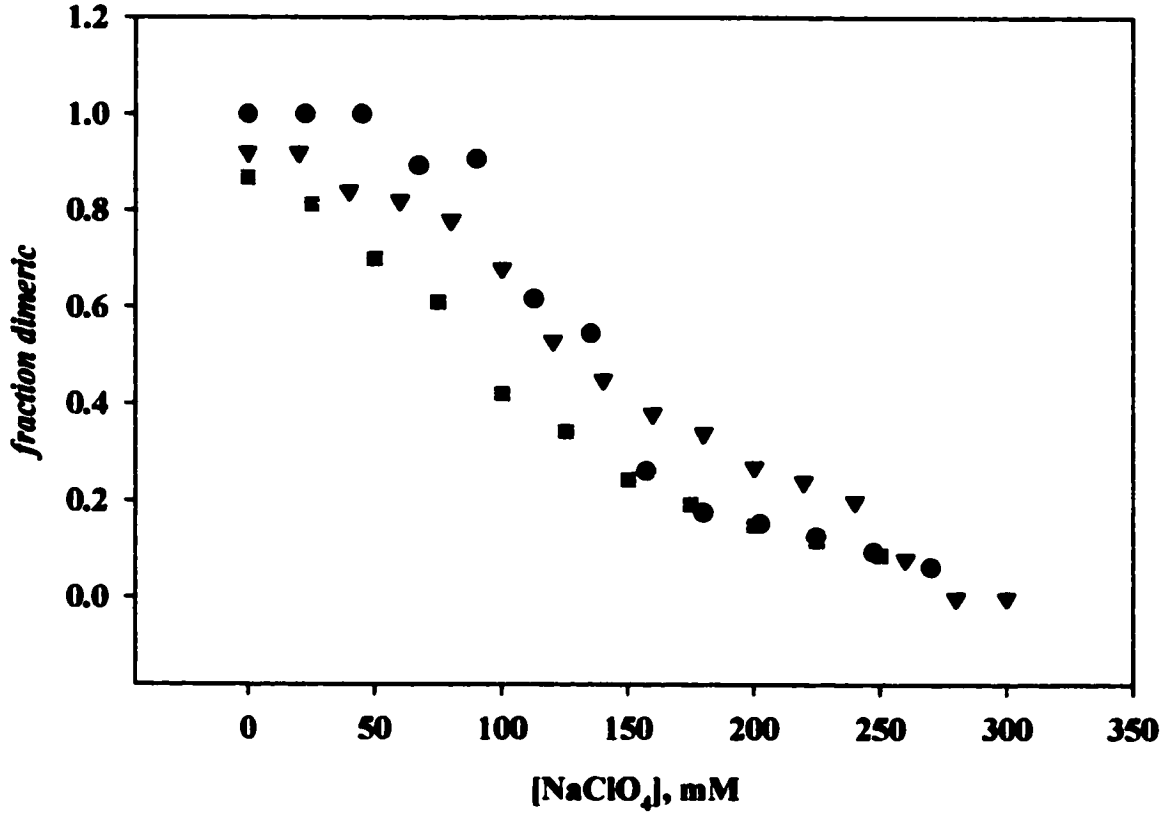

Figure 3.25 Comparison of activity, fourth derivative spectra r values, and $S_{20,w}$ values as probes of the effect on wild type yeast enolase of increasing [$NaClO_4$]. (●) Analytical ultracentrifugation data. ~10.6 μM protein samples were centrifuged at 20°C/42,000 RPM, scanning at 280 nm (as described in Section 2.2.11). (▾) Fourth derivative data. ~10.6 μM protein samples were scanned at 20°C/1 cm pathlength, as described (see Section 2.2.10). (▪) Activity data. ~8 nM enzyme were assayed at 20°C/240 nm in 50 mM Imidazole (pH 7.1)/1 mM $Mg(OAc)_2$/0.1 mM EDTA/250 mM KCl and 1 mM 2-PGA.

The W56F and E188D mutants were incubated in buffer containing varying concentrations of $NaClO_4$, as described for wild type. Their dissociation was monitored using activity and fourth derivative spectroscopy. Figure 3.27 illustrates their dissociation

Figure 3.26 Determination of K_d and $\Delta G_{(H2O)}$ constants.
A) $\ln K_d$ versus [$NaClO_4$]; B) ΔG versus [$NaClO_4$]. Graphs were obtained using activity data acquired for apo-wild type protein.

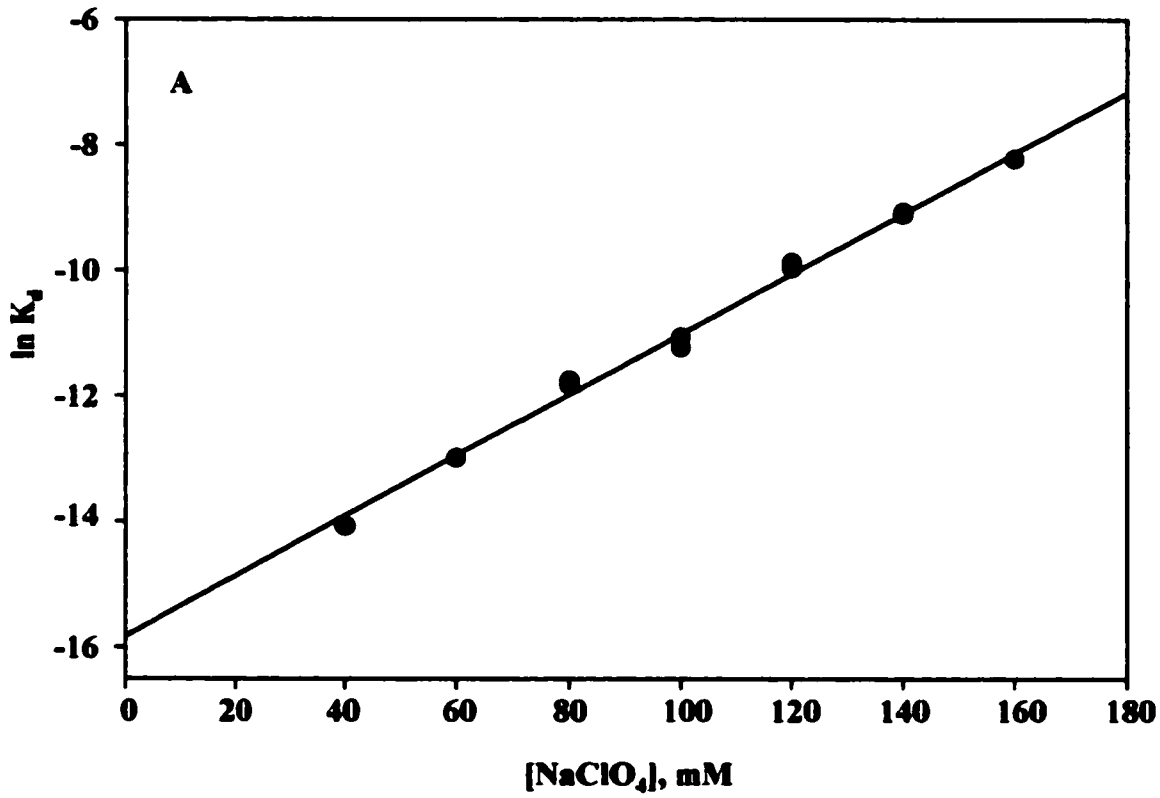
A
ln K_d
-6
-8
-10
-12
-14
-16
0
20
40
60
80
100
120
140
160
180
[$NaClO_4$], mM

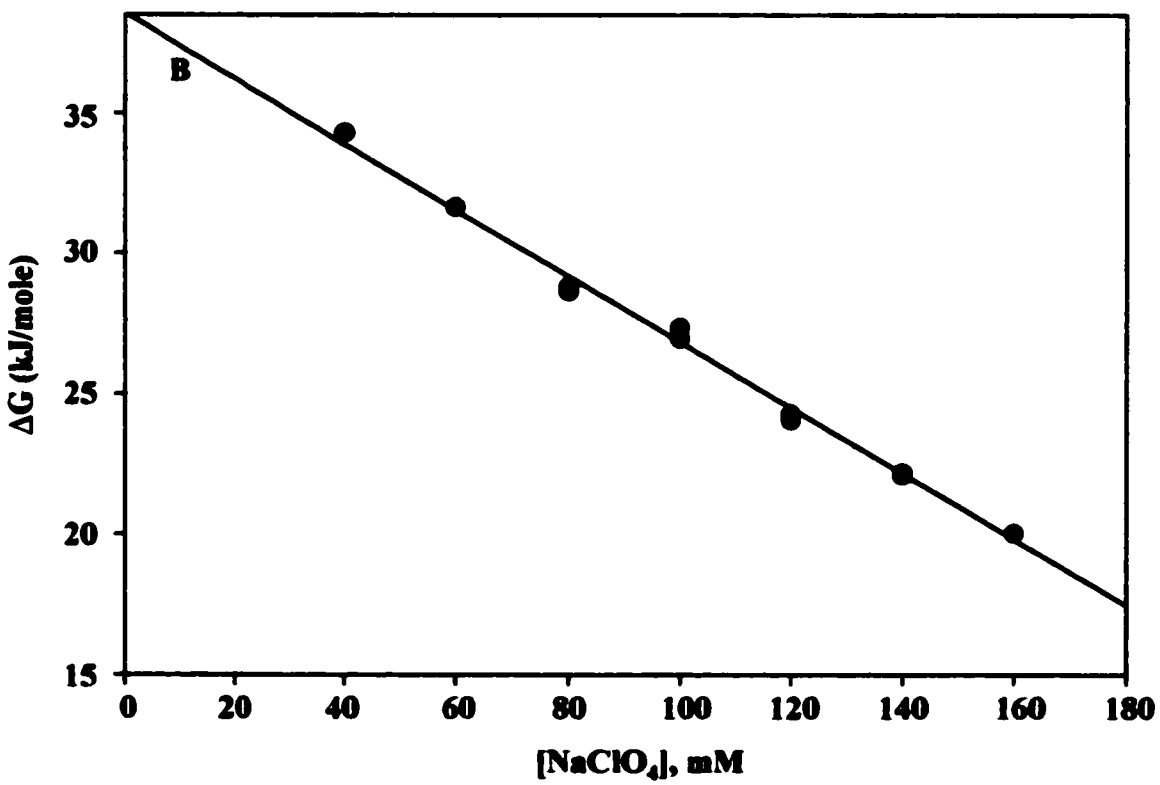
B
ΔG (kJ/mole)
35
30
25
20
15
0
20
40
60
80
100
120
140
160
180
[$NaClO_4$], mM

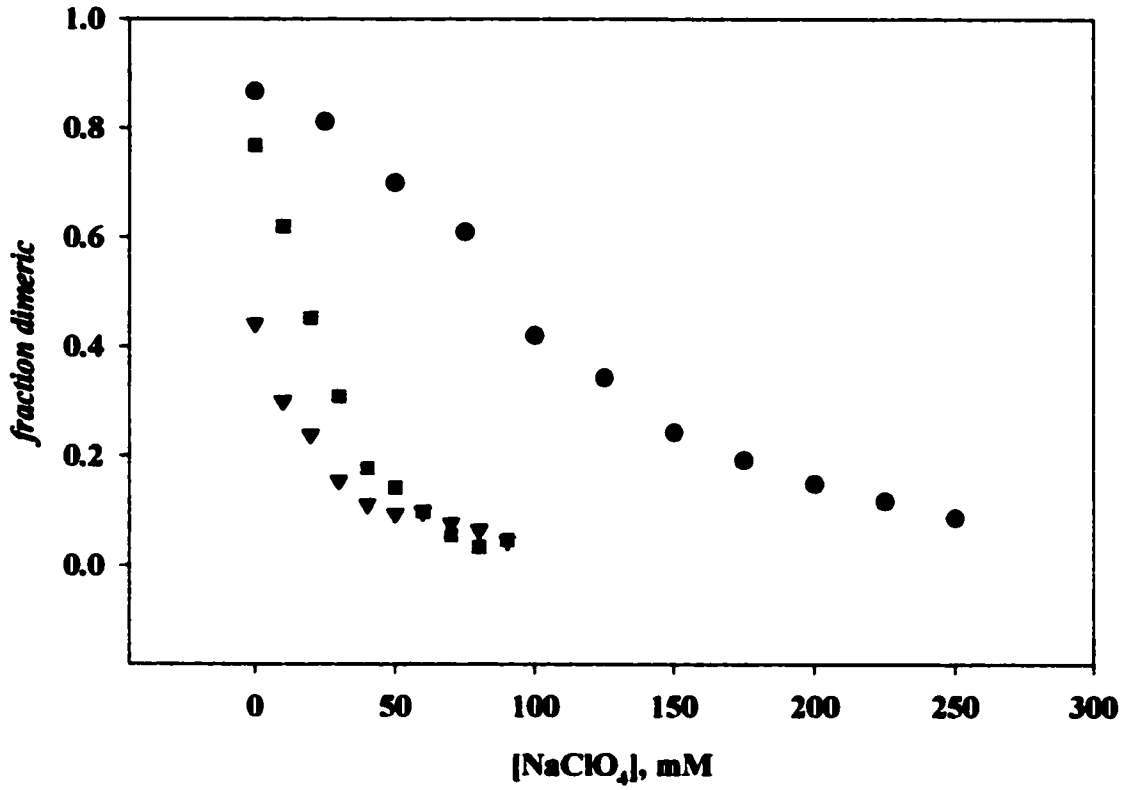

Figure 3.27 Comparison of the dissociation of the W56F and E188D mutants relative to that of wild type yeast enolase. Fraction dimeric enzyme is plotted versus [$NaClO_4$] using activity data obtained with apo-proteins. (●) Wild type; (▼) W56F; (■) E188D.

relative to that of wild type. The term dissociation is used appropriately here, as evidence presented in a previous section (see Figure 3.23(C), Section 3.4.1) shows that the chaotrope effectively brings about the dissociation of the dimer into its component monomers. In addition, dissociation is the single event monitored within the [$NaClO_4$] range utilized (see Figure 3.25, Section 3.4.1), and loss of secondary structure was not detected. The

differences are immediately and strikingly apparent. First, it is clear that both mutants are fully dissociated at considerably lower [$NaClO_4$]. Whereas wild type is fully dissociated by ~250 mM $NaClO_4$, the mutants are nearly completely dissociated ca. 60 mM perchlorate. Second, both mutants are not initially fully dimeric proteins, in accordance with analytical ultracentrifugation findings (see Section 3.2.5). The mutants thus dissociate substantially more readily than wild type, as they are already partially dissociated in their apo-forms in the absence of perchlorate. The dissociation constants determined for the apo-mutant proteins are also listed in Table 3.6. In cases where it was not possible to determine K_d from a dissociation curve, the dissociation constant was calculated from a single r and $S_{20,w}$ measured for the corresponding protein in 0 mM $NaClO_4$. The results demonstrate the weakened subunit dissociation of the mutants in a quantitative manner. That weakened subunit dissociation has resulted from the mutations is clear in both the range of $NaClO_4$ required for complete dissociation, and the sharpness with which dissociation occurs. This confirms that the targeted hydrogen bond at the subunit interface was successfully weakened by both mutations effected in its vicinity.

K_d values were calculated for each mutant. For each concentration of $NaClO_4$, the fraction of dimeric enzyme was calculated. As with the native enzyme, this was accomplished by comparing percent activity, r, and $S_{20,w}$ at a given [$NaClO_4$] with that of dimeric and monomeric enzyme. Dimeric values for activity, r, and $S_{20,w}$ were taken as those associated with each respective mutant in the presence of 1 mM Mg^{2+}/300 mM NaOAc and no perchlorate, as the mutants are dimeric in their cofactor-bound state (see Section 3.3.1, Figure 3.17). Monomeric r for each was taken as that associated with the respective spectra

Apo-protein	K_d (M)	$\Delta G_{(H2O)}$ (kJ/mole)	*m* (kJ-M^{-1}-mole^{-1})[a]	$[NaClO_4]_{1/2}$ (M)[b]
Wild Type	1.49×10^{-7} +/- 0.18	38.3 +/- 0.4	113.1 +/- 3.6	0.103
	1.50×10^{-7} +/- 0.30	38.3 +/- 0.7	92.3 +/- 7.0	0.131
	4.14×10^{-8} +/- 0.75	41.4 +/- 1.8	109.7 +/- 12.2	0.132
W56F	3.36×10^{-5} +/- 0.06	25.1 +/- 0.2	137.9 +/- 6.0	N.D.[c]
	3.33×10^{-5}	25.1	N.D.	N.D.
	2.4×10^{-5}	25.9	N.D.	N.D.
E188D	8.50×10^{-6} +/- 0.13	28.4 +/- 0.3	169.9 +/- 8.2	0.011
	5.29×10^{-6} +/- 0.22	29.6 +/- 0.5	248.0 +/- 14.6	0.012
	4.0×10^{-6}	30.3	N.D.	N.D.

Table 3.6 Thermodynamic constants for wild type and mutant enolases. Results based on activity are shown in black, whereas those obtained using fourth derivative UV spectra and AUC are shown in red and blue, respectively. All data are shown with corresponding standard errors on one single determination, with the exception of E188D's activity data, which represent an average of two determinations. Fourth derivative and AUC analysis was carried out on 10.6 μM protein samples. Activity assays were carried out using ~10 nM wild type, ~180 nM W56F, and ~20 nM E188D. Fourth derivative data for W56F, and AUC data for both W56F and E188D represent the constants calculated using the monomeric r and $S_{20,w}$ values reported in previous sections (see Sections 3.2.4 and 3.2.5).

[a] *m* is the slope when plotting ΔG versus $[NaClO_4]$.

[b] $[NaClO_4]_{1/2}$ is the concentration of the chaotropic salt needed to produce a 50% equilibrium mixture of monomers and dimers.

[c] N.D. These correspond to K_d obtained from single values of r and $S_{20,w}$ in the absence of perchlorate, *i.e.*, these data were not obtained from dissociation curves as a function of $NaClO_4$.

in 150 mM $NaClO_4$. Sedimentation coefficients for monomeric and dimeric mutants were assumed to be identical to those obtained for wild type.

The W56F mutant is particularly susceptible to dissociation, even at very low

[$NaClO_4$]. As a result, it was extremely difficult to obtain reproducible dissociation curves using the spectral probe, as very important changes occur in a very narrow and very low $NaClO_4$ concentration range. Activity thus proved to be the best probe of this apo-mutant's dissociation. Subunit association is weakened by 2-3 orders of magnitude for W56F, and by 1-2 orders of magnitude for E188D, with dissociation constants residing in the micromolar range for both. Data acquired using activity in the case of W56F is in very good agreement with K_d values calculated from a single point using the fourth derivative r and $S_{20,w}$ reported for the apo-mutant in 0 M perchlorate (see Sections 3.2.4 and 3.2.5). E188D data equally compare fairly well. $[NaClO_4]_{1/2}$ is most certainly considerably lower than is the case for wild type, although it was impossible to determine its precise value for W56F. This is due to the fact that the mutant is already >50% dissociated in the absence of perchlorate.

The dissociation of holo-W56F was monitored using fourth derivative spectroscopy. As discussed, the spectrum of W56 as it resides in the wild type protein may be obtained by subtracting the W56F spectrum from that of wild type (see Figure 3.14, Section 3.2.4). By obtaining such spectra as a function of [$NaClO_4$], it is possible to examine the changes in environment that occur at this position as the protein dissociates. It is also possible to compare the spectra of dissociating wild type protein to those of dissociating W56F. By making such a comparison, it is possible to determine which changes occurring in wild type upon dissociation are due to W56. An analogous shift occurring in both proteins cannot be attributed to W56. Figure 3.28 illustrates the spectral changes occurring in holo-W56F

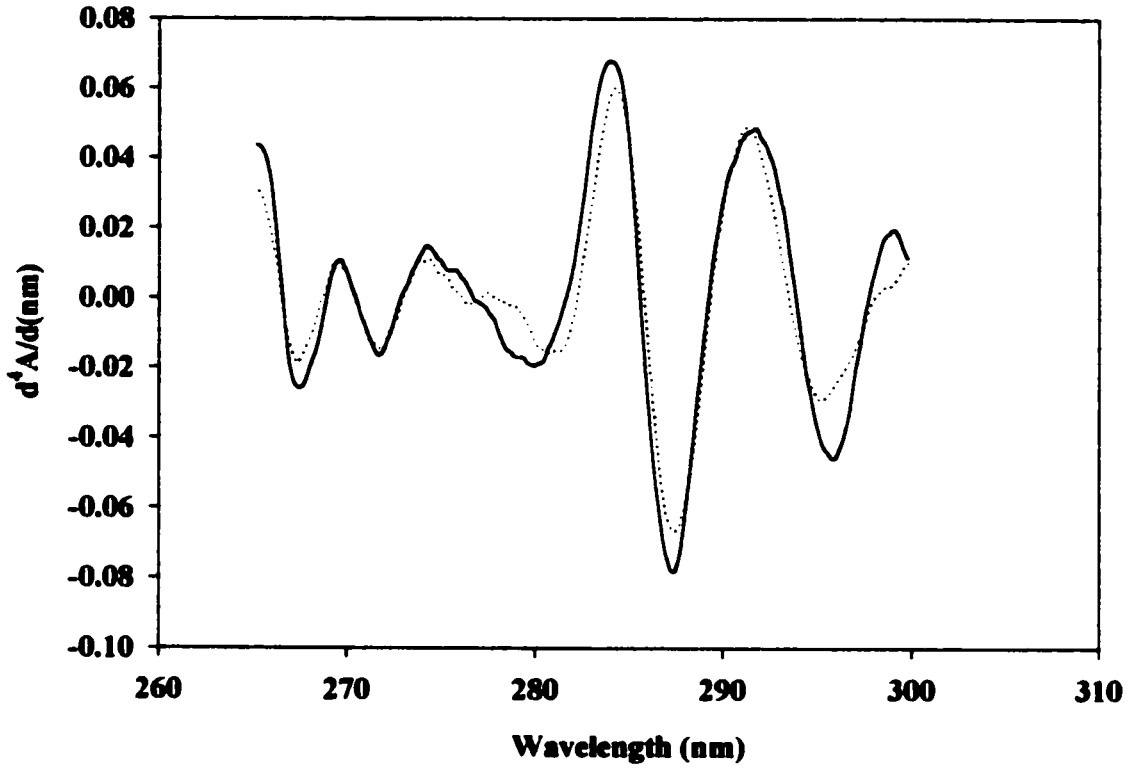

Figure 3.28 Dissociation of holo-W56F mutant yeast enolase with increasing [$NaClO_4$]. Holo-W56F is shown in 0 mM (—) and 180 mM $NaClO_4$ (·····).

mutant upon dissociation. The holo-mutant was used for this comparison, as the apo-form is already substantially dissociated in the absence of perchlorate. A comparison with the changes reported for wild type in Figure 3.23 (B) reveals that different changes occur at the 287 nm, 291 nm, and 295 nm peak positions. Thus, these can be attributed, at least in part, to W56.

Quantitative results confirm that subunit interactions have been weakened in the

mutant proteins, as revealed by the increased dissociation constants. The depressed subunit association observed is substantial, especially since it is attributed to one single weakened hydrogen bond. Plots of ΔG versus $[NaClO_4]$ show that the apo-mutants reside in a considerably more "loose" conformation upon dissociation. This is revealed by the increased slope, or *m*, which represents the solvent accessible protein surface area (89).

3.4.3 Mg^{2+} binding protects against dissociation: Determining K_d for the holo-mutants

$NaClO_4$ incubations were prepared for protein samples in the presence of 1 mM Mg^{2+}. These then were treated and analyzed in the manner described for apo-protein samples. This was carried out in order to determine the holo-mutant protein dissociation constants relative to wild type, and to study the effect of metal binding on K_d. It was of interest to determine if the dimeric mutants recovered wild type-range dissociation constants, as well as the extent of the protection against dissociation afforded them by Mg^{2+}. Figure 3.29 shows results obtained using wild type, as monitored by the three probes. These data clearly show that cofactor protects against dissociation, as higher $[NaClO_4]$ is needed to effect and complete the dissociation process. Apo-protein samples of wild type were monomeric by 250 mM $NaClO_4$, whereas holo-protein samples required closer to 300 mM $NaClO_4$ to bring about more complete dissociation. Analogous mutant results are shown in Figure 3.30. It is clear that Mg^{2+} protects both mutants against dissociation. Although W56F is almost fully dissociated within the same $[NaClO_4]$ range, the protection is nonetheless important given its stabilizing effect on K_d and $[NaClO_4]_{1/2}$. The protection of E188D against dissociation is further emphasized by the notable change in $[NaClO_4]$ required to

Figure 3.29 Comparing the dissociation of apo versus holo-wild type yeast enolase in the presence of $NaClO_4$. A) Activity data. A typical assay required ~14 nM of Mg^{2+}-pre-incubated enzyme. B) Fourth derivative data. Data were from scans of 10.6 μM protein samples. C) AUC data. Data were from centrifugations of 10.6 μM protein samples. (●) Apo-protein; (▼) holo-protein.

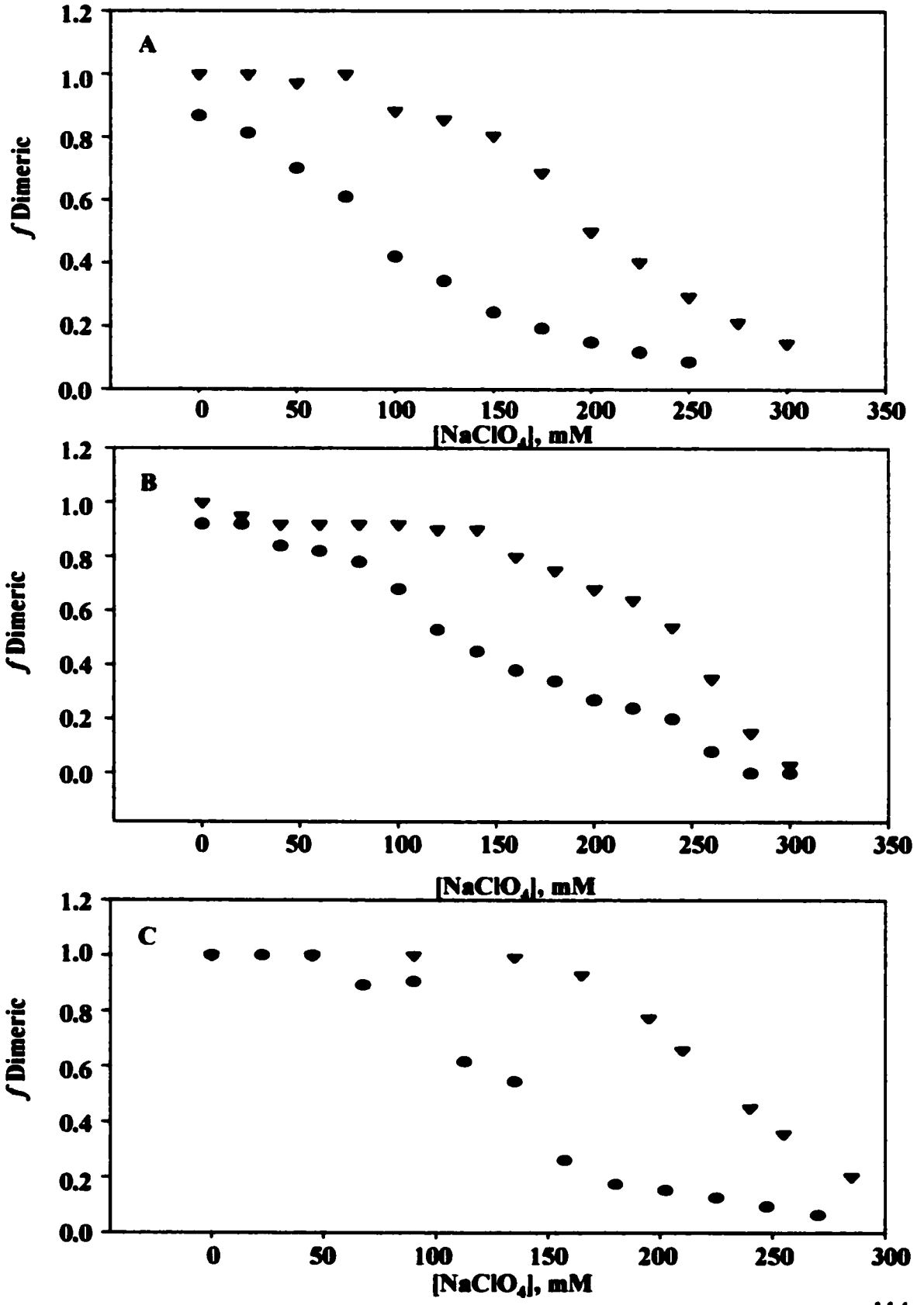
A
B
C
f Dimeric
[NaClO4], mM
1.2
1.0
0.8
0.6
0.4
0.2
0.0
0
50
100
150
200
250
300
350

Figure 3.30 Comparing the dissociation of apo versus holo-mutants of yeast enolase in the presence of $NaClO_4$. A) W56F activity data. A typical assay required ~26 nM of holo-W56F. B) E188D fourth derivative data. Data were from scans of 10.6 μM holo-E188D protein samples. C) E188D activity data. A typical assay required ~20 nM of holo-E188D enzyme. (●) Apo-enzymes; (▼) holo-enzymes.

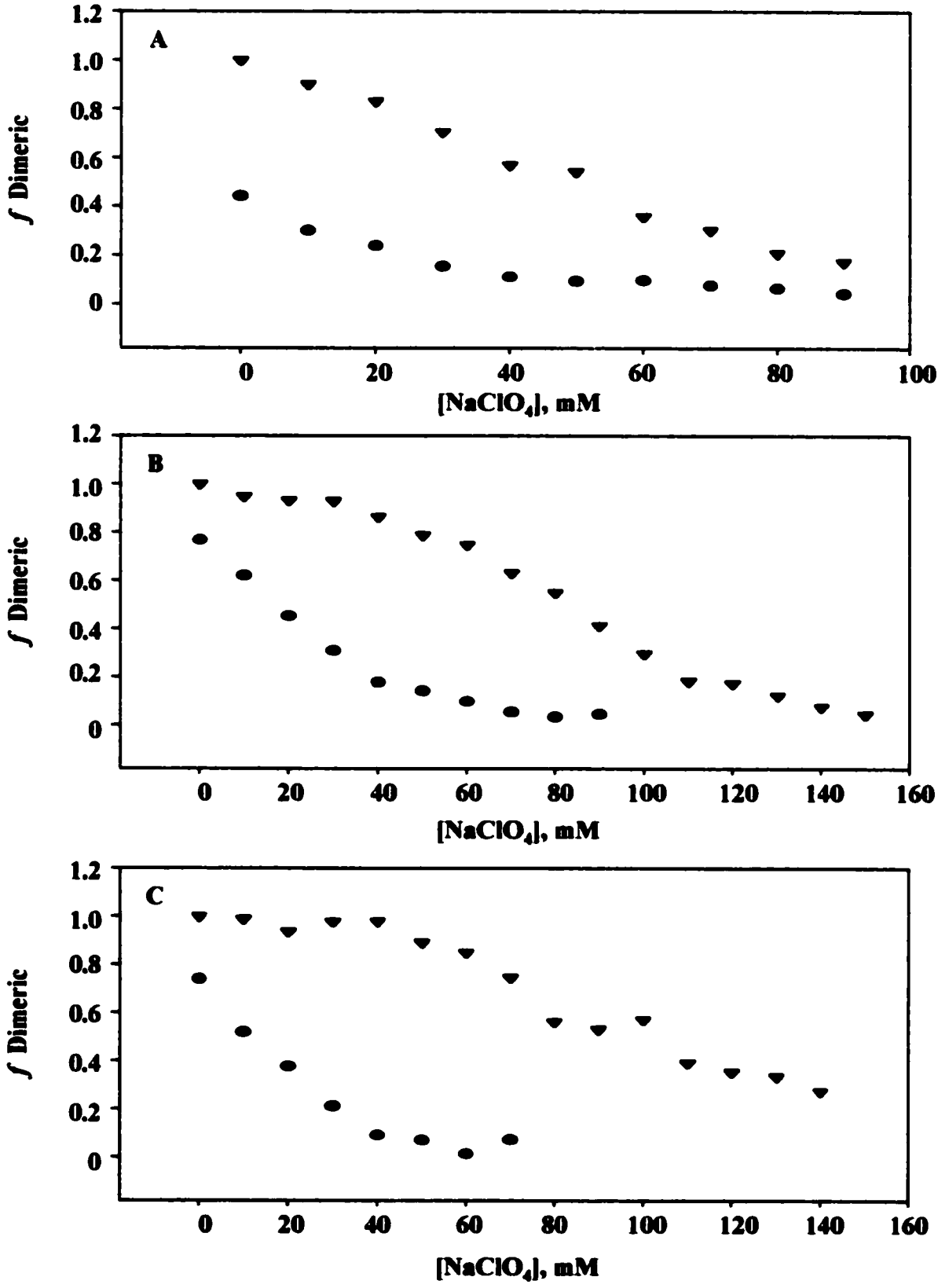
A
B
C
f Dimeric
[NaClO4], mM
1.2
1.0
0.8
0.6
0.4
0.2
0
0
20
40
60
80
100
120
140
160

Holo-protein	K_d (M)	$\Delta G_{(H2O)}$ (kJ/mole)	m (kJ-M^{-1}-$mole^{-1}$)	$[NaClO_4]_{1/2}$ (M)
Wild Type	3.40×10^{-9} +/- 0.20	47.5 +/- 0.5	101.7 +/- 2.2	0.205
	1.57×10^{-8} +/- 0.62	43.8 +/-1.5	72.6 +/- 7.1	0.240
	2.62×10^{-9} +/- 0.56	48.2 +/- 1.4	93.3 +/- 5.5	0.234
W56F	3.35×10^{-7} +/- 0.23	36.5 +/- 0.6	225.2 +/- 12.0	0.043
	1.07×10^{-7} +/- 0.10	39.1 +/- 0.2	185.7 +/- 4.2	0.062
	N.D.	N.D.	N.D.	N.D.
E188D	6.80×10^{-8} +/- 0.16	40.2 +/- 0.4	159.8 +/- 4.9	0.079
	2.80×10^{-8} +/- 0.54	42.4 +/- 1.3	158.1 +/- 14.8	0.101
	N.D.	N.D.	N.D.	N.D.

Table 3.7 Holo-protein constants. All data are shown with corresponding standard errors on one single determination, with the exception of activity data reported for W56F and E188D, which represent an average of two determinations. Activity assays typically required ~14 nM wild type, ~26 nM W56F, and ~20 nM E188D. Fourth derivative and AUC analysis was carried out on 10.6 μM protein samples. Color assignments are as described for Table 3.6.

effect complete dissociation. In either case, the holo-mutants' $[NaClO_4]_{1/2}$ remain substantially lower than for the holo-wild type protein. This suggests that although the mutants are dimeric in the presence of 1 mM Mg^{2+} (0 mM $NaClO_4$), they remain considerably more readily dissociable than wild type. The extrapolated constants for holo-proteins' dissociation are reported in Table 3.7.

Wild type data show considerable protection when incubated in the presence of Mg^{2+}. This is evident in the K_d, which has decreased by ~2 orders of magnitude. On average, m,

or the solvent accessible protein surface area, has also seen a decrease, which points to a more closed protein conformation in saturating Mg^{2+}. A substantial increase in $[NaClO_4]_{1/2}$ also relates to the dimeric enzyme's increased stability, whereby it is now much less readily dissociable. Protection is especially noted in the case of the variant proteins, as evidenced by data presented in Figure 3.30. The significant stabilization of the mutants is clear, although they retain significantly lower $[NaClO_4]_{1/2}$. They retain a measure of the weakened subunit association initially apparent in their apo-form, although K_d constants show improvement upon cofactor binding. Comparatively speaking, E188D has a tighter K_d relative to W56F, and higher $[NaClO_4]$ are required to fully dissociate the former, all of which make it more stable than the latter in their dimeric forms. Binding of Mg^{2+} decreases solvent exposure in E188D, whereas this is not apparent with W56F. The rapid reactivation of the latter in its apo-state, and the inherent difficulties in obtaining dissociation curves reflective of the apo-mutant's level of activity render a true estimate of this protein's *m* problematic. Mg^{2+}, based on previous evidence, most assuredly decreases the mutant's solvent accessibility, regardless of the reported apo and holo *m* values.

The protection from dissociation with Mg^{2+} is emphasized further for the mutants. An analogous experiment was carried out in which the [protein] was varied, and the effect on $S_{20,w}$ monitored (see Section 3.2.5). As discussed, an effect on the sedimentation coefficient suggests that the system under study is dissociating. As outlined, the mutants are fully dimeric in the presence of 1 mM Mg^{2+}. Table 3.8 illustrates $S_{20,w}$ for each mutant over a 10 fold [protein] range. The results show that dissociation is far less extensive, relative to results obtained for the apo-enzymes, at lower concentrations where dissociation tends

[Protein], mg/ml	$S_{20,w}$ (S)
1.0	5.451/5.457
0.5	5.299/5.382
0.1	5.144/5.297

Table 3.8 Protection against dissociation for mutants of yeast enolase in the presence of saturating Mg^{2+}. $S_{20,w}$ are listed in black for W56F, and in red for E188D.

to be favored, and this in support of the dimerizing influence of the cofactor.

3.4.4 Substrate binding also protects against dissociation: Determining K_d for 2-PGA-bound holo-proteins

Substrate protection was studied by preparing $NaClO_4$ incubations of holo-enzymes + 1 mM 2-PGA, enolase's natural substrate. Samples were assayed for activity as described, and the data compared. Figure 3.31 illustrates the dissociation patterns for the holo-proteins when pre-incubated with 2-PGA. Substrate protection is most marked for W56F, and stabilization of wild type and E188D proteins is observed. The dissociation constants extrapolated are listed in Table 3.9.

Protection by substrate is considerable in W56F, as association is tightened substantially. The substrate bound mutants are dimeric, and do not show further dimerization. Table 3.10 shows how 2-PGA binding has produced a more compact quaternary assembly of the proteins, as seen by the higher $S_{20,w}$ relative to values reported for holo-proteins. The mutants remain more readily dissociable, as is evident by their depressed $[NaClO_4]_{1/2}$. Although dimeric, the mutants equally retain significantly higher *m*,

Figure 3.31 Comparing the dissociation of holo versus 2-PGA-bound holo-proteins in the presence of $NaClO_4$. Activity data is shown. A) Wild type; B) W56F; C) E188D. (●) Holo-proteins; (▾) holo-proteins + 1 mM 2-PGA.

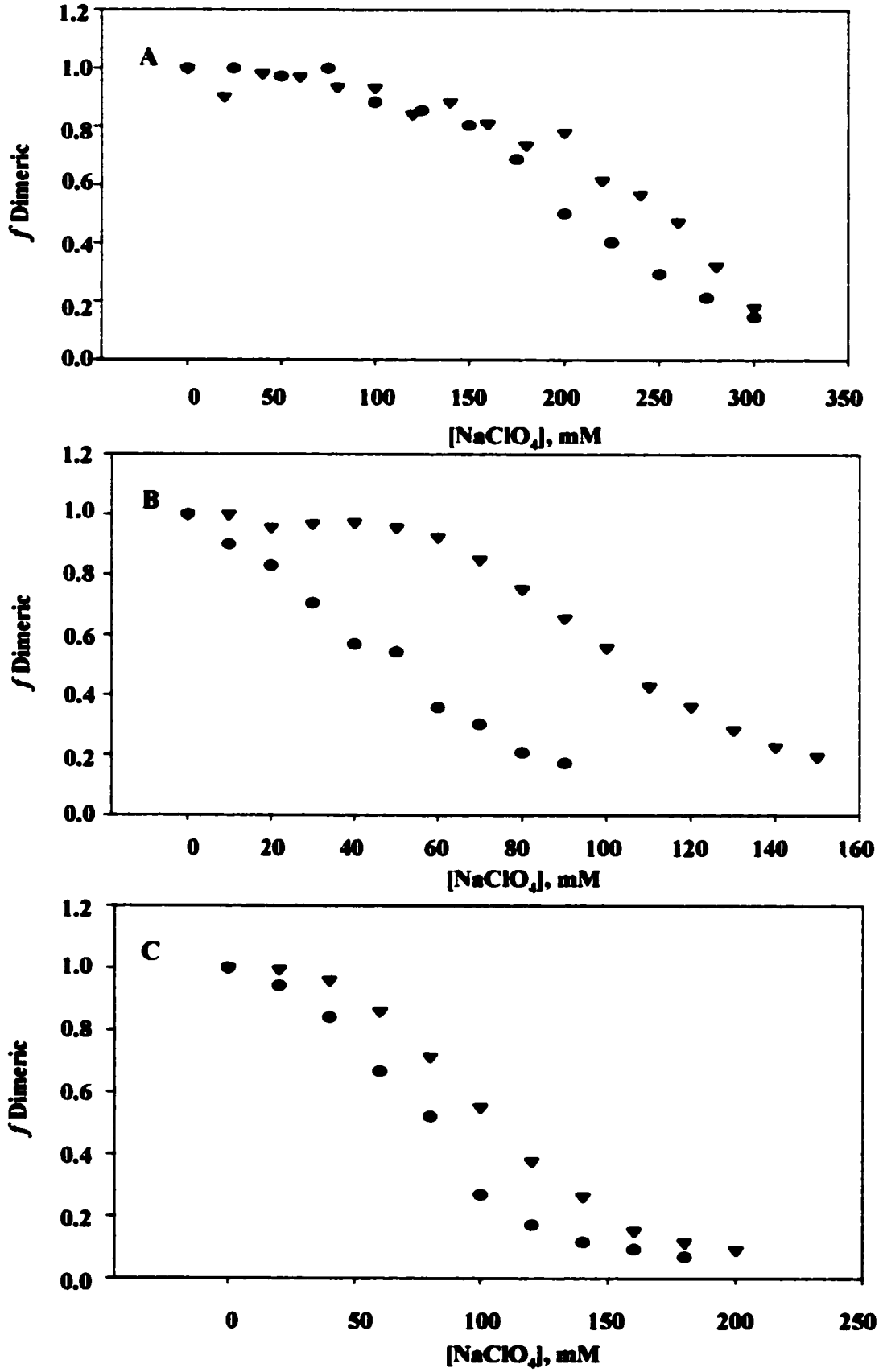
A
B
C
f Dimeric
[NaClO4], mM
1.2
1.0
0.8
0.6
0.4
0.2
0.0
0
50
100
150
200
250
300
350
20
40
60
80
120
140
160

Protein	K_d (M)	$\Delta G_{(H2O)}$ (kJ/mole)	*m* (Joules-M^{-1}-$mole^{-1}$)	$[NaClO_4]_{1/2}$ (M)
Wild Type	$2.0x10^{-9}$ +/- 0.5	48.8 +/- 1.2	87.9 +/- 4.7	0.253
W56F	$2.68x10^{-8}$ +/- 0.34	43.0 +/- 0.8	178.6 +/- 10.7	0.106
E188D	$2.35x10^{-8}$ +/- 0.28	42.8 +/- 0.7	153.4 +/- 7.5	0.101

Table 3.9 Dissociation constants for 2-PGA-bound holo-proteins. Activity data are represented as an average of two determinations +/- standard errors for W56F and E188D, and one single determination for wild type. Activity assays typically required ~14 nM wild type, ~28 nM W56F, and ~20 nM E188D.

Protein	$S_{20,w}$ (S)
Wild Type	5.488
W56F	5.556
E188D	5.452

Table 3.10 Effect of 2-PGA binding on $S_{20,w}$. Data were obtained from centrifugations of 10.6 μM protein samples in 1 mM Mg^{2+}/1 mM 2-PGA.

Protein	Fluorescence Intensity	λ_{max} (emission) (nm)
Wild Type	905	338
W56F	424	335
E188D	611	338

Table 3.11 Fluorescence data for 2-PGA-bound holo-proteins. Signals were monitored on 1.06 μM protein samples in 1 mM Mg^{2+}/1 mM 2-PGA.

suggesting that their quaternary packing is not as efficient as with wild type, and that solvent exposure is greater. Higher *m* values explain the increased readiness with which the mutants dissociate. The increased solvent exposure is also indicated in fluorescence data obtained for substrate bound mutants, which retain significantly lower signal intensities. The data shown in Table 3.11 supports the findings of *m*, as quenching may result from increased exposure to bulk solvent, especially with E188D. This, however, is coupled to the loss of one Trp in the case of W56F.

3.4.5 Evolution of protection

A summary of K_d and *m* values obtained for apo-proteins versus holo and substrate bound holo-proteins is presented in Tables 3.12 and 3.13, respectively. A graphical comparison of K_d as a function of dimerization is shown in Figure 3.32. The three proteins show that cofactor binding strengthens subunit association by two orders of magnitude. The impact of magnesium binding is important, as it re-associates the mutants. The binding of substrate also produces tighter association, and this is conveyed by favoring more compact/ closed overall quaternary packing. The effect of cofactor and substrate are each believed to be mediated via their respective effect on the conformation of the mobile loop regions. *m* values generally decrease as tighter protein assemblies are favored. However, the behavior of W56F in going from its apo to its holo-form is atypical. This is reflective of the difficulties encountered in obtaining *m* which are truly representative of the mutant's apo-state. The complexity arises in the rapid reactivation of the apo-W56F mutant under the assay conditions specified, as the presence of saturating magnesium leads to re-association.

Protein	Apo	Holo	Holo + 2-PGA
Wild Type	1.49×10^{-7} +/- 0.18	3.40×10^{-9} +/- 0.20	2.0×10^{-9} +/- 0.5
W56F	3.36×10^{-5} +/- 0.06	3.35×10^{-7} +/- 0.23	2.68×10^{-8} +/- 0.34
E188D	8.50×10^{-6} +/- 0.13	6.80×10^{-8} +/- 0.16	2.35×10^{-8} +/- 0.28

Table 3.12 A summary of K_d values. The dissociation constants of all proteins in apo, holo, and substrate bound holo-forms are compared. Data represents that obtained from activity assays.

Protein	Apo	Holo	Holo + 2-PGA
Wild Type	113.1 +/- 3.6	101.7 +/- 2.2	87.9 +/- 4.7
W56F	137.9 +/- 6.0	225.2 +/- 12.0	178.6 +/- 7.5
E188D	169.9 +/- 8.2	159.8 +/- 4.9	153.4 +/- 7.5

Table 3.13 A summary of *m*. *m* corresponding to data shown in Table 3.12 are listed.

Figure 3.32 K_d as a function of association. Graphs represent K_d values obtained from activity experiments. (A) Wild type; (B) W56F; (C) E188D. (●) Apo-proteins; (▼) holo-proteins; (■) substrate bound holo-proteins.

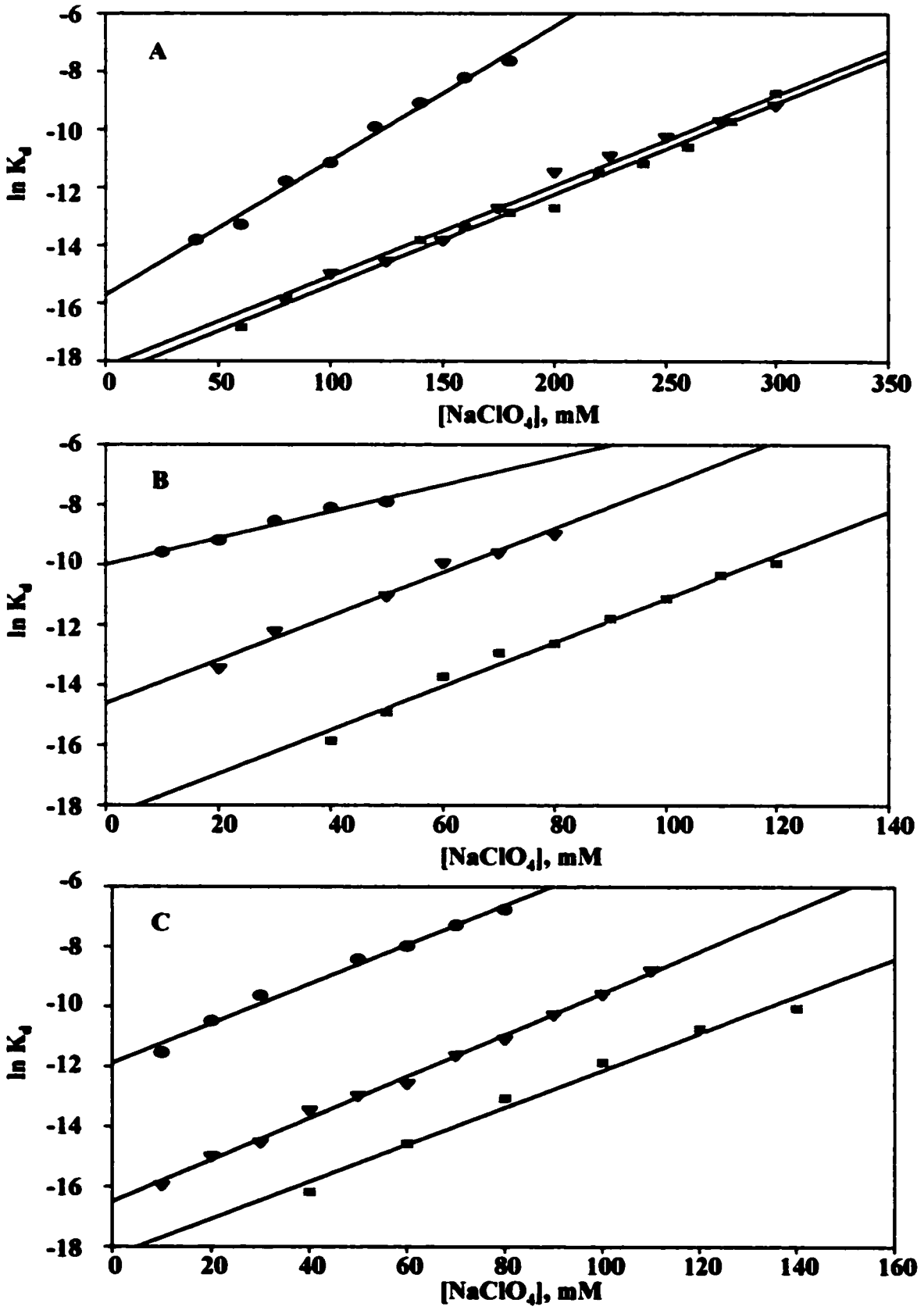
A
B
C
ln K_d
[$NaClO_4$], mM
-6
-8
-10
-12
-14
-16
-18
0
50
100
150
200
250
300
350
20
40
60
80
120
140
160

3.5 Kinetics

Having characterized the W56F and E188D mutants on a structural level, a detailed catalytic study was subsequently undertaken. The proteins were titrated with cofactor and substrate, and the kinetic parameters extracted. Kinetic experiments were also carried out using Mn^{2+} as the cofactor. As discussed, Mn^{2+} is third to Mg^{2+} in its ability to activate enolase (see Chapter 1, Section 1.3.3), and detailed kinetic studies using Mn^{2+} have been reported (53, 54). Results are listed in Table 3.14.

Results show decreased k_{cat} for both mutants when titrated with Mg^{2+}, with that of W56F retaining only ~30% of wild type activity, and E188D displaying ~65% activity. The Mg^{2+} kinetics are interesting in that they show slightly higher Michaelis constants for both mutants, and significantly higher K_i for magnesium in the case of E188D. Increased K_M may point to weaker magnesium binding in the mutants, although this could only be confirmed by determining K_d for Mg^{2+}. Inhibition by high [magnesium] is altered in W56F, and requires somewhat higher [Mg^{2+}] for inhibition, while E188D is barely inhibited even at 20 times the highest [Mg^{2+}] normally assayed. Catalytic efficiency is depressed for both mutants, and the energetic differences in their ability to carry out catalysis, relative to wild type, are significant.

W56F shows depressed activity when titrated with manganese and substrate, whereas E188D's catalytic ability is close to wild type's. K_M constants are unchanged for the two mutants with respect to Mn^{2+} and 2-PGA, and K_i is significantly higher for Mn^{2+} in E188D. However, the catalytic efficiency of the latter is unchanged relative to wild type. The catalytic differences are important for W56F, with substantially decreased kinetic efficiency,

Protein	k_{cat} (s^{-1})	K_M (μM)	K_i (μM)	k_{cat}/K_M (M^{-1}-s^{-1})	ΔΔG (kJ/mole)
Wild Type	64.4	107.1 +/- 8.4	5653 +/- 953	$6.0x10^5$	-
	39.4	7.1 +/- 0.7	60.8 +/- 6.2	$5.5x10^6$	-
	76.6	113.5 +/- 17.8	-	$6.7x10^5$	-
W56F	19.5	168.5 +/- 13.6	8817 +/- 1066	$1.2x10^5$	3.9
	12.3	9.7 +/- 1.8	33.0 +/- 6.4	$1.3x10^6$	3.5
	27.4	72.3 +/- 8.1	-	$3.8x10^5$	1.4
E188D	41.1	196.2 +/- 15.0	$2.0x10^5$ +/- 6408	$2.1x10^5$	2.6
	28.2	5.6 +/- 0.4	204.4 +/- 18.4	$5.0x10^6$	0.23
	74.4	116.6 +/- 11.2	-	$6.4x10^5$	0.11

Table 3.14 Kinetic parameters. Kinetics in the presence of Mg^{2+} are listed in black, whereas the kinetics in the presence of Mn^{2+} and 2-PGA are listed in red and blue, respectively.

as seen by the k_{cat}/K_M ratio, and the ΔΔG for activity. K_M for 2-PGA is unchanged for both.

Decreased catalysis for W56F is consistent, and is also more marked than is the case for E188D. This may be due to disruption of the mobile loop in which W56 resides. Long range conformational changes may have led to disruptions of the active site loop immediately (Pro35-Gly60), making it unable to undergo the closure needed for proper Mg^{2+} coordination, and, therefore, proper catalysis. The altered Mg^{2+} inhibition caused by the two mutations suggests that the third metal binding site may have been disrupted by these substitutions. In effect, the location of the inhibitory binding site is as yet unknown, but

these results suggest that it may lie in the vicinity of the subunit interface. Inhibition by Mn^{2+} is not as significantly affected by the mutations, suggesting that the disruption effected at the inhibitory binding site is such that Mn^{2+} is now even better accommodated at this site than is Mg^{2+}.

Specific activities were calculated for wild type and mutant proteins under the assay conditions described for inactivation experiments (*i.e.*, 1 mM Mg^{2+}/1 mM 2-PGA). For samples of enzyme pre-incubated in the presence of 1 mM Mg^{2+}, specific activities of $1.26*10^5$ μM-min^{-1}-mg^{-1} for wild type, $5.4*10^4$ μM-min^{-1}-mg^{-1} for W56F (~50 % loss of activity in its dimeric form) , and $8.3*10^4$ μM-min^{-1}-mg^{-1} for E188D were calculated. Samples of apo-incubated proteins showed much lower specific activities, with ~10 times more W56F enzyme needed to produce measurable activity slopes. Apo-mutants show decreased activity due to a higher fraction of the enzyme in its monomeric/inactive state.

Chapter 4: Discussion

4.1 Structural characterization of the W56F and E188D yeast enolase mutants

A purification scheme for recombinant yeast enolase has been optimized by adaptation of protocols previously reported (28, 47). The procedure includes $(NH_4)_2SO_4$ fractionation, along with two ion exchange chromatography steps. This method produces high yields of recombinant protein, frequently exceeding 200 mg from four liters of culture (see Table 3.1 in Section 3.1.2), in agreement with published purification results (47). The protein obtained is highly pure. Analysis by Coomassie Blue-stained SDS-PAGE and analytical ultracentrifugation has shown the preparations to be well over 90% homogeneous (see Figure 3.5, Section 3.1.2). The enzyme is highly active, with specific activities ca. 120 Units/mg when appropriately desalted. Protein pools are free of host *E. coli* enolase, as established in Section 3.1.3. A biophysical characterization of the recombinant protein demonstrated structural and catalytic integrity relative to its native counterpart, isolated and obtained commercially (see Figures 3.6 and 3.7, Section 3.1.4).

The W56F and E188D mutants were prepared using the Quickchange (Stratagene) method. DNA sequence analysis revealed that the desired substitutions had indeed been effected, and that unwanted spurious mutations had not been introduced. The mutant

proteins were expressed and purified as described for wild type. Both mutants showed increased interaction with anion and cation exchange resins, suggestive of dissociation-induced exposure of previously buried side chains (see Figure 3.8, Section 3.1.5). Increased solvent exposure of residues which were previously either buried or only partially solvent exposed may indicate a more open protein conformation. This in turn, may result from a more loosely-held hydrogen bond at the subunit interface, having been weakened in this case by site-directed mutagenesis. Purification results (see Figure 3.9 & Table 3.3, Section 3.1.5) indicate that the mutants are well expressed, and that activity has been depressed considerably in the case of W56F. This could be due to one or both of the following: 1) W56F shows decreased k_{cat} in its dimeric form; 2) W56F is dissociated at least in part, leading to an increased fraction of the enzyme present in its inactive monomeric form, thus producing the depressed k_{cat} observed. Further characterization of the mutant's catalytic properties was carried out, the results of which are discussed below.

W56F and E188D were characterized structurally in order to verify the effects of these substitutions on the enzyme. Both mutants showed identical secondary structural folding patterns relative to wild type, with peptide bond CD spectra which were virtually superimposable (see Figure 3.10, Section 3.2.1). In contrast, extensive changes were observed in their respective tertiary structures, relative to wild type, as revealed by circular dichroism and fluorescence spectroscopy (see below).

Circular dichroic spectra collected on the proteins were particularly informative. Some of the changes observed for the W56F variant are intuitive: phenylalanine signals intensify, whereas tryptophanyl signals diminish. Those seen with the E188D variant,

however, are not. In this case, an overall upward shift of the wild type spectrum is evident, a trend which is consistent with dissociation (see Figure 3.11, Section 3.2.2). A previous study has shown similar changes in CD spectra upon dissociation, when the enzyme was treated with a high concentration (1 M) of KCl (37). Similar results were obtained in the present study with high [$NaClO_4$] and high [KCl] (data not shown). Some changes in the W56F spectrum are also consistent with dissociation. These are seen at ~266 nm, where the Phe signal shows an intensity well above that typical of the residue, and in regions of Trp contributions (~284 nm and 294 nm), where the loss of negative peaks is also consistent with shifts taking place upon dissociation (37). The dramatic shift observed in E188D is not detected with W56F, but the argument can be made for this to be the result of the missing tryptophan at position 56. Aromatic signals are not discrete, nor can any one peak be assigned to any one type of side chain. This was touched upon briefly in Section 3.2.2. It is known that peaks may result from one or more types of residue(s), although general guidelines usually apply in the interpretation of aromatic signals, wherein Phe, Trp, and Tyr groups are known to produce signals in specified wavelength ranges. However, in a protein which contains a multitude of chromophores, the signals detected can be affected by that of neighboring aromatics, thus producing complex spectra. This may be the case for W56F. Whereas W56F may be partly dissociated, its spectrum may not indicate this as dramatically as with E188D, and this due to the substitution of Trp56 with a residue whose contributions are known to occur at shorter wavelengths.

Fluorescence spectroscopy of apo-proteins shows decreased emission intensities and red-shifting λ_{max} (emission) for both mutants (see Figure 3.12, Section 3.2.3). Red-shifting

is indicative of increased side chain mobility (91). The decrease in signal intensity may also reflect this in E188D, a result which is intensified by the loss of a tryptophan in W56F, as expected. The spectral differences point to changes in both tryptophan and tyrosine environments. The decrease in emission intensity in both mutants results from increased exposure to bulk solvent, a component of which is causing fluorescence quenching. This is consistent with dissociation, or at the very least, with weakened subunit association, as this may shift aromatics into positions with enhanced solvent accessibility.

Changes occurring in fourth derivative UV spectra are also consistent with subunit dissociation. First, there is a decrease in the peak ratio associated with the mutants, as discussed in Section 3.2.4. This is consistent with the dissociation process, as confirmed by results shown in Figure 3.23 (B) (Section 3.4.1) where the fourth derivatives of UV spectra of wild type enolase are shown as a function of increasing [$NaClO_4$]. The decreased peak-to-trough distance between A_{283nm}- A_{287nm} for both mutants, and the small increase in the A_{291nm}-A_{295nm} peak-to-trough distance in E188D are characteristic trends observed upon dissociation (see Figure 3.13). The decreased A_{291nm}-A_{295nm} peak-to-trough distance in W56F is atypical, and is probably due to the missing tryptophan.

Partial dissociation of both mutants was demonstrated conclusively using analytical ultracentrifugation. Here, W56F and E188D were determined to be ~52% and ~26% dissociated, respectively. This confirmed the spectral results which suggested dissociation, and allowed for the determination of a quantitative estimate of the shift in K_{eq} (see Section 3.2.5). Dissociation was more extensive in the case of W56F, which supported previous findings using fluorescence and fourth derivatives of UV spectra. Having confirmed that

partial dissociation had indeed taken place, it became apparent that protein samples of apo-mutant enzyme actually contained a mixed population of monomers and dimers, and that this was reflected in the spectroscopic changes obtained. It also added a measure of complexity to the interpretation of spectra obtained for W56F, a task already difficult in light of the replacement of one chromophore with another. It was, therefore, difficult to separate changes in absorbance due to the W→F substitution from those due to dissociation.

4.2 Subunit dissociation with $NaClO_4$

$NaClO_4$ causes changes in the fourth derivatives of UV spectra and enzymatic activity of yeast enolase. These changes have been reported (30, 80, 93, 94). The effect of $NaClO_4$, a chaotropic salt, on wild type enolase is also reported in the present study (see Figures 3.23 & 3.24, Section 3.4.1). It had been previously assumed that $NaClO_4$ dissociates the enzyme into its monomeric components, and that this is what led to the inactivation and spectral changes observed. However, conclusive evidence of dissociation was not obtained until samples of enzyme in varying [$NaClO_4$] were analyzed by centrifugation in an AUC. Data reported in this present study and other recently published results (94) show and confirm the dissociative effect of $NaClO_4$ on the enzyme (see Figure 3.23 (C), Section 3.4.1). Thus, proof of dissociation was presented, and this, in turn, is the process which leads to the other monitored effects (see Figure 3.23 (A) and (B), Section 3.4.1).

The decrease in r in second derivative spectra with increasing [$NaClO_4$] has been studied previously using pressure as the dissociative force (77). The decrease is interpreted as a decrease in tyrosine environment polarity upon dissociation. This, indeed, is contrary to what is expected. However, it was noted that, of the nine tyrosines in the molecule, four

of which are buried, two Tyr residues reside at the subunit interface (77). These, at positions 6 and 11, are more precisely situated near a cleft between the monomers, which is rich in ordered water molecules (77). The study postulated that the network of rigid waters in the crevice may actually create an environment of much greater polarity in the vicinity of Tyr6 and Tyr11 than that of bulk water. Therefore, environment polarity decreases as the subunits dissociate. This would be in agreement with aromatic circular dichroism results which show an upward shift, indicative of a shift into an environment of lesser polarity, in the protein spectrum upon dissociation with KCl (37). It would also explain the changes in Tyr signals obtained with the E188D variant (see Figure 3.11 (B)), as aromatic signals are generally intensified in less polar environments (90). Other changes in spectra occur with $NaClO_4$. The shifts observed ca. 272-280 nm in the fourth derivative spectra upon dissociation (see Figure 3.23 (B)) also reflect changes in tyrosine environments.

The dissociation of wild type enzyme by $NaClO_4$ was monitored using activity, fourth derivative UV spectroscopy, and analytical ultracentrifugation. A comparison of the three probes shows good agreement among the catalytic, tertiary, and quaternary changes taking place, which suggests a single process within the [$NaClO_4$] utilized (see Figure 3.25, Section 3.4.1). Results presented in Table 3.6 (and later in Table 3.7) show the use of AUC in K_d determinations (see wild type). In the results reported for apo and holo-wild type, reasonably good agreement is obtained among the K_d values associated with the different probes.

Studies carried out on the mutants with $NaClO_4$ quantitatively confirmed the dissociation observed with AUC in the absence of perchlorate. These monitored changes

in activity and fourth derivatives. Both mutants have elevated K_d relative to wild type, thus showing weakened subunit association. This, in turn, suggests that the targeted interface hydrogen bond was successfully weakened. Apo-mutant dissociation constants reside in the micromolar range, as opposed to wild type apo-values which are closer to nanomolar. The mutants were shown to reside in a more open conformation, as seen by higher *m* (see Table 3.6). They are much more readily dissociable, requiring considerably lower [$NaClO_4$] to bring about and complete the dissociation process (see Figure 3.27). This is reflected in the substantially lower $[NaClO_4]_{1/2}$ obtained for E188D (see Table 3.6). $[NaClO_4]_{1/2}$ is definitely lower in W56F as well, but this could not be quantitated, since apo-samples of this mutant were >50% monomeric. Where appropriate, K_d data were calculated from a single r or $S_{20,w}$ value for each mutant in its respective apo-state. The comparison between these constants and those obtained using $NaClO_4$ shows good agreement.

The dissociation of W56F is particularly informative. Changes occurring with $NaClO_4$ in fourth derivative spectra were monitored in W56F. As discussed, the spectrum of W56, as it resides in wild type, may be obtained by subtracting an equimolar spectrum of W56F from that of wild type (see Figure 3.14 , Section 3.2.4). By comparing the spectral changes occurring in W56F to those occurring in wild type upon dissociation, it is possible to attribute specific shifts in the native protein to the W56 residue. Shifts occurring at 287 nm, 291 nm, and 295 nm can be attributed to W56, as the changes at these peak positions upon dissociation differ in W56F (see Figure 3.28).

4.3 Binding of metal cofactor

The binding of Mg^{2+} at the metal site (1) lowers the subunit dissociation constant,

thereby driving the equilibrium in favor of the dimer (11). The stabilizing effect of Mg^{2+} on the wild type enzyme is seen here by an increase in fluorescence signal (see Figure 3.20), r (see Figure 3.18 (A)), and $S_{20,w}$ (see Figure 3.17 (A)). It is also shown through stabilization against denaturation (see Figure 3.22 (A)). The associative effect of Mg^{2+} is also accompanied by changes in aromatic CD signals (data not shown). Previous CD studies have been carried out in which important changes took place upon binding cofactor (37). These were proposed to reflect the changes in the loop conformations, the precise orientation of which is crucial for Mg^{2+} coordination (37). These same effects are observed in W56F and E188D upon binding of cofactor. Binding of Mg^{2+} leads to re-association of the partially dissociated apo-mutants. The dimerization is evident in results reported for analysis carried out using AUC, fluorescence, temperature denaturation, and fourth derivative UV spectroscopy. Cofactor binding produces analogous changes, but to far greater extent given the greater level of re-association taking place within the mutants.

Mg^{2+} protects wild type and mutants against dissociation (see Figures 3.29 and 3.30), as cofactor bound proteins necessitated higher [$NaClO_4$] to effect and complete the process. This is further substantiated by the establishment of the holo-mutants as fully dimeric (see Table 3.8). The presence of magnesium produced tighter subunit association, as quantitatively outlined in Table 3.7. Tightened subunit association is particularly the case for holo-W56F and holo-E188D. The decreased K_d values and increased $[NaClO_4]_{1/2}$ indicate that both are less easily dissociable than their respective apo-forms. Dissociation constants obtained for the holo-wild type protein are in very good agreement with reported values for the ββ-enzyme (mammalian), where K_d's of 1.2 nM and 6.5 nM based on activity

and fourth derivative spectroscopy measurements, respectively, were obtained (30). Similar results were obtained with the various probes. The holo-mutants retain elevated K_d's relative to wild type, particularly in the case of W56F. As a result, they remain substantially more readily dissociable than wild type, as seen by lower $[NaClO_4]_{1/2}$.

The effect of Mg^{2+} on apo-proteins is revealing in a number of ways. The increase in r observed is typical of re-association, and the quantitative increase is consistent with the extent of dissociation initially estimated for each apo-mutant. The comparison of the protein fourth derivative spectra thus reveals the extent of the shift attributable to the missing Trp residue in W56F, as the mutant is fully dimeric under the specified buffer conditions (see Figure 3.19, Section 3.3.2). The protection from dissociation with magnesium is especially telling when monitored by activity. As discussed, Mg^{2+} binding has a stabilizing effect on the mobile loop portions of the protein. The stabilization of these loops, which are crucial for proper catalysis, both in gating the active site and in coordinating to metals at sites I & II, is most certainly the catalyst for the recovery and maintenance of activity over larger ranges of $[NaClO_4]$.

4.4 Substrate binding

The binding of 2-PGA has a tightening effect on the overall structure of the protein, analogous to that observed with Mg^{2+}. This produces a more compact protein assembly, as seen by the increased $S_{20,w}$ of the three 2 -PGA-bound holo-proteins (Table 3.10). The effect on $S_{20,w}$, however, does not indicate any further dimerization of the mutants. The concomitant spectral changes of 2-PGA binding observed with aromatic CD (data not shown) and fluorescence spectroscopy are consistent with tighter subunit association, which

is further substantiated by the lowered dissociation constants obtained (Table 3.9). Substrate binding in effect provides further protection against dissociation for wild type and mutant proteins alike (Figure 3.31). This does not, however, result in tighter subunit association in the native protein. Rather, the structural effect of 2-PGA binding on the overall shape of the molecule, which is a much more closed and compact entity, is what offers the protection observed. This is evidenced by the lower extent of solvent exposed protein surface area, or *m*, upon substrate binding (Table 3.9). Just as in binding Mg^{2+}, the binding of substrate produces conformational changes in the protein, thus leading to the spectroscopic shifts detected. These are due to the effect of substrate binding on mobile loops in the protein.

Presence of substrate protects the mutants against dissociation, as shown through the tightened subunit dissociation constants obtained, and the increased $[NaClO_4]_{1/2}$ observed (Table 3.9). The mutants nevertheless remain more readily dissociable than wild type. Comparison of *m* reveals that, although dimeric, the variants remain in a significantly more 'open' protein conformation upon dissociation, with increased solvent exposure of protein surfaces. This is supported by comparative spectral data which show that substrate bound mutants retain substantially lower fluorescence signals (see Table 3.11) and important signal differences in their aromatic CD (data not shown). The increased exposure of mutant protein surfaces may allow chaotropes to hydrate buried surfaces more easily, thus rendering the mutants more readily dissociable.

4.5 Denaturation is a two-step process

As previously reported, the association of subunits stabilizes the enzyme against denaturation (40). In effect, results obtained in the present study agree, as Mg^{2+} binding

renders the proteins studied more thermostable (Figure 3.22). This is viewed as evidence that the enzyme must dissociate before denaturing, and that denaturation is, therefore, a two-step process (40). The binding of metal reduces subunit dissociation, and leads to increased thermostability. This consequence of metal binding on both processes lends support to the possibility of denaturation as a two-step mechanism. Although dissociation of a protein into its smaller oligomeric components may cause important changes in its peptide bond spectrum (96), this is not the case for enolase. Monomeric subunits of enolase have been shown to display identical far-UV region spectra as obtained for the dimeric protein (30). Although these published results were obtained using the mammalian enzyme isolated from rabbit muscle, they were confirmed in the present study using the yeast enzyme (Sections 3.4.1 & 3.4.2). Thus, intact peptide bond spectra do not discount the possibility of dissociation, as the monomers of enolase are folded regardless of subunit association in the absence of denaturing forces. It is not clear how readily denaturation takes place following dissociation at this point. However, higher [$NaClO_4$] are known to produce other effects on the enzyme following dissociation, as determined by aromatic CD measurements (unpublished data, M.J. Kornblatt), and these are believed to be possible denaturation. Further study into this matter would most certainly prove to be informative in answering these questions.

The stabilizing effect of Mg^{2+} is emphasized even more in the presence of substrate and tighter binding metals (40). The latter is consistent with the loss of metal ion upon dissociation, prior to denaturation, thus leading to inactivation (Section 1.4). The increased thermostability is believed to be mediated via the closure of the mobile loop portions in the

enzyme upon binding metals and substrate. The stabilization of loop conformations enhance subunit association, thereby leading to a more compact, "closed" protein conformation which is more thermostable (40).

4.6 Energy and catalytic considerations

The effect of the single mutations on dimer stability is large, as evidenced by the impact on K_d. In dimeric proteins, the energetics of subunit interactions may be distributed along oligomer interfaces, or alternatively, confined to relatively small areas (31). Single mutations in a case where the energetics are distributed over a large area of interaction fail to produce important changes in dimer stability (31). The substantial impact of the W56F and E188D mutations on dimer stability (~14 kJ/mole for W56F, and ~10 kJ/mole for E188D) for the apo-enzymes suggest that a relatively small area of the interface is responsible for the bulk of the energetic contributions to association. As a result, the area in the vicinity of the Pro35-Gly60 loop is directly implicated. Site-directed mutagenesis at the enolase subunit interface has been carried out previously in the ββ-enzyme isolated from rabbit muscle (94). A glutamate residue at position 414, which forms two salt bridges at the interface, was mutated to leucine to study the effect that abolishing these interactions had on the enzyme. The impact of this on dimer stability was significant, changing $\Delta G_{(H2O)}$ from 49.7 kJ/mole to 42.3 kJ/mole (94). In the yeast enzyme, position 414 is occupied by an arginine which is also implicated in two salt bridges at the interface (22). More precisely, close examination of the yeast x-ray structure revealed R414 to be situated in the water filled crevice between the monomers (77). Its mutational effect on stability supports the possibility that a relatively small area of interaction is responsible for the bulk of the

energetic contributions. In this case, at least two areas of interaction are known to contribute a great deal to the monomer association. The involvement of an area with a direct link to the Pro35-Gly60 mobile loop suggests its key importance in the enzyme's structural and functional stability.

The implication of the Pro35-Gly60 loop is undeniably crucial for catalysis. The most mobile portion(Pro35-His43) acts as a gate over the active site, and its closure is crucial for activity (see Sections 1.2.3 & 1.3.5). Under specified enzymatic assay conditions (1 mM Mg^{2+}/1 mM 2-PGA), the mutants are dimeric. The W56F mutation, situated in the loop, showed significant effect on catalysis, as seen by depressed k_{cat} for Mg^{2+}, Mn^{2+}, and 2-PGA (Table 3.14). The loss of activity could be due to the following: 1) The presence of a higher fraction of monomers, which are inactive, leads to an overall decrease in k_{cat}; 2) the dimeric mutant itself has a lower k_{cat}, the mutation having detrimentally affected the active site via the Pro35-Gly60 loop. Samples from protein pools of W56F showed decreased activity levels (~70%) in this buffer system (Table 3.3). The kinetics of 2-PGA are carried out using dimeric protein samples, as substrate is titrated into enzyme in the presence of 1 mM Mg^{2+}. Results showed a significantly depressed k_{cat} value (~65% loss of activity), and specific activities obtained for holo-W56F equally show ~50% loss of activity (see Section 3.5). Holo-E188D shows k_{cat} values comparable to that of wild type, and the somewhat lower activity levels obtained in the mutant's apo-form may be attributed to the presence of monomers. Thus, the mutation at position 56 has lowered the mutant dimer's catalytic efficiency.

The effect of the W56F mutation on activity is important, as reflected by catalytic

efficiency and $\Delta\Delta G$. This is all the more significant given the distance between the active site and subunit interface. Such long range interactions have been reported in other enzymes (31). The impact on activity in this case is mediated via the mobile loop which traverses the active site and extends to the subunit interface. This is evidenced by the inactivation observed in the mutation directly implicating a loop residue, as opposed to its more indirect involvement in the E188D mutant, which retains normal levels of catalysis.

4.7 It all comes down to the loops

The importance of the loop conformation is evident in many ways. First, it is clear that weakening a subunit interaction involving one of these, the Pro35-Gly60 loop, either directly or indirectly, has a significant impact on the structure of enolase apo-proteins. Second, the destabilization of the interaction, and consequently of the loop, has an important impact on the protein's behavior when subjected to dissociative and/or denaturative forces. Third, the mutation at the interface involving the Pro35-Gly60 loop has a long-range detrimental effect on the dimer catalytic ability. This destabilization of the loop at the interface results in an improper conformation of the active site loop. This, in turn, may affect its closure over the catalytic site. Alternatively, this may result in the loss of metals, possibly due to improper coordination, thus leading to loss of activity.

The central role of the mobile loops, and that of the Pro35-Gly60 loop in particular, is evident. The destabilization of loops and areas in close proximity to loops also has been shown to have definitive physiological consequences. Severe fatigue and exercise intolerance were observed in a man with muscle enolase deficiency (97). The enolase expressed was found to contain two mutations, G156D and G374E, each situated in loop

regions (12). These correspond to positions 157 and 376 in yeast, respectively, and G156 is in close proximity to His159, an active site residue. The glycines at these positions may act as loop hinges, much like G37 and G41 in the active site loop (see Section 1.2.3). The considerable effect of these mutations on activity (only 5% residual activity is detected) indicates the crucial importance of maintaining precise loop conformation, as previously postulated. The present study supports this premise.

Chapter 5: Conclusions

A number of conclusions can hereby be drawn based on the results reported in the present study. These are as follows:

A) The hydrogen bond between W56 and E188 has been successfully weakened in both variants prepared, as these are partially dissociated;

B) Important structural changes have taken place, and these are consistent with dissociation;

C) The weakened subunit association in W56F has resulted in a significant loss of activity, while E188D displays normal k_{cat} levels in its dimeric state;

D) The increase in K_i with Mg^{2+} for both mutants, particularly for E188D, suggests that the third inhibitory metal binding site may reside in close proximity to the subunit interface where the mutations were effected;

E) As for wild type, cofactor and substrate binding favors subunit association in the mutants, and Mg^{2+} contributes to the enzymes' thermostability;

F) The thermostability offered by Mg^{2+} binding supports the denaturation process as a two-step mechanism, beginning with the dissociation of the subunits;

G) Spectral shifts analogous to those in wild type occur upon binding Mg^{2+} and 2-PGA;

H) A change at position 56 alters catalysis and may be mediated through the Pro35-Gly60 loop;

I) The associative effect of Mg^{2+} and 2-PGA binding on K_d and the increased thermostability

with cofactor are conversely mediated through this same loop;

J) This suggests a two-way relationship between the active site and the subunit interface, thus providing an explanation for the occurrence of monomers as inactive entities.

References

(1) Holland, M.J., Holland, J.P., Thill, G.P., & Jackson, K.A. (1981) The primary structures of two yeast enolase genes. Homology between the 5' noncoding flanking regions of yeast enolase and glyceraldehyde-3-phosphate dehydrogenase genes. J. Biol. Chem. **256 (3)**: 1385-1395.

(2) Chin, CC., Brewer, J.M., Eckard, E., & Wold, F. (1981) The amino acid sequence of yeast enolase. Preparation and characterization of peptides produced by chemical and enzymatic fragmentation. J. Biol. Chem. **256 (3)**: 1370-1376.

(3) Chin, CC., Brewer, J.M., & Wold, F. (1981) The amino acid sequence of yeast enolase. J. Biol. Chem. **256 (3)**: 1377-1384.

(4) Chin, CC. Q. (1990) The primary structure of rabbit muscle enolase. J. Protein Chem. **9**: 427-432.

(5) McAlister, L., & Holland, M. J. (1982) Targeted deletion of a yeast enolase structural gene. Identification and isolation of yeast enolase isozymes. J. Biol. Chem. **257 (12)**: 7181-7188.

(6) Warburg, O., & Christian, W. (1942) Isolation and crystallization of enolase. Biochem. Z. **310**: 384-421.

(7) Brewer, John M. (1981) Yeast enolase: Mechanism of activation by metal ions. CRC Crit. Rev. Biochem. **11 (3)**: 209-254.

(8) Barnes, L.O., & Stell Wagen, E. (1973) Enolase from the thermophile Thermus x-1. Biochemistry. **12**: 1559-1565.

(9) Veronese, F.M., Schiavon, O., Boccu, E., Benassi, C.A., & Fontana, A. (1984) Enzymatically active subunits of *Bacillus stearothermophilus* enolase bound to sepharose. Int. J. Peptide Protein Res. **24**: 557-562.

(10) Schurig, H., Rutkat, K., Rachel, R., & Jaenicke, R. (1995) Octameric enolase from the hyperthermophilic bacterium *Thermotoga maritima*: Purification, characterization, and image processing. Protein Sci. **4**: 228-236.

(11) Wold, F. (1971) in The enzymes. Vol 5, 3rd edn. (Boyer, P.D., ed), 499-538, Academic Press, New York, USA.

(12) Lebioda, L., Stec, B., & Brewer, J.M. (1989) The structure of yeast enolase at 2.25Å resolution. An 8-fold β + α-barrel with a novel ββαα $(\beta\alpha)_6$ topology. J. Biol. Chem. **264 (7)**: 3685-3693.

(13) Kühnel, K., & Luisi, B.F. (2001) Crystal structure of the *Escherichia coli* RNA degradosome component enolase. J. Mol. Biol. **313**: 583-592.

(14) Duquerroy, S., Le Bras, G., & Janin, J. (1994) Lobster enolase crystallized by serendipity. Proteins. **18 (4)**: 390-393.

(15) Duquerroy, S., Camus, C., & Janin, J. (1995) X-ray structure and catalytic mechanism of lobster enolase. Biochemistry. **34**: 12513-12523.

(16) Zhang, E., Brewer, J.M., Minor, W., Carreira, L.A., & Lebioda, L. (1997) Mechanism of enolase: The crystal structure of asymmetric dimer enolase-2-phospho-D-glycerate/enolase-phosphoenolpyruvate at 2.0Å resolution. Biochemistry. **36**: 12526-12534.

(17) Babbitt, P.C., Hasson, M.S., Wedekind, J.E., Palmer, D.R.J., Barrett, W.C., Reed, G.H. Rayment, I.. Ringe, D., Kenyon, G.L., & Gerl, J.A. (1986) The enolase superfamily: A general strategy for enzyme-catalyzed abstraction of the α-protons of carboxylic acids. Biochemistry. **35**: 16489-16501.

(18) Gulick, A.M., Hubbard, B.K., Gerlt, J.A., & Rayment, I. (2000) Evolution of enzymatic activities in the enolase superfamily: Crystallographic and mutagenesis studies of the reaction catalyzed by D-glucarate dehydratase from *Escherichia coli*. Biochemistry. **39**: 4590-4602.

(19) Babbitt, P.C., Mrachko, G.T., Hasson, M.S., Huisman, G.W., Kolter, R., Ringe, D., Petsko, G.A., Kenyon, G.L., & Gerlt, J.A. (1995) A functionally diverse enzyme superfamily that abstracts the α-protons of carboxylic acids. Science. **267**: 1159-1161.

(20) Larsen, T.M., Wedekind, J.E., Rayment, I., & Reed, G.H. (1996) A carboxylate oxygen of the substrate bridges the magnesium ions at the active site of enolase: Structure of the yeast enzyme complexed with the equilibrium mixture of 2-phosphoglycerate and phosphoenolpyruvate at 1.8Å resolution. Biochemistry. **35**: 4349-4358.

(21) Lebioda, L., Zhang, E., Lewinski, K., & Brewer, J.M. (1993) Fluoride inhibition of yeast enolase: Crystal structure of the enolase-Mg(2+)-F(-)-Pi complex at 2.6Å resolution. Proteins: Struct. Func. Genet. **76**: 219-225.

(22) Stec, B., & Lebioda, L. (1990) Redefined structure of yeast apo-enolase at 2.25Å resolution. J. Mol. Biol. **211**: 235-248.

(23) Lebioda, L., Stec, B., & Brewer, J.M. (1997) Mechanism of enolase: The crystal structure of enolase-Mg^{2+}-2-phosphoglycerate/phosphoenolpyruvate complex at 2.2Å resolution. Biochemistry. **30**: 2877-2822.

(24) Reed, G.H., Poyner, R.R., Larsen, T.M., Wedekind, J.E., & Rayment, I. (1996) Structural and mechanistic studies of enolase. Curr. Opin. Struct. Biol. **6**: 736-743.

(25) Murzin, A.G., Brenner, S.E., Hubbard, T., & Chotia, C. (1995) SCOP: A structural classification of proteins database for the investigation of sequences and structures. J. Mol. Biol. **247**: 536-540.

(26) Hocker, B., Beisman-Driemeyer, S., Hettwer, S., Lustig, A., & Sterner, R. (2001) Dissection of a (beta-alpha) 8-barrel enzyme in two folded halves. Nature Struct. Biol. **8**: 32-36.

(27) Banner, D.W., Bloomer, A.C., Petsko, G.A., Philips, D.C., Pogson, C.I., Wilson, I.A., et al. (1975) Structure of chicken muscle triose phosphate isomerase determined crystallographically at 2.5Å (angstrom) resolution using amino acid sequence data. Nature. **255**: 609-614.

(28) Wedekind, J.E., Poyner, R.E., Reed, G.H., & Rayment, I. (1994) Chelation of serine 39 to Mg^{2+} latches a gate at the active site of enolase: Structure of the bis (Mg^{2+}) complex of yeast enolase and the intermediate analogue phosphonoacetohydroxamate at 2.7Å resolution. Biochemistry. **33**: 9333-9342.

(29) Brewer, J.M., Glover, C.V.C., Holland, M.J., & Lebioda, L. (1997) Effect of site-directed mutagenesis of His373 of yeast enolase on some of its physical and enzymatic properties. Biochim. Biophys. Acta. **1340**: 88-96.

(30) Kornblatt, M.J., Al-Ghanim, A., & Kornblatt, J.A.K. (1996) The effects of sodium perchlorate on rabbit muscle enolase. Spectral characterization of the monomer. Eur. J. Biochem. **236**: 78-84.

(31) Myers,, D.P., Jackson, L.K., Ipe, V.G., Murphy, G.E., & Philips, M.A. (2001) Long-range interactions in the dimer interface of ornithine decarboxylase are important for enzyme function. Biochemistry. **40**: 13230-13236.

(32) Williams, J.C., & McDermott, A.E. (1995) Dynamics of the flexible loop of triose phosphate isomerase: The loop motion is not ligand gated. Biochemistry. **34**: 8309-8319.

(33) Brewer., J.M., Glover, C.V., Holland, M.J., & Lebioda, L. (1998) Significance of the enzyme properties of yeast S39A enolase to the catalytic mechanism. Biochim. Biophys. Acta. **1383**: 351-357.

(34) Poyner, R.R., Larsen, T.M., Wong, S-W., & Reed, G.H. (2002) Functional and structural changes due to a serine to alanine mutation in the active site flap of enolase. Arch. Biochem. Biophys. **401 (2)**: 155-163.

(35) Vinarov, D., & Nowak, T. (1999) Role of His 159 in yeast enolase catalysis. Biochemistry. **38**: 12138-12149.

(36) Brewer, J.M., Holland, M.J., & Lebioda, L. (2000) The H159A mutant of yeast enolase 1 has significant activity. Biochem. Biophys. Res. Commun. **276(3)**: 1199-202.

(37) Kornblatt, M.J., Lange, R., & Balny, C. (1998) Can monomers of yeast enolase have enzymatic activity? Eur. J. Biochem. **251**: 775-780.

(38) Janin, J. Miller, S., & Chotia, C. (1988) Surface, subunit interfaces and interior of oligomeric proteins. J. Mol. Biol. **204**: 155-164.

(39) Jones, S., & Thornton, J.M. (1996) Principles of protein-protein interactions. Proc. Natl. Acad. Sci. USA. **93**: 13-20.

(40) Brewer, J.M., & Wampler, J.E. (2001) A differential scanning calorimetric study of the effects of metal ions, substrate/product, substrate analogues, and chaotropic anions on the thermal denaturation of yeast enolase 1. Int. J. Biol. Macromolecules. **28**: 213-218.

(41) Sangadala, V.S., Glover, C.V.C., Robson, R.L., Holland, M.J., Lebioda, L., & Brewer, J.M. (1995) Preparation by site-directed mutagenesis and characterization of the E211Q mutant of yeast enolase 1. Biochim. Biophys. Acta. **1257**: 23-37.

(42) Stubbe, JA., & Abeles, R.H. (1980) Mechanism of action of enolase: Effect of the β-hydroxy group on the rate of dissociation of the α-carbon-hydrogen bond. Biochemistry. **19**: 5505-5512.

(43) Dino Vo, E.C., & Boyer, P.D. (1997) Isotopic probes of the enolase reaction mechanism. J. Biol. Chem. **246**: 4586-4593.

(44) Anderson, S.A., Anderson, V.E., & Knowles, J.R. (1994) Primary and secondary kinetic isotope effects as probes of the mechanism of yeast enolase. Biochemistry. **33**: 10545-10555.

(45) Kornblatt, M.J. (1996) The mechanism of rabbit muscle enolase: Identification of the rate-limiting steps and the site of Li^+ inhibition. Arch. Biochem. Biophys. **330 (1)**: 12-18.

(46) Cohn, M., Pearson, J.E., O'Connell, E.L., & Rose, I.A. (1970) Nuclear magnetic resonance assignment of the vinyl hydrogens of phosphoenolpyruvate. Stereochemistry of the enolase reaction. J. Am. Chem. Soc. **92 (13)**: 4095-8.

(47) Poyner, R.R., Laughlin, T., Sowa, G.A., & Reed, G.H. (1996) Toward identification of acid/base catalysts in the active site of enolase: Comparison of the properties of K345A, E168Q, and E211Q variants. Biochemistry. **35**: 1692-1699.

(48) Brewer, J.M. (1985) Specificity and mechanism of action of metal ions in yeast enolase. FEBS Lett. **182 (1)**: 8-14.

(49) Brewer, J., Robson, R.L., Glover, C.V.C., Holland, M.J., & Lebioda, L. (1993) Preparation and characterization of the E168Q site-directed mutant of yeast enolase 1. Proteins: Struct. Funct. Genet. **17**: 426-434.

(50) Anderson, V.E., Weiss, P.M., & Cleland, W.W. (1984) Reaction intermediate analogues for enolase. Biochemistry. **23**: 2779-2786.

(51) Faller, L.D., Baroudy, B.M., Johnson, A.M., & Ewall, R.X. (1977) Magnesium ion requirements for yeast enolase activity. Biochemistry. **16**: 3864-3869.

(52) Brewer, J.M., Carreira, L.A., Collins, K.M., Duvall, M.C., Cohen, C., & DerVartanian, D.V. (1983) Studies of activating and non-activating metal ion binding to yeast enolase. J. Inorg. Biochem. **19 (3)**: 255-267.

(53) Chien, J.C., & Westhead, E.W. (1971) Electron paramagnetic resonance study of the interaction of yeast enolase with activating metal ions. Biochemistry. **10 (17)**: 3198-3203.

(54) Zhang, E., Hatada, M., Brewer, J.M., & Lebioda, L. (1994) Catalytic metal ion binding in enolase: The crystal structure of an enolase-Mn^{2+}-phosphonoacetohydroxamate complex at Å resolution. Biochemistry. **33**: 6295-6300.

(55) Spencer, S.G., Brewer, J.M.., & Ellis, P.E. (1985) Cadmium (II)-113 NMR studies of the mechanism of metal ion activation of yeast enolase. J.Inorg. Biochem. **24 (1)**: 47-57.

(56) Spencer, S.G., & Brewer, J.M. (1984) Activation of yeast enolase by Cd (II). J.Inorg. Biochem. **20 (1)**: 39-52.

(57) Sinha, U., & Brewer, J.M. (1984) Cu (II) activates yeast enolase. J. Inorg. Biochem. **22 (3)**: 175-177.

(58) Wang, S., Scott, R.A., Lebioda, L., Zhou, Z.H., & Brewer, J.M. (1995) An x-ray absorption spectroscopy study of the interactions of Ni^{2+} with yeast enolase. J. Inorg. Biochem. **58 (3)**: 209-227.

(59) Rose, S.L., Dickinson, C., & Westhead, E.W. (1984) Kinetic and physical properties of Co^{2+} enolase. J. Biol. Chem. **259 (7)**: 4405-4473.

(60) Lebioda, L., Stec, B., Brewer, J.M. & Tykarska, E. (1991) Inhibition of enolase: The crystal structure of enolase-Ca^{2+}-phosphoglycerate and enolase-Zn^{2+}-phosphoglycolate complexes at 2.2Å resolution. Biochemistry. **30**: 2823-2827.

(61) Brewer, J.M., & Collins, K.M. (1982) Studies of the role of catalytic and conformational metals in producing enzymatic activity in yeast enolase. J. Inorg. Biochem. **13**: 151-164.

(62) Collins, K.M. & Brewer, J.M. (1982) Circular dichroism (CD) studies on yeast enolase: Activation by divalent cations. J. Inorg. Biochem. **17**: 15-28.

(63) Hanlon, D.P., & Westhead, E.W. (1969) Equilibrium measurements of the interaction of yeast enolase with activating metal ions. Biochemistry. **8**: 4247-4255.

(64) Hanlon, D.P., & Westhead, E.W. (1969) Kinetic studies on the activation of yeast enolase by divalent cations. Biochemistry. **8**: 4255-4260.

(65) Elliott, J.I., & Brewer, J.M. (1980) Binding of inhibitory metals to yeast enolase. J. Inorg. Biochem. **12**: 323-334.

(66) Lee, B.H., & Nowak, T. (1982) Influence of pH on the Mn^{2+} activation of and binding to yeast enolase: A functional study. Biochemistry. **31**: 2165-2171.

(67) Kornblatt, M.J., & Musil, R. (1990) The inhibition of yeast enolase by Li^{+} and Na^{+}. Arch. Biochem. Biophys. **277 (2)**: 301-305.

(68) Kornblatt, M.J. & Klugerman, A. (1989) Characterization of the enolase isozymes of rabbit brain: Kinetic differences between mammalian and yeast enolases. Biochem. Cell. Biol. **67 (2-3)**: 103-107.

(69) Poyner, R.R., & Reed. G.H. (1992) Structure of the bis divalent cation complex with phosphonoacetohydroxamate at the active site of enolase. Biochemistry. **31**: 7166-7173.

(70) Wedekind, J.E., Reed, G.H., & Rayment, I. (1995) Octahedral coordination at the high-affinity metal site in enolase: Crystallographic analysis of the Mg^{II}-enzyme complex from yeast at 1.9Å resolution. Biochemistry. **34**: 4325-4330.

(71) Brewer, J.M., Faini, G.J., Wu, C.A., Goss, L.P., Carreira, L.A., & Wojcik, R. (1978) Characterization of the subunit dissociation of yeast enolase. Physical aspects of protein interactions. (Catsimpoolas, N., ed.) pp.57-78, Elsevier/North-Holland, Amsterdam.

(72) Brewer, J.M., & Weber, G. (1968) The reversible dissociation of yeast enolase. Proc. Natl. Acad. Sci. USA. **59**: 216-223.

(73) Brewer, J.M. (1969) Interactions of potassium chloride and acetate with yeast enolase. Arch. Biochem. Biophys. **134**: 59-66.

(74) Brewer, J.M. (1975) Isoionic titration and isopycnic density gradient centrifugation studies of magnesium activation and subunit dissociation in yeast enolase. Arch. Biochem. Biophys. **171**: 466-473.

(75) Paladini, A.A., & Weber, G. (1981) Pressure-induced reversible dissociation of enolase. Biochemistry. **20**: 2587-2593.

(76) Kornblatt, J., Kornblatt, J. & Hui Bon Hoa, G. (1982) The pressure-induced, reversible inactivation of mouse brain enolases. Eur. J. Biochem. **128**: 577-581.

(77) Kornblatt, J.A., Kornblatt, M.J., & Hui Bon Hoa, G. (1995) Second derivative spectroscopy of enolase at high hydrostatic pressure: An approach to the study of macromolecular interactions. Biochemistry. **34**: 1218-1223.

(78) Keresztes-Nagy, S., & Orman, R. (1971) Dissociation of yeast enolase into active monomers. Biochemistry. **10**: 2506-2508.

(79) Holleman, W.H. (1973) The use of absorption optics to measure dissociation of yeast enolase into enzymatically active monomers. Biochim. Biophys. Acta. **327**: 176-185.

(80) Trepanier, D., Wong, C. & Kornblatt, M.J. (1990) The salt-induced dissociation and inactivation of a mammalian enolase: Evidence for the formation of active monomers. Arch. Biochem. Biophys. **283 (2)**: 271-277.

(81) Sambrook, J., Fritsch, E.F., & Maniatis, T. (1989) in Molecular Cloning: A Laboratory Manual. Vol. 1, 2, 3. Cold Spring Harbor Laboratory Press, N.Y., USA.

(82) Good, L., & Nazar, R.N. (1997) Plasmid mini-preparations from culture streaks. Benchmarks, BioTechniques. **22**: 404-406

(83) Molecular Biology LabFax. (1991) (Brown, T.A. ed.) Academic Press Inc and Bios Scientific Publishers Ltd., San Diego, USA.

(84) Laemmli, U.K. (1970) Cleavage of structural proteins during the assembly of the head of bacteriophage T4. Nature. **227**: 680-685.

(85) Lange, R., Frank, J., Saldana, J-L., & Balny, C. (1996a) Fourth derivative UV-spectroscopy of proteins under high pressure. I. Factors affecting the fourth derivative spectrum of the aromatic amino acids. Eur. Biophys. J. **24**: 277-283.

(86) Ragone, R., Colonna, G., Balestrieri, C., Servillo,L., & Irace, G. (1984) Determination of tyrosine exposure in proteins by second-derivative spectroscopy. Biochemistry. **23**: 1871-1875.

(87) Ralston, G. (1993) Introduction to analytical ultracentrifugation, for Beckman Instruments Inc.

(88) Enzyme LabFax. (1996) (Edited by P.C. Engel). Bios Scientific Publishers, Oxford, UK & Academic Press, San Diego, USA.

(89) Pace, C.N., Shirley, B.A., & Thomson, J.A. (1989) in Protein structure: A practical approach. (Creighton, T.E., ed.) pp. 311-330, IRL Press, Oxford.

(90) Strickland, E.H. (1974) Aromatic contributions to circular dichroism spectra of proteins. CRC Crit. Rev. Biochem. **2**: 113-175.

(91) Lakowicz, J. (1999) Principles of Fluorescence Spectroscopy. Kluwer Academic and Plenum Publishers, New York, USA.

(92) Kornblatt, J.A., Kornblatt, M.J., Lange, R., Mombelli, E., & Guillemette, J.G. (1999) The individual tyrosines of proteins: Their spectra may or may not differ from those in water or other solvents. Biochim. Biophys. Acta. **1431**: 238-248.

(93) Lin, T., & Kornblatt, M.J. (2000) The binding of Na^+ to apo-enolase permits the binding of substrate. Biochim. Biophys. Acta. **1476**: 279-286.

(94) Kornblatt, M.J., Zheng, S-X., Lamande, N., & Lazar, M. (2002) Cloning, expression and mutagenesis of a subunit contact of rabbit muscle-specific (ββ) enolase. Biochim. Biophys. Acta. (In Press).

(95) Arakawa, T, & Timasheff, S.N. (1982) Preferential interactions of proteins with salts in concentrated solutions. Biochemistry. **21**: 6545-6552.

(96) Johnson, C.W. Jr. (1990) Protein secondary structure and circular dichroism: A practical guide. Proteins: Struct. Funct. Genet. **7**: 205-214.

(97) Comi, G.P., Fortunato, F., Lucchiari, S., Bordoni, A., Prelle, A., Jann, S., Keller, A., Ciscato, P., Galbiati, S., Chiveri, L., Torrente, Y., Scarlato, G., & Bresolin, N. (2001) β-enolase deficiency, a new metabolic myopathy of distal glycolysis. Ann. Neurol. **50**: 202-207.